Investigation of Gold α-Oxo Carbene/Carbenoid Complexes as Key Intermediates in Gold(I) Catalysis

by

Caroline P. Stow

Department of Chemistry
Duke University

Date:_____

Approved:

_____
Ross A. Widenhoefer, Advisor

_____
Dorian Canelas

_____
Stephen L. Craig

_____
Jiyong Hong

Dissertation submitted in partial fulfillment of
the requirements for the degree of Doctor
of Philosophy in the Department of
Chemistry in the Graduate School
of Duke University

2022

ABSTRACT

Investigation of Gold α-Oxo Carbene/Carbenoid Complexes as Key intermediates in Gold(I) Catalysis

by

Caroline P. Stow

Department of Chemistry
Duke University

Date:_____

Approved:

_____
Ross A. Widenhoefer, Advisor

_____
Dorian Canelas

_____
Stephen L. Craig

_____
Jiyong Hong

An abstract of a dissertation submitted in partial fulfillment of the requirements for the degree of Doctor of Philosophy in the Department of Chemistry in the Graduate School of Duke University

2022

Abstract

Cationic gold(I) complexes have recently contributed to significant developments in homogenous catalysis. Such complexes have been praised as highly effective catalysts for the functionalization of C-C multiple bonds, leading to research on cationic gold-catalysts developing at an aggressive pace. Despite the progress being made surrounding gold(I)-catalysis, there are still many gaps in our fundamental understanding of the key intermediate complexes and their reactivity in these transformations, exemplified by the often evoked gold α-oxo carbene species. While there are existing computational studies suggesting the instability of gold α-oxo carbene species, there lacks any experimental evidence to support the stability and reactivity of alternate key intermediate species, such as gold α-oxo carbenoid species and gold *N*-alkenoxypyridinium/sulfonium complexes. Herein, we address the issues surrounding the formation of gold α-oxo carbene species in reported literature. We report the synthesis and reactivity of gold pyridinium α-oxo carbenoid complexes, gold sulfonium α-oxo carbenoid complexes, and gold α,α-dioxo carbenoid complexes. We then report the direct observation of a gold *N*-alkenoxysulfonium complex in a gold-catalyzed alkynyl sulfoxide rearrangement reaction and the synthesis of a series of gold-oxide compounds. Together, this research addresses the gaps in knowledge surrounding key intermediate species in gold(I)-catalyzed transformations.

To Mom and Dad.

None of this would have been possible without

your love and support.

Contents

List of Tables

List of Figures

List of Schemes

Acknowledgements

I would first like to thank my family for their unwavering support throughout my entire life, and especially my graduate school journey. I want to thank my Mom, Carol, for the constant encouragement, my Dad, John, for always making me laugh during the rough times, my sister, Allison, for always letting me vent to her, and my Aunt Pat for being such a strong positive role model my whole life.

I would also like to thank my advisor, Professor Ross Widenhoefer, for his support and encouragement, as well as my committee members throughout my graduate school career: Professor Jiyong Hong, Professor Stephen Craig, Professor Dorian Canelas, and Professor Steven Malcolmson. I would also like to thank the amazing NMR center staff, Dr. Benjamin Bobay, Dr. Donald Mika, and Dr. Ronald Venters. I additionally want to thank the Department of Chemistry staff, especially Meg and Chrissy, for helping me with every request I've had over the years.

To the past and present Widenhoefer lab members, Bob, Nana, Yichen, Liqi, Mitch, Daniel, and Xujun, I want to extend my sincerest thank you for making every day in lab memorable. I also want to say a special thank you to my friends for supporting me outside the lab as well; Nana, Caroline, Amanda, Sara, Mitch and Dottie. You all made this entire experience fun and enjoyable and I definitely could not have gotten through it all without you guys.

1. Introduction

1.1 Interest in Gold(I)-Catalyzed Reactions

Gold(I) catalysis has been an expanding topic in the field of synthetic chemistry over the past two decades since the first reported gold(I)-catalyzed hydroalkoxylation reaction.[1] One of the most significant developments since the emergence of cationic gold(I) complexes as effective catalysts in homogeneous catalysis has been their use for the functionalization of C–C multiple bonds, prompting the synthetic application of gold(I) catalysis to develop at a rapid pace.[2-6]

The ability of gold(I) catalysts to perform distinct transformations stems from the properties of gold that other transition metals do not possess, which can, in part, be explained within the context of the innate large relativistic effect of gold.[7,8] Specifically, the maximized relativistic effect compared to other transition metals results in gold displaying distinguishing electronic structure and subsequent distinct reactivity.[9,10] The direct relativistic effect due to the large contraction of the 6*s*-orbital and the indirect relativistic effect due to the expansion of the 5*d*-oribital causes features in the Au-L such as: increased bond strength, linear bicoordinate geometry, enhanced Lewis acidity, low oxophilicity, and high electrophlicity.[11-16] Additionally, the cationic gold fragment, $[(L)Au]^+$, can act as a highly electrophilic soft Lewis acid resistant to oxidation

addition/reductive elimination reactions, allowing for gold(I) catalysts to be suitable for myriad reactions.[6,7,15,16]

Reactions utilizing gold(I) catalysts, such as cyclopropanations[29,40,50] and hydrofunctionalization of C-C multiple bonds[4-6], allow for development of the field interested in the investigation of such mechanisms and key intermediate. While the reactions themselves are worthy of investigation due to the ability of gold(I) catalysts to form complex molecular structures from simple starting materials, it is still important to understand the fundamentals of these transformations to aid in increased efficiency and applications in organic synthesis. Although computational efforts have been made to probe and predict the intermediates in gold(I)- catalyzed reactions,[59-64] efforts to experimentally generate and observe and hypothesized intermediate complexes have been limited.[23-28,37-46] Therefore, to better understand these reactions, herein is a study on the observation and characterization of proposed key intermediates evoked in gold(I)-catalyzed transformations.

1.2 Reported Gold(I) Carbene Complexes

Cationic gold carbene complexes have been invoked as intermediates in many significant gold(I)-catalyzed transformations.[17-22,29,35,141,142] Notable examples that propose to generate cationic gold(I) carbene intermediates include the cycloaddition of 1,*n*-

enynes, cyclopropene ring opening, and reactions with diazo compounds (Figure 1).[4,17-22,50,143]

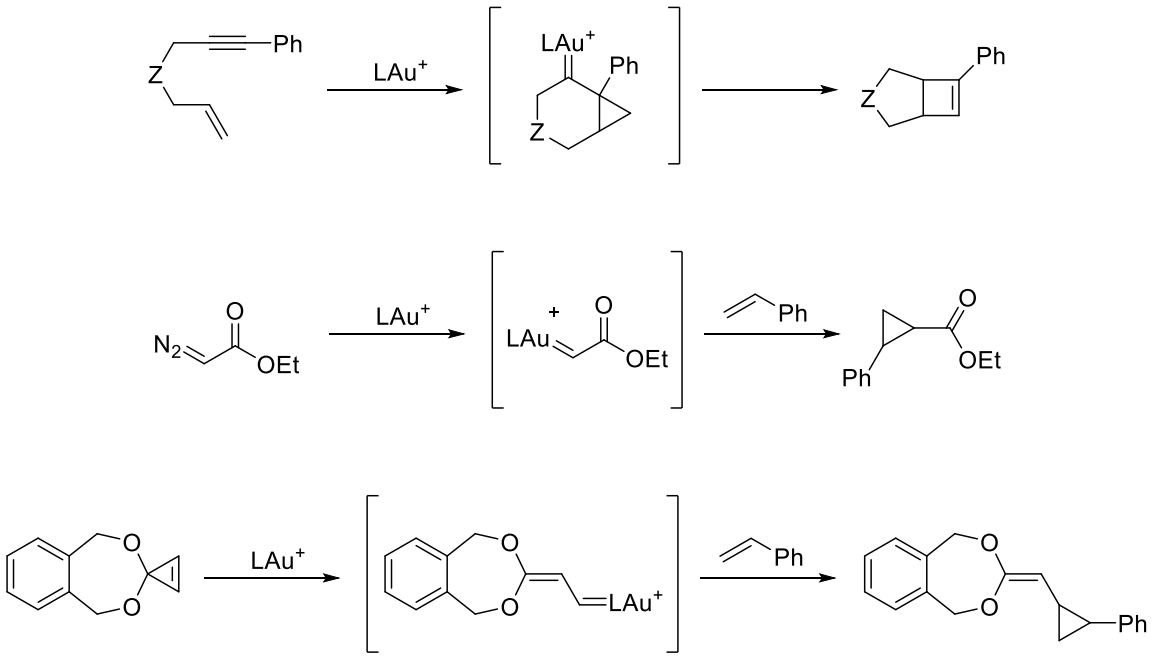

Figure 1. Examples of cationic gold(I) carbene intermediates generation in gold-catalyzed reactions.

Gold carbenes are often the hypothesized intermediate in cycloaddition and carbene transfer reactions, causing increased interest in the structure and reactivity of such species.[23] Despite this recent focus on cationic gold(I) carbenes, direct experimental evidence regarding gold carbene complexes remains limited, largely due to the absence of a well-defined, unstabilized gold carbene compound suitable for investigation.

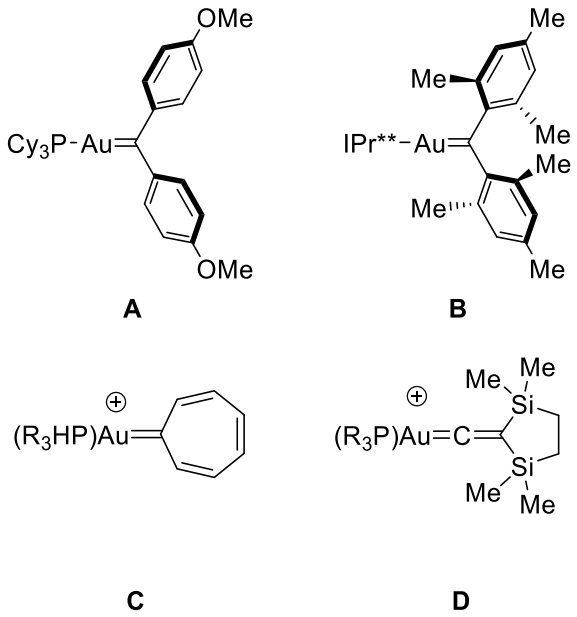

Figure 2. Four reported examples of gold carbene complexes.

The interest surrounding experimental evaluation of the fundamental bonding features of gold carbene complexes has been of focus in order to better understand the species' unique properties and improve their performance in a catalytic system. Early reported gold(I) carbene complexes are strongly stabilized by electron-donating heteroatom substituents, thus favoring the electronic structure toward a carbenium ion.[27,155-157] Thus far, four examples of Fischer gold carbene complexes have been characterized in the solid state (Figure 2).[23-28] However, each of these complexes relies on supporting stability factors such as resonance from 4-methoxy aromatic rings, hindered steric effect, or aromatic stabilization. Furthermore, of these examples, only the gold carbene complex isolated by Fürstner (**A**)[27] has been shown to undergo carbene transfer

to an alkene. The structural and spectroscopic information gleaned from the study of these complexes has provided insight into the nature of the gold to carbon electron donation.[26-28] However, there is still an absence of a gold(I) carbene complex suitable for carbene transfer study that is not reliant on heavily stabilizing substituents.

1.3 Gold(I) Carbene Transfer Reactions

Gold to alkene carbene transfer reactions and similar transformations have proven to be some of the more essential gold(I)-catalyzed reactions that evoke gold carbene intermediates.[29] In the vast reported literature on transition metal to alkene carbene transfer, three mechanisms prevail to apply to gold to alkene carbene transfer.[36,63,64,144-153] In these mechanisms involving nucleophilic attack on the α-carbon of the carbene, three intermediates/transition states are proposed, which could then collapse by (1) backside displacement of the gold-carbon bond on the γ-carbon, (2) frontside displacement of the gold-carbon bond on the γ-carbon, or (3) oxidative addition/reductive elimination via a metallacyclobutane intermediate (Scheme 1).

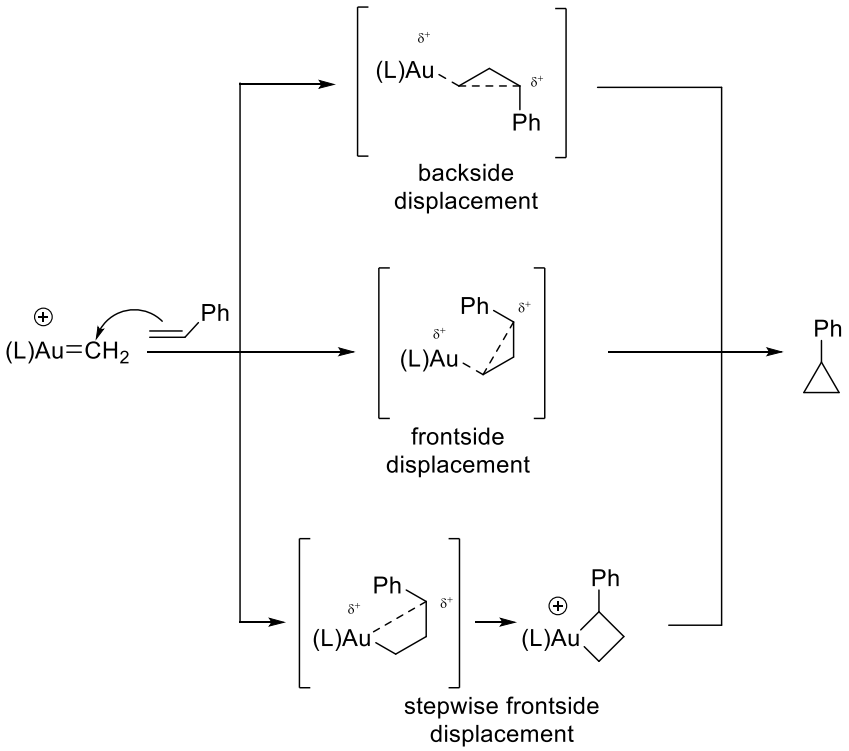

Scheme 1. Three proposed transition states with a full or partial positive charge on the γ-carbon.

However, due to the established unique characteristics of gold, such as poor *d* to *p* back bonding and the ability to form stable π-complexes,[30] it is expected that the mechanism of gold to alkene carbene transfer is different than similar reactions using other transition metals. Most knowledge of the gold(I)-catalyzed carbene transfer mechanism is drawn from experimental observations— e.g., stereochemistry or product ratios[29]—or from computational analysis.[29,31-34] With no direct observation of reaction intermediates, the experimental observations and computational analyses frequently offer differing opinions and conclusions, resulting in no proposed mechanism being

conclusively supported. Additionally, for some gold(I)-catalyzed reactions, alternative pathways have been proposed that do not invoke a gold carbene species at all.[35]

1.3.1 Reactive Gold Carbenoid Complexes

As opposed to a gold(I) carbene intermediate species in gold to alkene carbene transfers, it is hypothesized a gold(I) carbenoid complex is the key intermediate.[35,62] It is important to clarify definitions of carbene and carbenoid terminology used throughout this dissertation, as there are many inconsistencies in literature. Carbenes will be defined as divalent gold(I) complexes with a formal positive charge on the gold atom and a double bond between the gold and the adjacent α-carbon. Carbenoids will refer to complexes where the gold atom is bound to a formally uncharged sp^3-carbon atom, with an additional leaving group on the α-carbon (Figure 3, **E** and **F**).[35] Additionally, a carbenoid can also refer to a complex where the leaving group binds to the b-atom to form a conjugated g-leaving group (Figure 3, **G**)

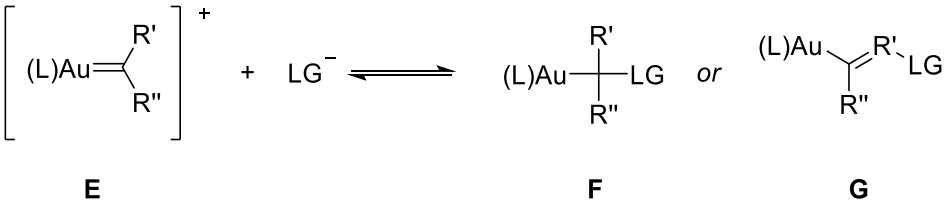

Figure 3. Depiction of a cationic gold(I) carbene (E) and cationic gold(I) carbenoid complexes (F and G). The rightmost structure depicts an example of a carbenoid with a conjugated γ-leaving group (G).

Notably, there is limited information available concerning kinetic and stereochemical analysis of the gold to alkene carbene transfer mechanism from a well-defined gold carbene or carbenoid complex intermediate to product under stoichiometric conditions. Such techniques have been proven to provide essential mechanistic insight for similar iron alkylidene complexes involved in carbene transfer reactions.[36] In order to study the transformation from intermediate to product, an appropriate gold carbene or carbenoid complex must be observed that is suitable for such mechanistic investigation.

Therefore, there is a need for a suitable gold carbenoid complex that could generate a reactive gold carbene complex reversibly in solution under mild conditions that would allow for kinetic analysis of gold to alkene carbene transfer from otherwise inaccessible gold carbene complexes. While many gold carbenoid complexes have been identified, none are suitable for the needed analysis for various reasons (Figure 4). Carbenoid **H** requires Lewis acid activation, carbenoid **I** requires forcing conditions for activation, and complex **J** involves irreversible carbene formation.[37-46] Each of these factors would mask the desired data surrounding the rate of carbene transfer in a kinetic analysis.

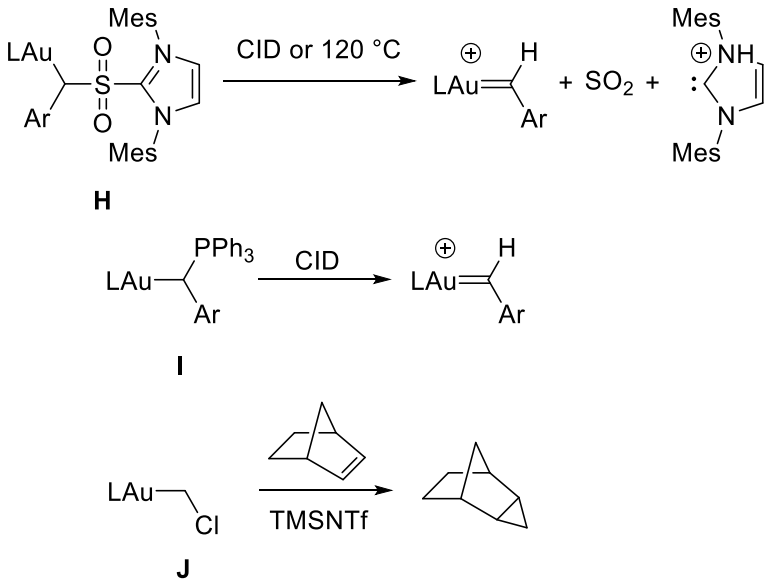

Figure 4. Examples of carbenoids not suitable for kinetic analysis.

1.3.2 Gold α-Oxo Carbene and Carbenoid Complexes

One prominent subset of cationic gold carbene complexes are α-oxo carbene complexes. Such species are often the hypothesized intermediate in gold(I)-catalyzed carbene transfer reaction of stabilized diazo compounds such as ethyldiazoacetate (EDA) with alkenes, alkynes, and arenes (Figure 5).[47-52] These compounds are also the proposed intermediate in gold-catalyzed oxidation of alkynes with aromatic and aliphatic amine *N*-oxides, sulfoxides, nitrones, epoxides, and nitro groups and subsequent carbene transfer (Scheme 2).[53-57]

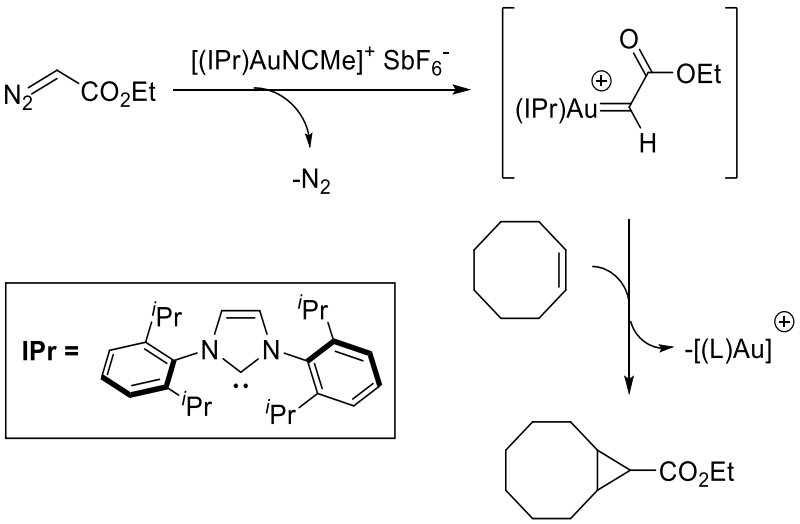

Figure 5. Example of gold-catalyzed cyclopropanation with EDA. The (IPr) (IPr = 1,3-bis(2,6-diisopropylphenyl)imidazol-2-ylidene) ligand is a commonly used (NHC) ligand in gold catalysis.

The reported literature of these reactions often hypothesizes an α-oxo gold carbene intermediate. However, there is no direct evidence for the existence of a free α-oxo gold carbene species. Rather, evidence suggests the key intermediate is an α-oxo gold carbenoid species. In similar computational studies of gold-catalyzed oxidation/carbene transfer reactions of alkynes with amine *N*-oxides, there is data disputing the formation of an α-oxo gold carbene. Instead, studies suggest carbene transfer reactivity to an *N*-alkenoxypyridinium complex (Scheme 2, **K**).[59-62] Complex **K** is then suggested to undergo rearrangement to form an α-oxo gold pyridinium carbenoid complex (**M**) without proceeding through an α-oxo gold carbene species (**L**).[59] Notably, similar mechanisms have been considered, but not confirmed, for comparable copper-

catalyzed reactions of EDA with alkenes.[63,64] Therefore, synthesis of compounds similar to complex **M** would be an ideal place to start probing such reactions.

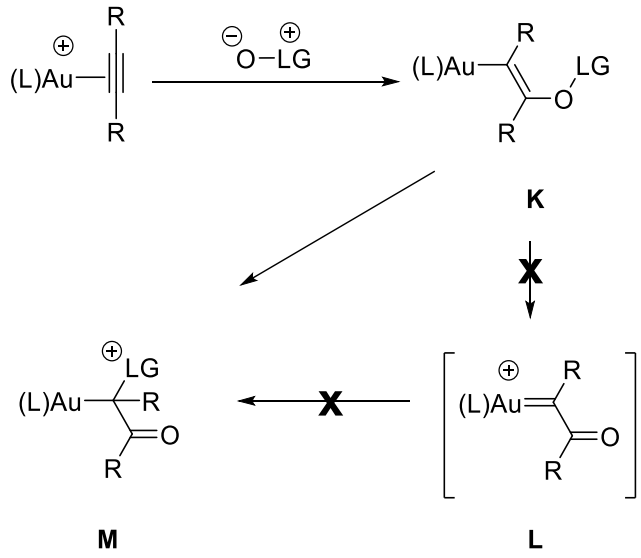

Scheme 2. Mechanism for the hypothesized direct converstion from an *N*-alkenoxypyridinium/sulfonium (K) complex to a gold α-oxo carbenoid complex (M).

1.4 Summary and Outlook

Even with increased interest in the structure and reactivity of gold(I)-catalyzed reactions, the knowledge of key intermediates is widely limited to computational studies. There are still significant gaps in the knowledge surrounding the structure and reactivity of cationic gold(I) carbene complexes despite recent research. Additionally, there is very little reported experimental data surrounding α-oxo carbene/carbenoid

complexes. Reported herein are a series of studies on the observation and characterization of gold α-oxo carbene species and/or gold α-oxo carbenoid species as the key intermediates proposed in various gold(I)-catalyzed reactions.

2. An Overview of α-Oxo Gold(I) Carbenes/Carbenoids in Gold-Catalyzed Transformations

2.1 Background

One of the key intermediates most often evoked in gold(I)-catalyzed carbene transfer reactions of stabilized diazo compounds[47-52] and in gold-catalyzed oxidation of alkynes[53-57] are α-oxo gold carbenes (**B**). These transformations are the two commonly utilized strategies in the generation of the α-oxo gold carbene species (Scheme 3).[56] Due to the hazardous and potentially explosive nature of diazo compounds, gold-catalyzed oxidation of an alkyne (Scheme 3, a) is often favored in the formation of these α-oxo gold carbenes. The carbonyl diazo compounds required in pathway (b) require small scale processes and highly energetic precursors, thereby further favoring pathway (a).

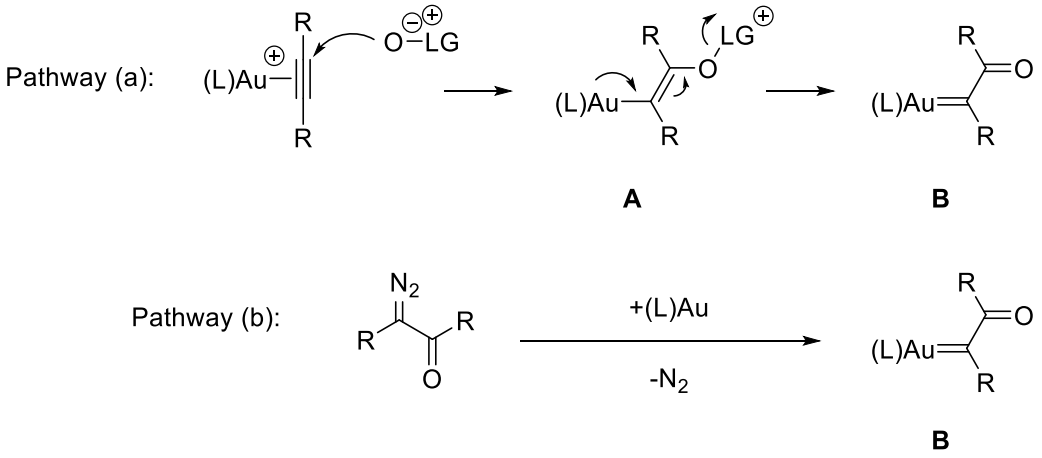

Scheme 3. Generation of α-oxo carbenes via (a) alkyne oxidation or (b) diazo carbonyl compounds.

While α-oxo gold carbenes are often proposed in these transformations, there is no direct evidence of these species, as they are unstable and often computationally bypassed in favor of lower energy pathways.[59,60,62] Instead, reported evidence suggests the pathway follows an α-oxo gold carbenoid complex as the active intermediate in these reactions, or direct conversion of *N*-alkenoxypyridinium/sulfonium species (**A**) to product.[62] However, there has been little to no reported experimental data regarding either α-oxo gold carbenoids or *N*-alkenoxypyridinium/sulfonium species and the role these species may play in gold(I)-catalyzed reactions. In this chapter, we report the existing research and evidence surrounding the involvement of α-oxo gold carbenoids versus α-oxo gold carbenes.

2.2 α-Oxo Carbenes from α-Diazocarbonyl Compounds

Many transition metals, such as Cu, Rh, and Ru, facilitate carbene transfer via decomposition of various diazo compounds.[68-74] Since 2005, gold has also been shown to decompose diazo compounds and perform cycloadditions, C-H/X-H insertions, and coupling reactions (Scheme 4).[48,49,50] In each featured reaction, an α-oxo gold carbene is evoked as the key intermediate. Recently, there have been mechanistic studies concerning the cyclopropanation and C-H insertion reaction between diazo compounds and styrenes.[58]

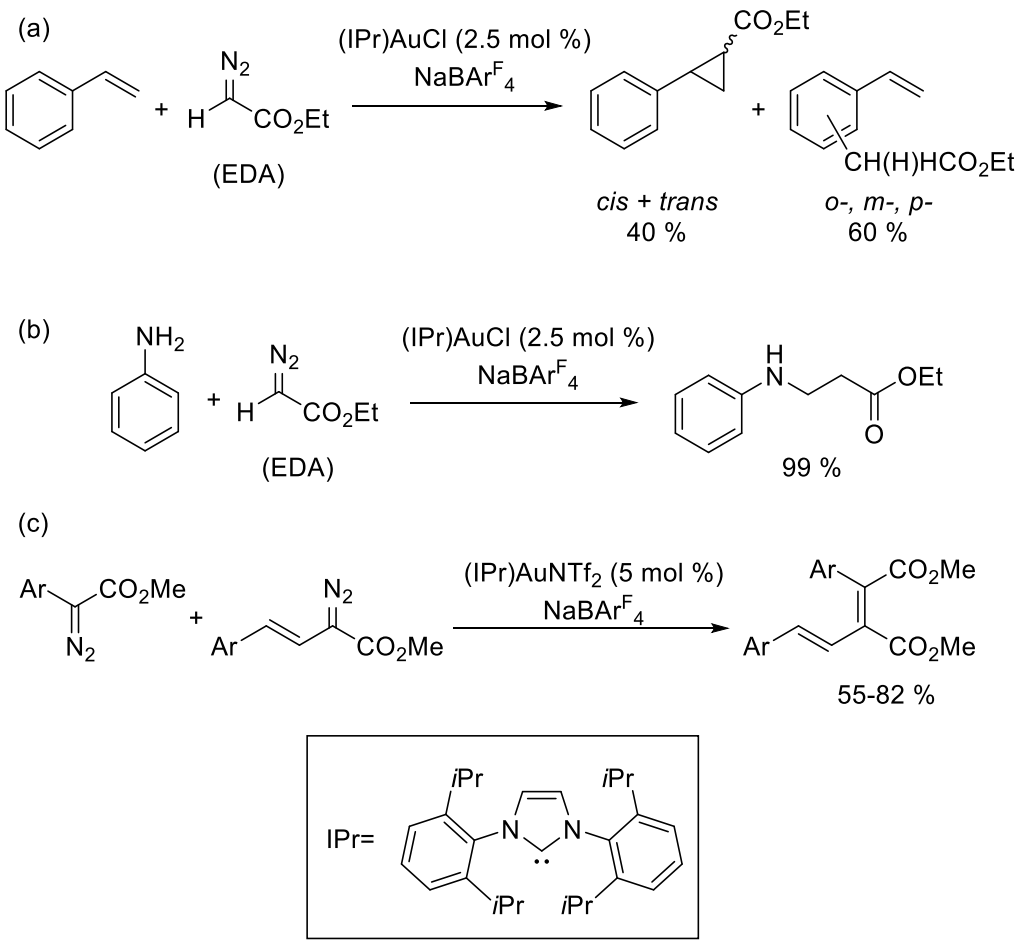

Scheme 4. Reported examples of gold-catalyzed carbene transfer reactions with proposed α-oxo carbene intermediates.

One of the most prominent gold-catalyzed carbene transfer reactions is the cyclopropanation reaction (Scheme 4a). Pérez and coworkers reported treatment of styrene with ethyl diazoacetate (EDA) to form cyclopropane and the C-H insertion product, hypothesizing the reaction progresses through a traditional metal-catalyzed carbene transfer reaction with an α-oxo gold carbene intermediate (Scheme 5).[58]

However, when the mechanism was further probed by the group, no α-oxo carbene was isolated or detected.[58]

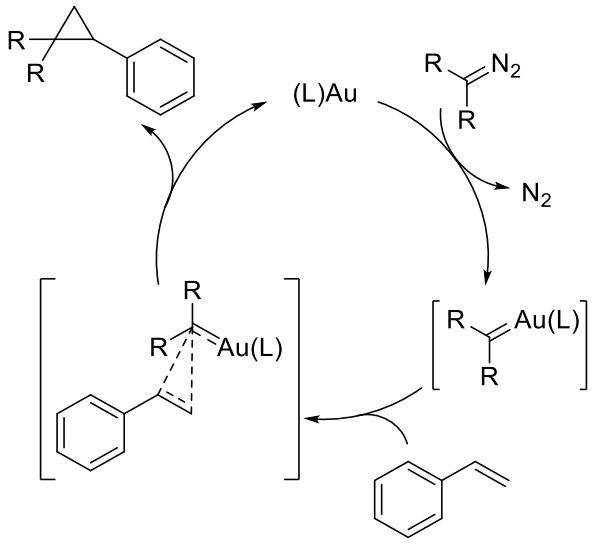

Scheme 5. Proposed mechanism for carbene transfer reaction from a diazo compound to styrene.

In 2015, Pérez and coworkers published kinetic studies probing their two proposed mechanisms for the transformations of styrene with EDA (Scheme 6).[58] By monitoring the amount of nitrogen evolved from the reaction and changing the substrate concentration, Pérez concluded that the observed data could only support the inner-sphere mechanism. When the substrate (i.e. styrene) concentration was increased, there was an observed increase in nitrogen production directly correlating with the substrate increase. Although the outer-sphere mechanism (Scheme 6, top) is the commonly hypothesized pathway, the experimental data directly contradicts the mechanism, as an increase in substrate should hinder the nitrogen production.

Therefore, the inner-sphere mechanism (Scheme 6, bottom) is the logical conclusion, as it was observed that an increase in substrate causes and increase in nitrogen evolution, which is in agreement with an inner-sphere mechanism.

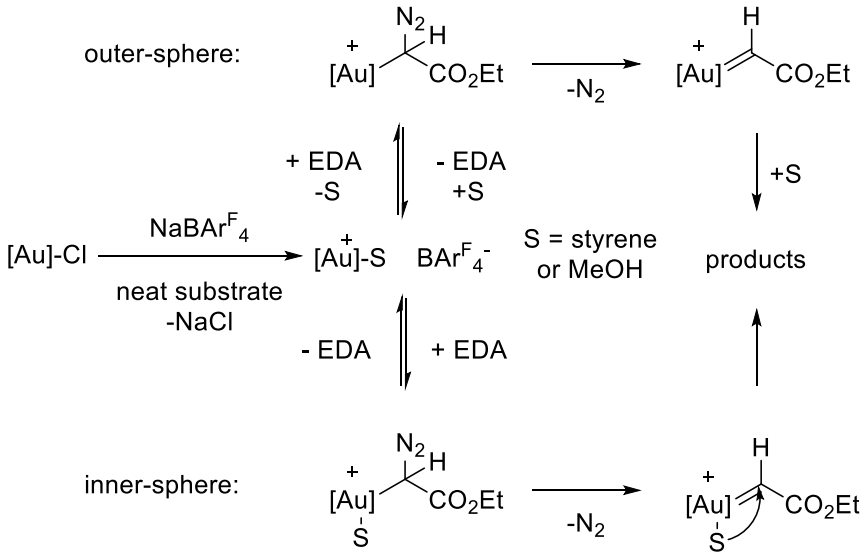

Scheme 6. Outer-sphere vs. inner-sphere mechanisms. $BArF_4^-$ counter ion removed for clarity.

Similarly, in 2017, Echavarren reported density-functional theory (DFT) calculations for the cyclopropanation of styrene with gold carbenoid complex, (L)$AuCH_2OTf$.[38] Their findings also supported a mechanism involving direct attack of the alkene on the methyl triflate complex without formation of a methylidene complex. Therefore, formation of an α-oxo carbene intermediate is neither supported by observational data nor calculations.

2.3 α-Oxo Carbenoids in Alkyne Oxidations

Rather than using dangerous diazo compounds, α-oxo carbenes/carbenoids are generated for study via the gold-catalyzed oxidation of alkynes with aromatic and aliphatic amine *N*-oxides, sulfoxides, nitrones, epoxides, and nitro groups, followed by carbene transfer (Scheme 7). Computational studies offer pathways that bypass an α-oxo carbene intermediate (**D**), and instead provide evidence for direct conversion of an *N*-alkenoxypyridinium complex (**C**) into an α-oxo carbenoid complex (**E**).[35,62] As there is little to no direct observational experimental evidence of the formation of species **C**-**E**, we must hypothesize key intermediates in the gold-catalyze oxidation of alkynes and subsequent carbene transfer reactions based off of computational studies, isotopic labeling experiments, and observed product formation to form our conclusions on the involvement of α-oxo carbenes/carbenoids.

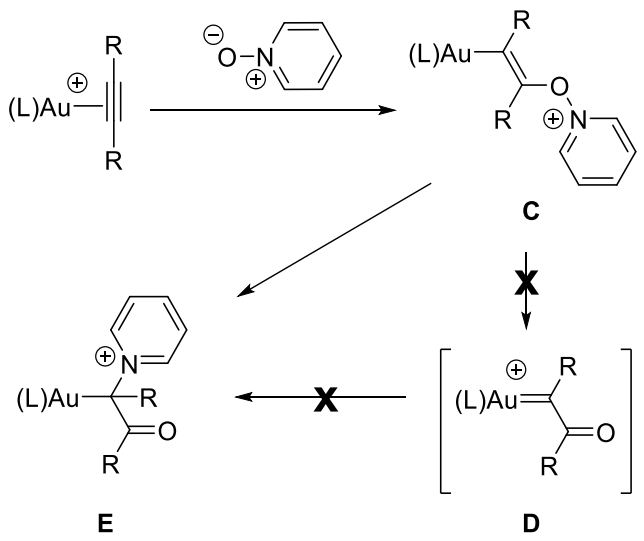

Scheme 7. Hypothesized pathway wherein the carbene (D) does not form. Instead, the *N*-alkenoxypyridinium species (C) converts directly to the carbenoid (E).

Gold-catalyzed alkyne oxidation has been implemented in both intramolecular and intermolecular transformations and utilizing various leaving groups (e.g. pyridine, sulfides).[60,62] In this text, we will examine both intermolecular and intramolecular transformations, but will limit the scope of oxidants to *N*-oxides and sulfoxides, which would form the *N*-alkenoxypyridinium/sulfonium species (Scheme 7, **C**).

2.3.1 Intermolecular Alkyne Oxidation

Roithová and coworkers studied the oxygen atom transfer reaction from pyridine *N*-oxide (PNO) to alkynes and subsequent carbene transfer by examining the reaction through mass spectrometry, infrared multiphoton dissociation spectroscopy (IRMPD), DFT, and isotopic labeling experiments.[62] In order to support the mechanism

wherein an *N*-alkenoxypyridinium complex (**C**) converts directly to and α -oxo carbenoid complex (**E**) (Scheme 7), a series of terminal alkynes, [(IPr)Au(CH_3CN)][BF_4], and pyridine *N*-oxide were subjected to collision-induced dissociation (CID) experiments. If an α-oxo carbene species were formed (**D**), it would be transferred to the gas-phase and observed by the probe. However, there was no conclusive data to support the formation of **D**.

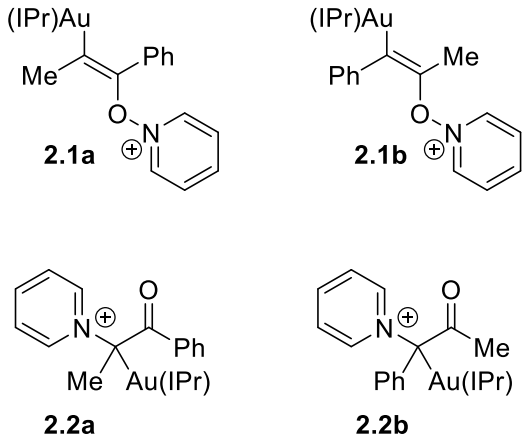

Figure 6. Isomers of potential intermediates formed in IRMPD experiments.

Using IRMPD, a signature spectrum of the intermediate formed when 1-phenylpropyne was treated with gold complex and PNO was compared to theoretical spectra of the possible intermediates formed (Figure 6). Based on the experimental IRMPD values observed, the theoretical intermediate that best fit the experimental data was the α-oxo carbenoid complex (**2.2a**). As the reaction progressed, additional experimental IRMPD spectra were obtained to see if **2.2a** would progress to an α-oxo

carbene. However, no experimental spectra matched the theoretical spectra for the corresponding α-oxo carbene. Alternatively, a mechanism was developed using DFT calculations which also supported the lowest energy pathway did not involve a carbene intermediate. Additionally, when deuterium labeled PNO-d_5 was added to an already mixed solution of gold complex, alkyne, and PNO, there was no integration of deuterium into the existing gold complex, thus indicating that the α-oxo carbenoid (Figure 6, **2.2a)** is directly formed from *N*-alkenoxypyridinium complex (**2.1a)**, rather than the release of pyridine to form an α-oxo carbene and recapture of pyridine. Altogether, these studies indicate the formation of a free α-oxo carbene species is highly unlikely.[62]

2.3.2 Intramolecular Alkyne Oxidation

2.3.2.1 Gold-Catalyzed Alkynyl Sulfoxide Rearrangement

In 2007, multiple teams reported the synthesis of tetrahydrobenzothiepinone from phenyl homopropargyl sulfoxide using gold catalysts (Scheme 8).[68-69] Two potential mechanisms came to fruition: 1) an *N*-alkenoxysulfonium species (**2.3**), the 5-*exo*-dig intermediate, is formed, followed by ring opening to form an α-oxo carbene (**2.4**), subsequently followed by attack of the aromatic ring to form the dihydrobenzothiepinone product (**2.5**) or 2) the *N*-alkenoxysulfonium species (**2.3**) can undergo a [3,3]-sigmatropic rearrangement to form the product (Scheme 8, dotted line).

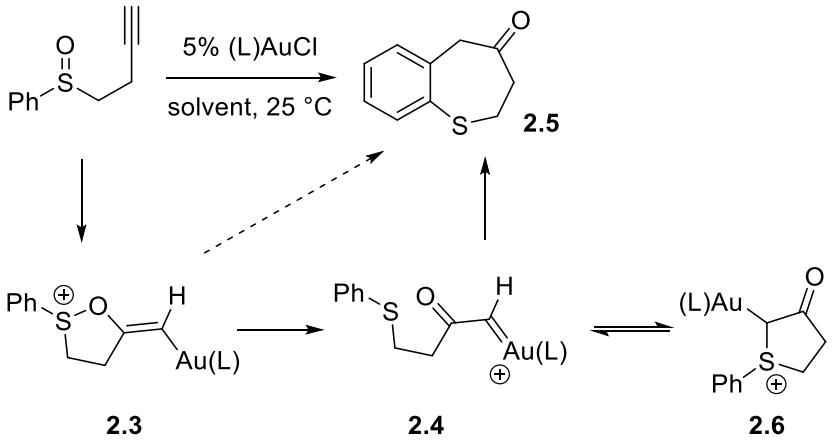

Scheme 8. Intramolecular alkyne oxidation mechanism. Instead of a carbene intermediate (2.4) forming, there is a hypothesized sigmatropic rearrangement pathway (dotted line).

Zhang and coworkers[60] initially hypothesize that the carbene (**2.4**) is unlikely to form, as observation of a sulfonium ion (Scheme 5, **2.6**) should hypothetically also form. However, **2.6** is not observed in these reactions. Furthermore, when **2.4** was attempted to be synthesized independently via treatment of an α-diazoketone with a gold catalyst, compound **2.4** was not observed, and the reaction yielded a carboxylic acid, as opposed to the expected product (**2.5**).[60] When DFT was applied, the lowest energy pathway did not favor the formation of a carbene, and instead supported the proposed [3,3]-sigmatropic rearrangement (Scheme 9).[60]

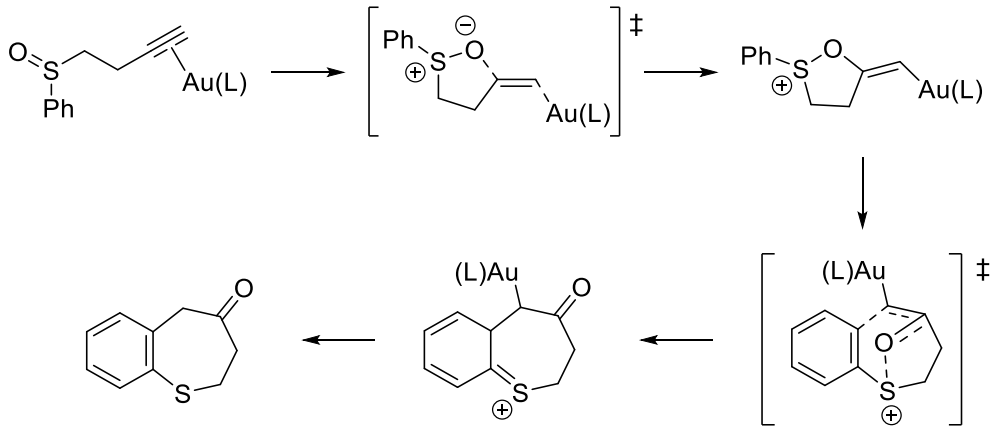

Scheme 9. Lowest energy pathway supported by DFT calculations favors a sigmatropic rearrangement without formation of an α-oxo carbene.

2.3.2.2 Gold-Catalyzed Alkynyl Amine-*N*-Oxide Rearrangement

Zhang and coworkers reported the gold-catalyzed synthesis of piperidin-4-ones and azepan-4-ones from acetylenic amine *N*-oxides,[77,78] presumably through an α-oxo carbene (Scheme 10). Computations of the activation barriers for the reaction, however, suggest that the formation of carbene intermediate **2.8** would form alternate products that are not observed. Alternatively, the energy pathway leading directly from **2.7** to **2.9** is more energetically favorable (Scheme 10, dotted line).[59]

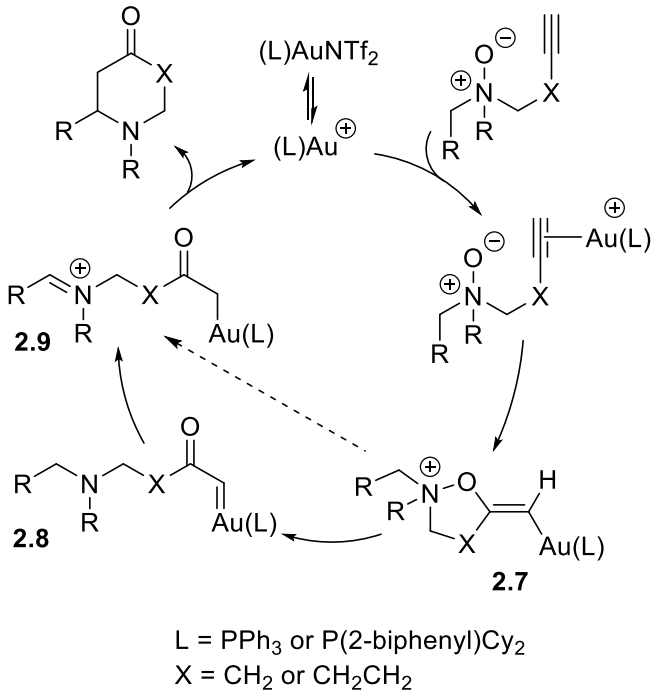

Scheme 10. Catalytic cycle of intramolecular alkyne oxidation with an acetylenic amine-*N*-oxide. Proposed pathway bypassing a carbene intermediate shown with a dotted line.

To further support the direct conversion from **2.7** to **2.9**, alkyne **2.10**-d_2 was synthesized and treated with an oxidant, followed by gold (Scheme 11, top).[59] The product mixture was obtained with little loss of deuterium labeling, despite excess m-CPBA present, suggesting the intramolecular pathway occurs without a distinct ring opening step. Lastly, observation of α-oxo carbene **2.12** was attempted via synthesis from diazo ketone **2.11** (Scheme 11, bottom). However, the predicted azepan-4-one product was not observed, once again indicating α-oxo gold carbene is not the active intermediate.

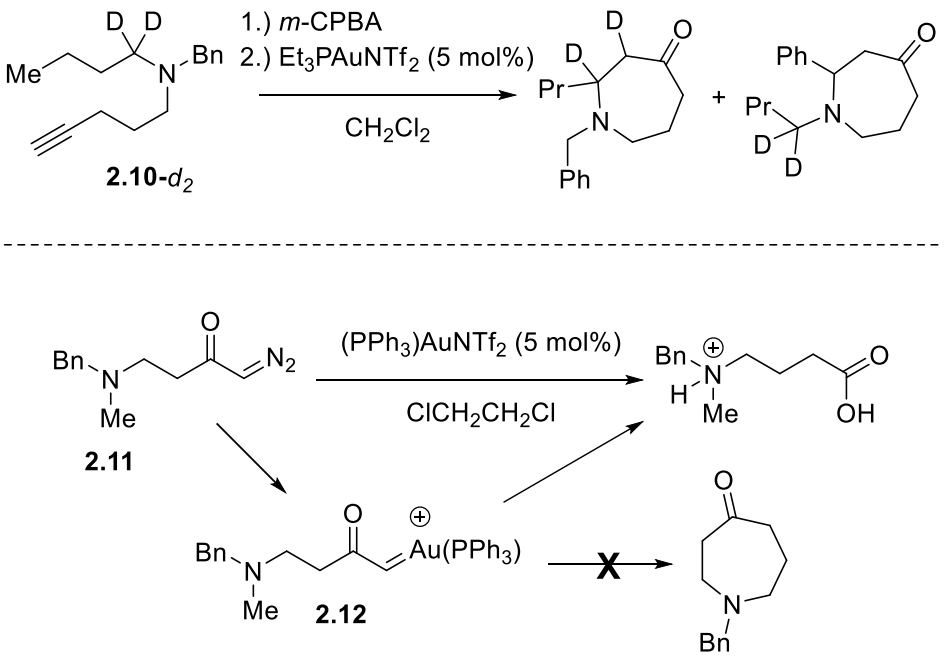

Scheme 11. Isotopic labeling experiment to form deuterium labeled products showing no detectable deuterium loss (top). Independent synthesis of carbene (2.12) resulted in the Wolff rearrangement product instead of proposed azepan-4-one product (bottom).

2.5 Summary

Despite the common hypothesized mechanistic pathway for gold-catalyzed oxygen atom transfers and carbene transfers from stabilized diazo compounds invoking an α-oxo gold carbene, there is no existing evidence to support these claims. An α-oxo carbene has yet to be experimentally observed, and when attempted to be independently synthesized, the obtained products do not agree with the hypothesized products. Furthermore, when applying DFT computations to these reactions, none of them agree with the hypothesized α-oxo carbene intermediate. Instead, the pathways of least energy

often directly convert from the *N*-alkenoxypyridinium/sulfonium complex to an α-oxo carbenoid species. These alternate intermediates are supported by gas-phase experiments, isotopic labeling experiments, and computational studies. As there is no computational or experimental evidence to support the mechanism wherein an a-oxo gold carbene forms, it is essential to learn more about N-alkenoxypyridinium/sulfonium species and α-oxo gold carbenoid complexes to determine what role they may play in these carbene transfer mechanisms.

3. Synthesis, Structure, and Reactivity of Gold(I) α-Oxo Carbenoid Complexes

Portions of this chapter have been published[79]:

C. P. Stow and R. A. Widenhoefer, *Organometallics.* **2020**, *39*, 1249-1257.

(DOI: 10.1021/acs.organomet.0c00033)

3.1 Background

Over the past decade, cationic gold(I) complexes have emerged as versatile catalysts for the functionalization of C− C multiple bonds. In addition to these π-activation processes, a diverse range of gold-catalyzed transformations have been developed that are thought to proceed via cationic two-coordinate gold carbene or carbenoid intermediates, [3,29,80-85] and considerable effort has been directed toward understanding the structure and reactivity of these complexes.[35,86] An important subset of these cationic intermediates are gold α-oxo carbene or carbenoid complexes generated via decomposition of α-diazo carbonyl compounds (Figure 7)[47-49] or, more conveniently, from the oxidation of alkynes with pyridinium *N*-oxides, sulfoxides, and related reagents.[53-57] These α-oxo carbene/carbenoid intermediates engage in a range of transformations, including alkene and alkyne cyclopropanation, carbene−carbene cross-coupling, C−H and X−H insertion, and cycloaddition.[47-49,53−57]

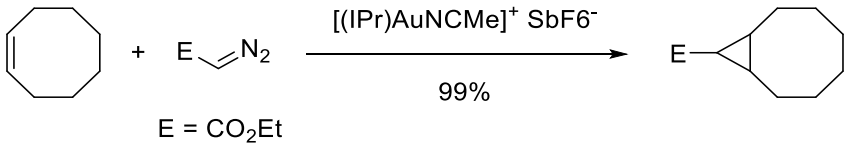

Figure 7. Decomposition of α–diazo carbonyl compounds into α–oxo carbene or carbenoid complexes.

Although the gold-catalyzed decomposition of α-diazo carbonyl compounds and the gold-catalyzed oxidation of alkynes are often assumed to proceed via discrete gold α-oxo carbene intermediates, there is no direct evidence for the existence of the free two-coordinate carbene complex,[87-89] and computational[59-61,90,91] and experimental[58,62,92] evidence suggests that an α-oxo carbenoid complex, rather than a free α-oxo carbene, might be the reactive species, at least under certain conditions. For example, Pérez showed that the rate of N_2 evolution in the cyclopropanation of styrene with ethyl diazoacetate catalyzed by a mixture of (IPr)AuCl and $NaBAr^{F_4}$ {BAr^{F_4} = B[3,5-$(CF_3)_2C_6H_3]_4$} displayed a linear dependence on [styrene],[58] which is inconsistent with rate-limiting N_2 dissociation from $[(IPr)AuC(H)(CO_2Et)(N_2)]^+$. Similarly, tandem mass spectrometry/ion spectroscopy analysis of the reactions of alkynes with pyridine *N*-oxide and $(IPr)Au^+$ suggested that the initially formed *N*-alkenoxypyridinium complex **A** undergoes intramolecular rearrangement to form the gold(I) pyridinium α-oxo carbenoid complex **B**, which can alternatively be viewed as a gold complex bearing a carbonyl-stabilized pyridinium ylide, without the intermediacy of the α-oxo carbene

complex **C** (Scheme 12).[62,92] These observations suggest the possible involvement of either **A** or **B** as the reactive species in the gold-catalyzed oxidation of alkynes with pyridine *N*-oxides.

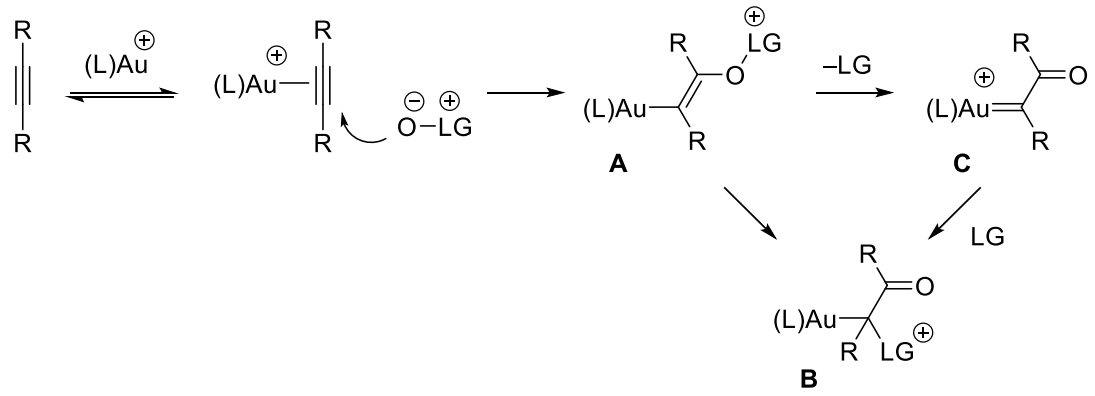

Scheme 12. Potential intermediates in the gold(I)-catalyzed oxidation of alkynes with pyridine *N*-oxides (O–LG).

Because of safety and practicality issues associated with employment of α-diazo carbonyl compounds on a large scale, there has been long-standing interest in the use of carbonyl-stabilized sulfonium ylide compounds as surrogates for α-diazo carbonyl compounds in transition-metal-catalyzed transformations.[93-95] Included in this body of work are gold-catalyzed cycloaddition,[96,97] cyclopropanation,[65-67,98,99] and N–H activation[100] processes employing carbonyl-stabilized sulfonium ylides. Both inner-sphere and outer-sphere pathways have been proposed for these transformations, which may likewise involve gold α-oxo carbene or carbenoid intermediates.[65-67,96-100] In any event, the potentially strong ligating abilities of stabilized sulfonium ylides suggest the

potential involvement of gold sulfonium ylide complexes as on-cycle or off-cycle intermediates in these transformations.

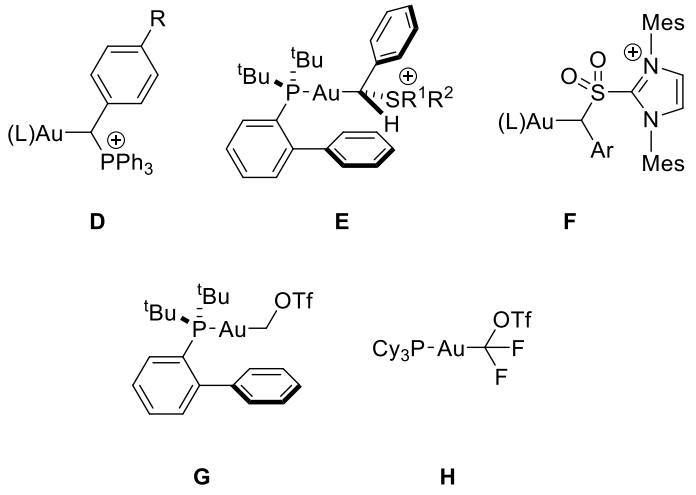

Figure 8. Reactive gold carbenoid complexes.

The observations outlined in the preceding paragraphs raise questions regarding the potential involvement of gold α-oxo carbenoid complexes in a number of gold-catalyzed transformations. Indeed, a handful of gold carbenoid complexes have recently been shown to function as gold carbene precursors or surrogates.[33,34,37-41,101-104] Chen showed that gold phosphonium benzylide complexes **D** generate reactive gold benzylidene complexes in the gas phase,[33,34,39,109] and we recently showed that sulfonium benzylide complexes **E** generate gold benzylidene complexes in solution under mild conditions (Figure 8).[103] Chen similarly showed that the gold SO_2- imidazolium complex **F** generates reactive gold arylidene complexes in solution.[37,41] Echavarren and Fürstner independently reported thermally unstable (trifluoromethanesulfonyloxy)methyl

carbenoid complex **G** and (trifluoromethanesulfonyloxy)-difluoromethyl carbenoid complex **H**, respectively, which undergo gold to alkene carbene transfer at or below room temperature.[38,104] Additionally, it has been reported that gold chloromethyl carbenoid complexes and related complexes undergo gold to alkene carbene transfer at elevated temperatures.[105-107] In comparison with gold benzyl and methyl carbenoid complexes, the structures and reactivity of gold α-oxo carbenoid complexes remain largely unexplored, and therefore, the potential for these complexes to serve as precursors or surrogates to gold α-oxo carbene complexes has not been evaluated. Although gold α-oxo carbenoid complexes bearing an α-phosphonium group are known,[43,108-112] the structures and reactivity of these complexes have not been extensively explored, nor is it likely that these compounds display significant reactivity in view of the high stability of the phosphonium ylide ligand.[113] Therefore, to gain insight into the potential role of gold α-oxo carbenoid complexes in gold(I) catalysis, we have investigated the synthesis, structure, and reactivity of gold α-oxo carbenoid complexes bearing a pyridinium, sulfonium, or trifluoromethanesulfonate group.

3.2 Synthesis of Gold(I) α-Oxo Carbenoid Complexes

3.2.1 Gold α-Trifluoromethanesulfonyl α-Oxo Carbenoid Complexes

As an entry point to the synthesis of gold α-oxo carbenoid complexes, we targeted the synthesis of gold trifluoromethanesulfonate α-oxo carbenoid complexes via

reaction of (IPr)Au(OTf) with α-diazo carbonyl compounds, which was modeled after Echavarren's synthesis of gold halomethyl carbenoid complexes.[38] To this end, treatment of (IPr)Au(OTf) with ethyl diazoacetate in CH_2Cl_2 at room temperature for 30 min followed by crystallization from CH_2Cl_2/pentane led to the isolation of the gold α-trifluoromethanesulfonate ester enolate complex (IPr)AuCH(OTf)CO_2Et (**3.1a**) in 70% yield. In a similar manner, the gold α-trifluoromethanesulfonate ketone enolate complex (IPr)AuCH(OTf)C(O)(4-MeC_6H_4) (**3.1b**) was isolated in 57% yield from the reaction of (IPr)Au(OTf) with *p*-methyl-2-diazoacetophenone (Figure 9). In contrast to the

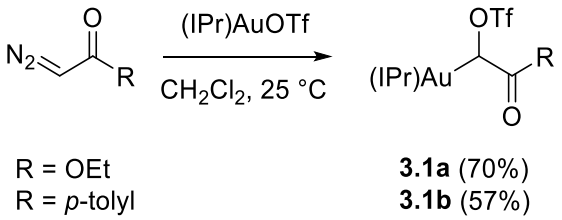

Figure 9. Reaction of α-diazo carbonyl compounds with gold to form complexes 3.1a and 3.1b.

(trifluoromethanesulfonyloxy)methyl carbenoid complexes **G** and **H**, complexes **3.1** were stable for hours in solution at room temperature and were characterized in solution by NMR spectroscopy and mass spectrometry. For example, the ^{1}H NMR spectra of complexes **3.1** displayed a diagnostic one-proton singlet at δ 5.27 (**3.1a**) and 6.31 (**3.1b**) assigned to the carbenoid proton, and the ^{13}C NMR spectra displayed a resonance at δ 96.2 (**3.1a**) and 104.0 (**3.1b**) assigned to the carbenoid carbon atom. The IR

spectra of complexes **3.1** displayed a strong C=O stretching band at 1723 (**3.1a**) and 1669 (**3.1b**) cm^{-1}, which established the presence of a carbon-bound enolate ligand.

3.2.2 Gold Pyridinium and Sulfonium α-Oxo Carbenoid Complexes

3.2.2.1 Synthesis and Isolation of Gold Pyridinium and Sulfonium α-Oxo Carbenoid Complexes

The α-trifluoromethanesulfonate enolate complexes **3.1a** ad **3.1b** reacted cleanly with 4-picoline within 30 min at room temperature to form the pyridinium α-oxo carbenoid complexes $[(IPr)AuCH(4\text{-}MeC_5H_4N)CO_2Et]^+ OTf^-$ (**3.2a**) and $[(IPr)AuCH(4\text{-}MeC_5H_4N)C(O)(4\text{-}MeC_6H_4)]^+ OTf^-$ (**3.2b**), which were isolated in 55–61% yield as colorless crystals from CH_2Cl_2/pentane (Scheme 3.2). In a similar manner, complexes **3.1a** and **3.1b** reacted with dimethyl sulfide at room temperature over 18 h to form the dimethyl sulfonium α-oxo carbenoid complexes $[(IPr)AuCH(SMe_2)CO_2Et]^+ OTf^-$ (**3.3a**) and $[(IPr)AuCH(SMe_2)C(O)(4\text{-}MeC_6H_4)]^+ OTf^-$ (**3.3b**), respectively, which were isolated as colorless crystals in 42–48% yield (Scheme 13).

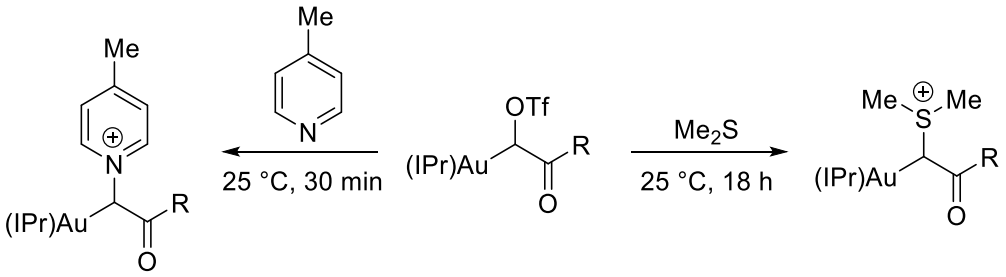

3.2a (55%)
3.2b (61%)

3.1a (R = OEt)
3.1b (R = *p*-tolyl)

3.3a (48%)
3.3b (42%)

Scheme 13. Reactions of 4-picoline and dimethyl sulfide with complexes 1.

3.2.2.2 Gold Pyridinium α-Oxo Carbenoid Kinetics

To probe the mechanism of the nucleophilic displacement of the trifluoromethanesulfonate group in the conversion of complexes **3.1** to complexes **3.2** and **3.3**, we analyzed the kinetics of the conversion of **3.1a** to **3.2a**. To this end, an equimolar mixture of **3.1a** (4.0 mM) and 4-picoline (4.1 mM) in $CD2Cl_2$ at 25 °C was monitored periodically by ^1H NMR spectroscopy.

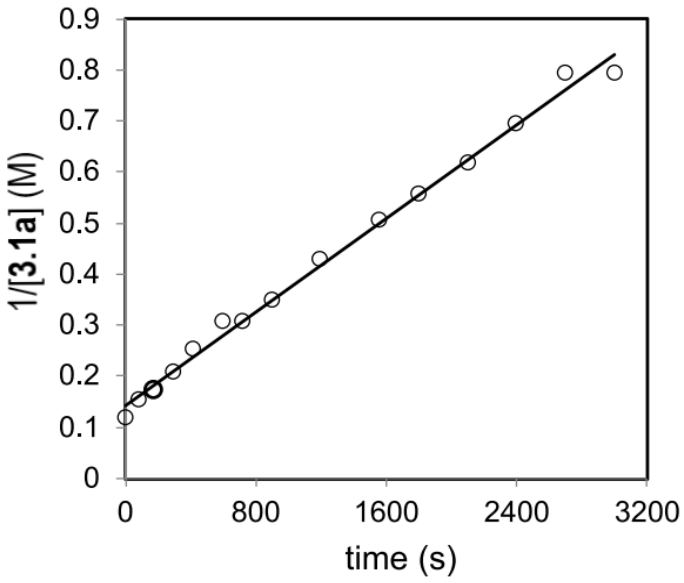

Figure 10. Second-order plot for the reaction of 1a (4.0 mM) with 4-picoline (4.1 mM) in CD_2Cl_2 at 25 °C.

A plot of 1/[**3.1a**] versus time was linear for more than three half-lives with a second-order rate constant of k = 2.30 ± 0.05 $M^{-1}s^{-1}$ (Figure 10). The second-order behavior is consistent with a bimolecular pathway for the conversion of **3.1a** and 4-picoline to **3.2a**,

presumably via direct S_N2 displacement of the trifluoromethanesulfonate group by 4-picoline.

3.2.2.3 Gold Diphenylsulfonium α-Oxo Carbenoid Synthesis

The attempted synthesis of the diphenylsulfonium α-oxo carbenoid complex $[(IPr)AuCH(SPh_2)(CO_2Et)]^+ OTf^-$ (**3.4a**) via reaction of trifluoromethanesulfonate carbenoid complex **3.1a** with diphenyl sulfide proved to be unsuccessful, presumably because of the lower nucleophilicity of diphenyl sulfide relative to 4-picoline or dimethyl sulfide. Rather, complex **3.4a** was isolated as colorless crystals in 85% yield from the direct reaction of the sulfonium ylide Ph_2SCHCO_2Et with (IPr)Au(OTf) at room

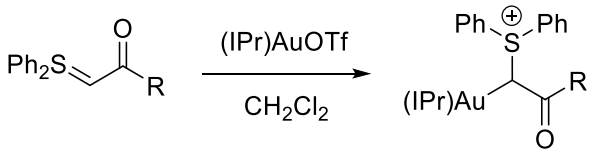

R = OEt — **3.4a** (48%)
R = *p*-tolyl — **3.4b** (42%)

Figure 11. Reaction of sulfur ylide with gold to form complexes 3.4.

temperature for 15 min (Figure 11). In a similar manner, the corresponding diphenylsulfonium phenacyl complex $[(IPr)AuCH(SPh_2)C(O)(4\text{-}MeC_6H_4)]^+ OTf^-$ (**3.4b**) was isolated as a white solid in 48% yield from the reaction of $Ph_2SCHCO(4\text{-}MeC_6H_4)$ with (IPr)Au(OTf) at 0 °C (Figure 3.5).

3.2.2.4 Characterization and Structures of Gold Pyridinium and Sulfonium α-Oxo Carbenoid Complexes

The pyridinium carbenoid complexes **3.2** and the sulfonium carbenoid complexes **3.3** and **3.4** were thermally stable and were characterized in solution and, in the cases of **3.2** and **3.3**, in the solid state. In the ^{1}H NMR spectra of complexes **3.2–3.4**, as was the case with trifluoromethanesulfonate complexes **3.1**, particularly diagnostic was the carbenoid proton resonance in the ^{1}H NMR spectrum, which ranged from δ 3.41 (**3.3a**) to 6.10 (**3.2b**), and the carbenoid carbon resonance in the ^{13}C NMR spectra, which ranged from δ 61.1 (**3.3a**) to δ 84.2 (**3.2b**). Similarly, the presence of the stereogenic carbenoid carbon atom in complexes **3.2**–**3.4** was established by the presence of four sets of doublets in the range δ 1.25−0.80 corresponding to the diastereotopic IPr methyl groups.

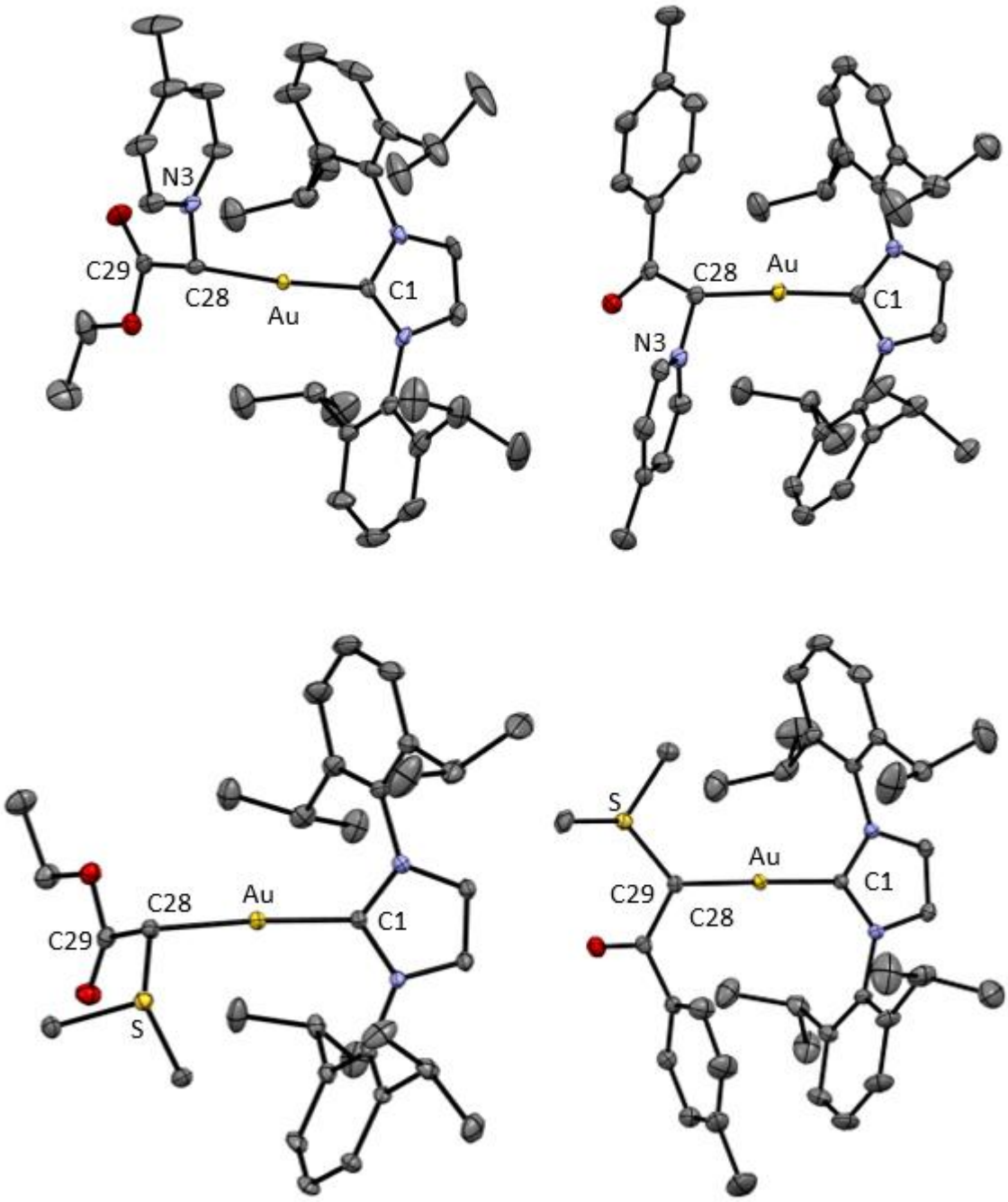

Figure 12. ORTEP diagrams of 3.2a (upper left), 3.2b (upper right), 3.3a (lower left) and 3.3b (lower right).

The molecular structures of gold α-oxo carbenoid complexes **3.2a**, **3.2b**, **3.3a**, and **3.3b**. were determined by single-crystal X-ray diffraction (Figure 12 and Table 1). In the solid state, the gold atom of these carbenoid complexes adopts a linear conformation with C−Au−C angles in the range of 174.5− 179°. The gold−carbenoid bond (Au−C28) is 0.065−0.084 Å longer than is the gold−IPr (Au−C1) bond, with the ketone complexes **3.2b** and **3.3b** having a nominally larger difference in the Au−C1/Au−C28 bond distances than the corresponding ester complexes **3.2a** and **3.3a**. The carbenoid ligand of complexes **3.2** and **3.3** is oriented with a syn-periplanar arrangement of the heteroatom group and the carbonyl oxygen atom, with O−C− C−X (X = N, S) dihedral angles ranging from 11.7° for **3.3b** to 27.4° for **3.3a**. The gold-bound carbon atom of the carbenoid ligand of complexes **3.2** and **3.3** adopts a distorted sp^3 geometry with two smaller angles (106−108°) and one larger angle (111−116°), with the ester derivatives **3.2a** and **3.3a** displaying the largest deviations between the large and small angles. For complexes **3.2a**, **3.2b**, and **3.3b**, the Au−C28−S/N3 angle is the larger one, whereas in the case of **3.3a**, the C29−C28−S angle is the larger one.

Table 1. Selected bond lengths (Å), bond angles (deg), and dihedral angles (deg) for complexes 3.2a, 3.2b, 3.3a, and 3.3b.

	3.2a	**3.2b**	**3.3a**	**3.3b**
Au–C1	2.016(5)	2.013(3)	2.012(3)	2.005(1)
Au–C28	2.081(5)	2.087(3)	2.088(4)	2.084(1)
C28–S/N3	1.491(8)	1.484(4)	1.782(4)	1.785(1)
C28–C29	1.501(9)	1.491(4)	1.492(5)	1.486(2)

C1–Au–C28	174.4(2)	176.9(1)	175.4(1)	179.01(5)
Au–C28–S/N3	115.3(4)	112.6(2)	108.7(2)	111.27(6)
Au–C28–C29	106.5(4)	104.7(2)	106.5(2)	106.15(8)
S/N3–C28–C29	105.9(4)	110.0(2)	114.9(3)	107.95(9)
S/N3–C28–C30–O1	20.5(9)	14.6(4)	27.4(5)	11.7(2)

3.2.3 α,α-Dioxo Carbenoid Complexes

We also sought to synthesize pyridinium and sulfonium α,α-dioxo carbenoid complexes, which could be compared to α-oxo carbenoid complexes **3.2–3.4** with regard to stability and/or reactivity. To this end, treatment of (IPr)Au(OTf) with 4-picolinium bis(methoxycarbonyl)methylide in CH_2Cl_2 at room temperature led to the isolation of $[(IPr)AuC(4\text{-}MeC_5H_4N)(CO_2Me)_2]^+ OTf^-$ (**3.**5) in 70% yield (Figure 13). Similarly, reaction of (IPr)Au(OTf) with diphenylsulfoxonium bis(methoxycarbonyl)methylide led to the

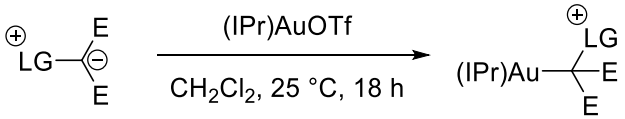

E = CO_2Me, LG = 4-picoline — **3.5** (70%)
E = CO_2Me, LG = SPh_2 — **3.6** (39%)

Figure 13. Treatment of dis-(methoxycarbonyl)methylide complexes with gold to form complexes 3.5 and 3.6.

isolation of $[(IPr)AuC(SPh_2)(CO_2Me)_2]^+ OTf^-$ (**3.6**) in 39% yield. The formation of complexes **3.5** and **3.6** was established by the ~0.3 ppm upfield shift of the methoxy resonances of complexes **3.5** and **3.6** relative to the free methylide.

3.3 Reactivity of Gold(I) α-Oxo Carbenoid Complexes

3.3.1 Reactions of Carbenoid complexes with Neutral Two-Electron Donors

As noted above, the trifluoromethanesulfonate group of complexes **3.1** was readily displaced by 4-picoline or dimethyl sulfide to form pyridinium and sulfonium α-oxo carbenoid complexes **3.2** and **3.3** (Figure 9). In contrast, complexes **3.2** and **3.3** displayed no reactivity toward 4-picoline or dimethyl sulfide. For example, treatment of pyridinium α-oxo carbenoid complex **3.2b** with excess dimethyl sulfide in DCE-d_4 at 75 °C for 9 hours led neither to C–N bond cleavage to form sulfonium complex **3.3b** nor to Au–C bond cleavage to form the free pyridinium ylide (4-MeC_5H_4N)CHCO(4-MeC_6H_4) and (IPr)AuSMe$_2$ (Scheme 14). Similarly, heating a solution of sulfonium α-oxo carbenoid complex **3.3b** with excess 4-picoline led to no detectable C–S or Au–C bond cleavage. Complex **3.3b** likewise failed to react with the pyridinium ylide (4-MeC_5H_4N)CHCO(4-MeC_6H_4) at 75 °C.

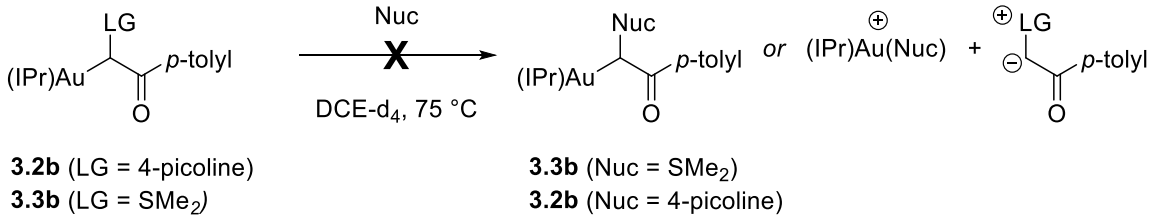

Scheme 14. Stability of complexes 3.2 and 3.3 toward nucleophiles.

In contrast to the α-oxo carbenoid complexes **3.2** and **3.3**, the α,α-dioxo carbenoid complex **3.5** underwent facile ligand displacement with 4-picoline and dimethyl sulfide. For example, treatment of **3.5** with excess 4-picoline at room temperature resulted in immediate (≤ 5 min) displacement of 4-picolinium bis(methoxycarbonyl)methylide to form the gold picoline complex $[(IPr)Au(4\text{-}MeC_5H_4N)]^+$ OTf^- [114] and the free methylide (Scheme 15). Similarly, treatment of **3.5** with excess dimethyl sulfide led to the immediate formation of the gold sulfide complex $[(IPr)Au(SMe_2)]^+$ OTf^- and the free methylide (Scheme 15).

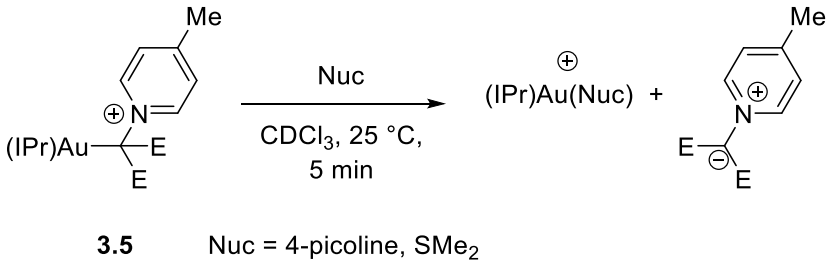

3.5 Nuc = 4-picoline, SMe_2

Scheme 15. Displacement of methylide from complex 3.5.

3.3.2 Reactions of α-Oxo Carenoid Complexes with C–C Multiple Bonds

Skrydstrup[96] and Maulide[97] described the gold(I)-catalyzed annulation of terminal alkynes with stabilized sulfonium ylides to form furans, which was proposed to occur via outer-sphere addition of ylide on a gold π-alkyne complex, presumably formed in competitive equilibrium with the σ-sulfonium ylide complex. To evaluate whether sulfonium or pyridinium α-oxo carbenoid complexes were viable intermediates

in furan formation, we investigated the reactions of α-oxo carbenoid complexes **3.2b, 3.3a,** and **3.3b** with terminal alkynes in DCE-d_4 at 75 °C. However, as shown in Scheme 16, various combinations of leaving group (LG), carbonyl substituent (R^1), and alkyne substituent (R^2) led to no detectable consumption of the carbenoid complex and no detectable formation of the furan.

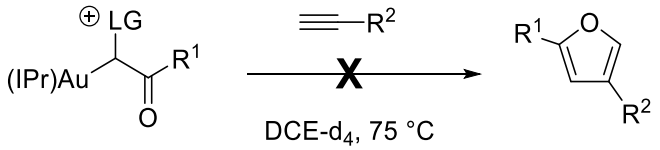

LG	complex	R^1	R^2
SMe_2	**3.3b**	*p*-tolyl	*n*-hexyl
SMe_2	**3.3b**	*p*-tolyl	*t*-butyl
SMe_2	**3.3b**	*p*-tolyl	*p*-tolyl
SMe_2	**3.3a**	OEt	*n*-hexyl
4-picoline	**3.2b**	*p*-tolyl	*n*-hexyl

Scheme 16: Attempted reactions of α-oxo carbenoid complexes 3.2 and 3.3 with terminal alkynes.

We likewise evaluated the potential of the gold carbenoid complexes to engage in gold to alkene carbene transfer. Treatment of pyridinium α-oxo carbenoid complex **3.2a** or the diphenylsulfonium analogue **3.4a** with excess 4-methoxystyrene in either CD_3CN at 70 °C or toluene-d_8 at 95 °C led to no detectable consumption of the carbenoid

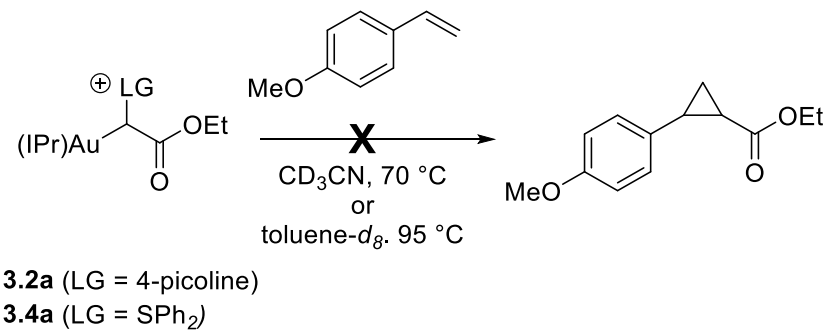

Figure 14. Attempted reaction to form cyclopropanes by treating complexes 3.2a and 3.4a with 4-methoxystyrene.

complex or formation of the cyclopropane after 9 h (Figure 14). In comparison, heating a suspension of trifluoromethanesulfonate α-oxo carbenoid complex **3.1b** in neat cyclohexene at 75 °C for 18 h led to complete consumption of **3.1b** to form the bicyclo[4.1.0]- heptane derivative **3.7** in 33% yield (^{1}H NMR) and (IPr)Au(OTf), which precipitated from solution (Figure 15).[115] In an effort to increase the efficiency of gold to

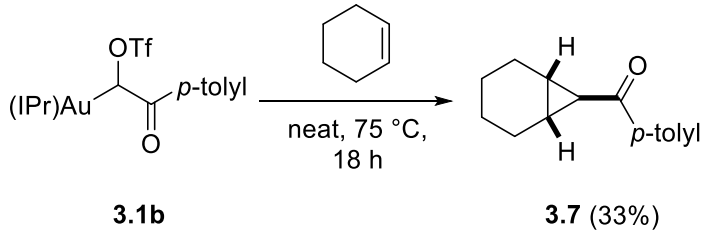

Figure 15. Cyclopropanation by treating cyclohexene with 3.1b to yield 3.7.

carbene alkene transfer from **3.1b**, we likewise investigated the Lewis acid-promoted ionization of **3.1b** in cyclohexene. However, slowly warming a solution of **3.1b** and $SbCl_5$ in cyclohexene from −78 °C to room temperature over the course of 4 hours led to

complete consumption of **3.1b** to form (IPr)AuCl without detectable formation of **3.7** or 1,4-di-*p*-tolylbut-2-ene-1,4-dione.[115]

3.3.3 Reactivity Interpretation

The studies described above provide some insights into the potential roles of α-oxo carbenoid complexes in gold-catalyzed transformations. First, the stabilities of the pyridinium and sulfonium α-oxo carbenoid complexes with respect to ligand displacement and the absence of gold to alkene carbene transfer behavior argue strongly against the participation of these complexes in the gold-catalyzed reactions of alkynes with pyridine *N*-oxides, sulfoxides, and related reagents.[53-57] However, these results do not rule out gold *N*-alkenoxypyridinium complexes (**A** in Scheme 12) and their variants as the reactive species generated in gold-catalyzed alkyne oxidation reactions. Here it should be noted that Bourissou characterized a three-coordinate gold α-oxo carbene complex and established this species as a viable intermediate in the carbene transfer reactions of α-diazo carbonyl reactions catalyzed by three-coordinate gold bis(phosphine) complexes.[87] Likewise, Hofmann validated a three-coordinate copper α-oxo carbene complex in the analogous copper-catalyzed process.[88,89] However, because three-coordinate gold and copper carbene complexes are significantly more stable than are cationic two-coordinate gold carbene complexes,[30,35,86,116,117] the relevance of these observations to the behavior of cationic two-coordinate gold complexes is not clear.

The gold trifluoromethanesulfonate α-oxo carbene complexes **3.1** are significantly more stable than the (trifluoromethanesulfonyloxy)methyl carbenoid complexes **G** and **H** reported by Echavarren[38] and Fürstner,[104] respectively. Nevertheless, the slow gold to alkene carbene transfer from complex **3.1b** to cyclohexene is in line with the observations of Echavarren and Fürstner, who showed that complexes **G** and **H** engage readily in gold to alkene carbene transfer.[38,104] Importantly, density functional theory calculations and kinetic analysis of gold to alkene carbene transfer from the (trifluoromethanesulfonyloxy)methyl carbenoid complexes supported a mechanism involving direct displacement of the trifluoromethanesulfonate group by the alkene without formation of the free gold methylidene complex.[38]

The results described herein also provide some insight into the mechanisms of the gold-catalyzed cycloaddition and cyclopropanation of alkenes and alkynes with stabilized sulfonium ylides.[65-67,96-99] For example, Maulide reported a range of gold-catalyzed cycloaddition and cyclopropanation processes employing sulfonium ylides derived from malonates and β-keto esters.[65-67,97-99] Computational analysis of these transformations supports pathways involving outer-sphere addition of the sulfonium ylide on a gold π-alkene, π-alkyne, or π-allene complex as opposed to inner-sphere pathways involving α-oxo carbene intermediates or sulfonium α-oxo carbenoid intermediates.[65-67,97-99] In comparison, Skrydstrup described the gold(I)-catalyzed

annulation of terminal alkynes with ketonestabilized sulfonium ylides to form furans, which was proposed to occur via outer-sphere addition of the ylide on a gold π-alkyne to form sulfonium intermediate I followed by expulsion of sulfide and subsequent attack of the ketone oxygen atom on the carbon atom α to gold in the resulting vinylogous oxo carbene intermediate II (Scheme 17).[96]

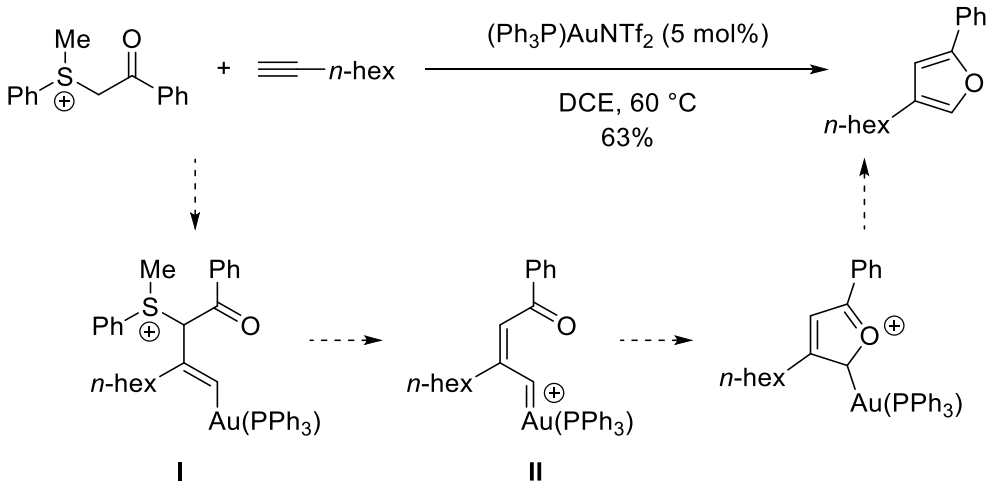

Scheme 17. Proposed mechanism for the gold-catalyzed annulation of stabilized sulfonium ylide with 1-octyne.[96]

Our observations inform on the feasibility of the mechanism depicted in Scheme 17. First, the resistance of sulfonium α-oxo carbenoid complexes **3.3** and **3.4** to loss of sulfide either spontaneously or via nucleophilic displacement argues against the formation of the vinylogous oxo carbene intermediate II and points to the direct attack of the ketone oxygen atom on the C1 atom of intermediate I, as was proposed by Maulide.[97] Second, the proposed outer-sphere mechanism requires the formation of a π-

alkyne complex in the presence of the sulfonium ylide. However, the failure of 4-picoline, which is a much stronger ligand for gold than is the alkyne,[114,118] to displace the sulfonium ylide from the sulfonium α-oxo carbenoid complex **3.3a** and the failure of **3.3a** to react with 1-octyne causes us to question the feasibility of alkyne complexation in the presence of a ketone-stabilized sulfonium ylide. In comparison, the transformations reported by Maulide employ sulfonium ylides derived from malonates and β-keto esters.[65-67,97-99] Here, the facile displacement of the pyridinium ylide ligand from pyridinium α-oxo carbenoid complex **3.5** (Scheme 15) supports the feasibility of alkyne, alkene, or allene complexation to gold in the presence of a sulfonium ylide derived from a malonate or β-keto ester.

3.4 Summary

We have synthesized several families of gold α-oxo carbenoid complexes, including trifluoromethanesulfonate (**3.1**), pyridinium (**3.2**), and sulfonium (**3.3**, **3.4**) α-oxo carbenoid complexes and α,α-dioxo carbenoid complexes (**3.5** and **3.6**), all of which are stable at room temperature in solution and in the solid state. The stability of these α-oxo carbenoid complexes with respect to displacement of the ylide ligand or the leaving group attached to the carbenoid carbon varied significantly. For example, the triflate group of the gold trifluoromethanesulfonate α-oxo carbenoid complexes **3.1** was readily displaced in an S_N2 process by 4-picoline or dimethyl sulfide, whereas the methylide

ligand of the α,α-dioxo carbenoid complex **3.5** was readily displaced by these same neutral two-electron donors. In contrast, the gold pyridinium and sulfonium α-oxo carbenoid complexes **3.2**–**3.4** displayed no reactivity toward neutral two-electron donors.

The gold trifluoromethanesulfonate α-oxo carbene complex **3.1b** underwent gold to alkene carbene transfer to cyclohexene at 75 °C, albeit slowly and in modest yield, whereas the gold sulfonium and pyridinium α-oxo carbenoid complexes displayed no reactivity toward terminal alkynes or *p*-methoxystyrene. An intriguing but as yet unresolved question raised by these studies relates to the reactive intermediate generated in the gold-catalyzed oxidation of alkenes with pyridine *N*-oxides, sulfoxides, and related reagents.[53-57] The stability of gold pyridinium α-oxo carbenoid complexes **3.2** argues strongly against the participation of these compounds and their variants in gold-catalyzed alkyne oxidation processes. Similarly, the mass spectrometry studies of Roithová argued against the involvement of the free gold α-oxo carbene complex in these transformations.[62,92] These observations suggest the involvement of an *N*-alkenoxypyridinium complex as the reactive intermediate in these transformations, as was likewise suggested by Gagosz,[61] but this hypothesis remains to be experimentally verified.

3.5 Experimental Details

3.5.1 General Methods

Reactions were run under a nitrogen atmosphere in flame-dried glassware using standard glovebox and Schlenk techniques. NMR spectra were obtained on a 400 MHz Varian Inova spectrometer and a 500 MHz Bruker spectrometer. ^{13}C NMR spectra were referenced to residual $CDCl_3$ (δ 77.2) or CH_2Cl_2 (δ 53.8). The ^{1}H NMR spectra were referenced to residual $CDCl_3$ (δ 7.26) or CH_2Cl_2 (δ 5.32). Infrared (IR) spectra were obtained on a Nicolet 380 FT-IR spectrometer at 25 °C. Diethyl ether, CH_2Cl_2, and tetrahydrofuran were purified by passage through columns of activated alumina under nitrogen. Silver-free (IPr)Au(OTf) was synthesized employing published procedures.[119,120] *p*-Methyl-2-diazoacetophenone,[121] Ph_2SCHCO_2Et,[122,123] $Ph_2SCHC(O)(4\text{-}MeC_6H_4)$,[122,123] diphenylsulfonium bis(methoxycarbonyl)methylide,[99] and 4-picolinium bis(methoxycarbonyl)methylide[124] were synthesized employing known procedures. All of the other reagents were obtained through major chemical suppliers and used as received.

3.5.2 Gold α-Oxo Carbenoid Complexes

(IPr)AuCH(OTf)CO_2Et (**3.1a**). Ethyl diazoacetate (8.6 μL, 8.2×10^{-2} mmol) was added dropwise to a solution of (IPr)Au(OTf) (60 mg, 8.2×10^{-2} mmol) in CH_2Cl_2 (5 mL) under nitrogen at 25 °C, and the resulting solution was stirred for 30 min and then

concentrated under vacuum. Vapor diffusion of pentane into a concentrated CH_2Cl_2 solution at 4 °C formed white crystals that were rinsed with hexanes and dried under vacuum to give **3.1a** (47 mg, 70%). ^{1}H NMR (400 MHz, CD_2Cl_2): δ 7.53 (t, *J* = 7.8 Hz, 2H), 7.32 (d, *J* = 7.8 Hz, 4H), 7.22 (d, *J* = 0.9 Hz, 2H), 5.27 (s, 1H), 3.87 (dq, *J* = 10.7, 7.1 Hz, 1H), 3.78 (dq, *J* = 10.7, 7.2 Hz, 1H), 2.54 (sept, *J* = 6.8 Hz, 2H), 2.51 (sept, *J* = 6.8 Hz, 2H), 1.29 (d, *J* = 6.9 Hz, 12H), 1.22 (d, *J* = 6.9 Hz, 12H), 0.97 (t, *J* = 7.1 Hz, 3H). ^{13}C{^{1}H} NMR (126 MHz, CD_2Cl_2): δ 188.2, 174.3, 145.8, 133.9, 130.5, 124.0, 123.4, 96.2, 59.6, 28.7, 24.1, 24.1, 23.6, 14.0. ^{19}F NMR (376 MHz, CD_2Cl_2): δ −76.57. IR (CH_2Cl_2): 1723 cm^{-1} (ν C=O). HRMS (ESI) calcd (found) for $C_{32}H_{42}AuN_2O_5S$ (MH^+): 764.3485 (764.3496).

(IPr)AuCH(OTf)C(O)(4-MeC_6H_4) (**3.1b**). A solution of p-methyl-2-diazoacetophenone (33.5 mg, 0.209 mmol) in benzene (2 mL) was added dropwise to a solution of (IPr)Au(OTf) (102.5 mg, 0.139 mmol) in benzene (2 mL), and the resulting solution was stirred for 30 min at room temperature, during which time nitrogen evolution was observed and (IPr)Au(OTf) dissolved to afford a homogeneous solution. The solution was then cooled at −20 °C until frozen and then thawed, forming a white precipitate. The solution phase was decanted, and the precipitate was rinsed with hexanes and dried under vacuum to give **3.1b** (23 mg, 57%) as a white solid. ^{1}H NMR (400 MHz, CD_2Cl_2): δ 7.50 (t, *J* = 7.8 Hz, 2H), 7.39–7.34 (m, 4H), 7.30− 7.26 (m, 4H), 7.25–7.20 (m, 4H), 7.19 (s, 2H), 6.94 (d, *J* = 8.1 Hz, 2H), 6.31 (s, 1H), 2.46 (sept, *J* = 6.8 Hz,

2H), 2.45 (sept, *J* = 6.8 Hz, 2H), 2.37 (s, 3H), 1.21 (d, *J* = 6.9 Hz, 6H), 1.19 (d, *J* = 6.9 Hz, 6H), 1.17 (d, *J* = 6.9 Hz, 6H), 1.11 (d, *J* = 6.9 Hz, 6H). $^{13}C\{^{1}H\}$ NMR (126 MHz, CD_2Cl_2): δ 194.8, 188.3, 146.0, 142.1, 134.2, 133.3, 130.8, 129.2, 128.7, 127.3, 124.4, 124.4, 123.8, 104.5, 29.1, 29.1, 24.4, 24.2, 24.1, 21.6. ^{19}F NMR (376 MHz, CD_2Cl_2): δ −76.70. IR (CD_2Cl_2): 1669 cm−1 (ν C=O). HRMS (ESI) calcd (found) for $C_{37}H_{44}AuN_2O_4S$ (M^+): 867.2712 (867.2708).

[(IPr)AuCH(4-MeC_5H_4N)CO_2Et]$^+OTf^-$ (**3.2a**). 4-Picoline (11.3 μL, 0.116 mmol) was added dropwise to a solution of **3.1a** (80 mg, 9.7 × 10^{-2} mmol) in CH_2Cl_2 (3 mL) at 25 °C, and the resulting solution was stirred for 30 min and then concentrated under vacuum. The resulting residue was crystallized via vapor diffusion of pentane into a concentrated CH_2Cl_2 solution at −20 °C to give **3.2a** (12 mg, 55%) as white crystals. ^{1}H NMR (500 MHz, CD_2Cl_2): δ 7.84 (d, *J* = 6.2 Hz, 2H), 7.62 (t, *J* = 7.8 Hz, 2H), 7.45 (d, *J* = 6.2 Hz, 2H), 7.39 (d, *J* = 7.7 Hz, 2H), 7.35 (d, *J* = 7.8 Hz, 2H), 7.32 (s, 2H), 4.96 (s, 1H), 3.96 (dq, *J* = 10.8, 7.1 Hz, 1H), 3.80 (dq, *J* = 10.7, 7.1 Hz, 1H), 2.60 (s, 3H), 2.53 (sept, 6.8 Hz, 1H), 2.51 (sept, 6.8 Hz, 1H), 2.49 (sept, 6.8 Hz, 1H), 2.46 (sept, 6.8 Hz, 1H), 1.27 (d, *J* = 6.8 Hz, 6H), 1.25 (d, *J* = 6.8 Hz, 6H), 1.23 (d, *J* = 6.8 Hz, 6H), 1.15 (d, *J* = 6.8 Hz, 6H), 1.05 (t, *J* = 7.1 Hz, 3H). $^{13}C\{^{1}H\}$ NMR (126 MHz, CD_2Cl_2): δ 173.5, 157.7, 146.4, 145.4, 134.3, 131.2, 127.7, 124.8, 124.3, 77.0, 61.3, 29.2, 24.8, 24.1, 22.0, 14.3. HRMS (ESI) calcd (found) for $C_{37}H_{49}AuN_3O_2$ (M^+): 764.3485 (764.3496).

[(IPr)AuCH(4-MeC$_5$H$_4$N)C(O)(4-MeC$_6$H$_4$)]$^+$OTf$^-$ (**3.2b**). 4-Picoline (3.4 mg, 3.7 × 10^{-2} mmol) was added dropwise via syringe to a solution of **3.1b** (27 mg, 3.2 × 10^{-2} mmol) in benzene (2 mL), and the mixture was stirred at room temperature for 1 h to form a yellow solution. The reaction mixture was cooled at −20 °C to form a precipitate as the benzene froze. The frozen mixture was then warmed to room temperature to form a suspension. The solution phase was decanted from the precipitate, which was rinsed with hexanes and dried under vacuum. The precipitate was then dissolved in diethyl ether containing one drop of CH_2Cl_2, and the solution was cooled to −20 °C to form thin crystals. The solution was decanted from the crystals, which were washed with hexanes and dried under vacuum to give **3.2b** (18 mg, 61%) as thin white crystals. Slow liquid/liquid diffusion of hexanes into a concentrated CH_2Cl_2 solution gave crystals of **3.2b** suitable for X-ray diffraction. ^{1}H NMR (400 MHz, CD_2Cl_2): δ 7.87 (d, *J* = 6.3 Hz, 2H), 7.60 (t, *J* = 7.8 Hz, 2H), 7.50 (d, *J* = 8.0 Hz, 2H), 7.44 (d, *J* = 6.3 Hz, 2H), 7.38 (d, *J* = 7.8 Hz, 2H), 7.28 (d, *J* = 0.9 Hz, 2H), 7.22–7.18 (m, 2H), 6.99 (d, *J* = 8.0 Hz, 2H), 6.10 (s, 1H), 2.62 (s, 3H), 2.45 (sept, 6.8 Hz, 1H), 2.42 (sept, 6.8 Hz, 1H), 2.40 (s, 3H), 2.37 (sept, 6.8 Hz, 1H), 2.33 (sept, 6.8 Hz, 1H), 1.23 (d, *J* = 6.9 Hz, 6H), 1.21 (d, *J* = 6.9 Hz, 6H), 1.14 (d, *J* = 6.9 Hz, 6H), 0.81 (d, *J* = 6.9 Hz, 6H). ^{13}C{^{1}H} NMR (126 MHz, CD_2Cl_2): δ 191.7, 185.6, 157.0, 145.9, 145.8, 145.2, 143.2, 133.8, 132.1, 130.6, 129.2, 127.2, 127.0, 124.2, 124.2, 123.7, 84.2, 28.8,

28.6, 24.2, 23.8, 23.7, 23.6, 21.6, 21.3. HRMS (ESI) calcd (found) for $C_{42}H_{51}AuN_3O$ (M^+): 810.3692 (810.3696).

[(IPr)AuCH(SMe_2)CO_2Et]+OTf− (**3.3a**). Dimethyl sulfide (7.6 μL, 1.0 × 10−2 mmol) was added via syringe to a solution of **3.1a** (30 mg, 3.5×10^{-2} mmol) in CH_2Cl_2 (3 mL) at room temperature. The resulting solution was stirred for 18 h and then concentrated under vacuum. The resulting white solid was recrystallized from toluene at room temperature to give **3.3a** (16 mg, 48%) as colorless crystals. ^{1}H NMR (400 MHz, CD_2Cl_2): δ 7.56 (t, *J* = 7.8 Hz, 2H), 7.36 (d, *J* = 1.5 Hz, 2H), 7.34 (d, *J* = 1.5 Hz, 2H), 7.31 (s, 2H), 3.89 (dq, *J* = 10.7, 7.1 Hz, 2H), 3.84 (dq, *J* = 10.8, 7.1 Hz, 1H), 3.41 (s, 1H), 2.51 (sept, *J* = 7.0 Hz, 2H), 2.47 (sept, *J* = 7.0 Hz, 2H), 2.43 (s, 3H), 2.27 (s, 3H), 1.28 (d, *J* = 6.9 Hz, 6H), 1.27 (d, *J* = 6.9 Hz, 6H), 1.24 (d, *J* = 6.9 Hz, 12H), 0.99 (s, 3H). ^{13}C{^{1}H} NMR (126 MHz, CD_2Cl_2): δ 185.0, 170.6, 145.9, 133.7, 131.0, 124.3, 123.9, 61.1, 49.2, 28.8, 28.8, 28.5, 27.2, 24.4, 24.3, 23.7, 23.7, 13.9. HRMS (ESI) calcd (found) for $C_{33}H_{48}AuN_2O_2S$ (MH^+): 733.3097 (733.3102).

[(IPr)AuCH(SMe_2)C(O)(4-MeC_6H_4)]$^+$$OTf^-$ (**3.3b**). Dimethyl sulfide (10 μL, 1.4 × 10^{-2} mmol) was added via syringe to a solution of **3.1b** (40 mg, 4.6×10^{-2} mmol) in benzene (3 mL) at room temperature. The resulting solution was stirred for 18 h at room temperature and then cooled to −20 °C, forming a precipitate as the benzene froze. The frozen mixture was warmed to room temperature, and the thawed benzene solution was decanted from the precipitate, which was rinsed with hexanes and dried under vacuum.

The resulting solid residue was dissolved in diethyl ether containing one drop of CH_2Cl_2 and cooled to −20 °C to give **3.3b** (18 mg, 42%) as a white solid. ^{1}H NMR (400 MHz, CD_2Cl_2): δ 7.59 (t, *J* = 7.8 Hz, 2H), 7.48−7.42 (m, 4H), 7.38 (d, *J* = 7.9 Hz, 4H), 7.28 (s, 2H), 7.15 (d, *J* = 7.8 Hz, 2H), 6.96 (d, *J* = 7.8 Hz, 2H), 4.80 (s, 1H), 2.52 (s, 3H), 2.50 (sept, *J* = 6.9 Hz, 1H), 2.47 (sept, *J* = 6.9 Hz, 1H), 2.43 (sept, *J* = 6.9 Hz, 1H), 2.39 (sept, *J* = 6.9 Hz, 1H), 2.41 (s, 3H), 2.20 (s, 3H) 1.26 (d, *J* = 6.9 Hz, 6H), 1.21 (d, *J* = 6.9 Hz, 6H), 1.16 (d, *J* = 6.9 Hz, 6H), 1.05 (d, *J* = 6.9 Hz, 6H). ^{13}C{^{1}H} NMR (126 MHz, CD_2Cl_2): δ 193.3, 185.3, 145.7, 145.7, 143.4, 133.6, 132.8, 130.8, 129.1, 128.3, 127.4, 124.1, 124.1, 123.7, 61.6, 31.6, 28.8, 28.7, 28.3, 26.7, 24.3, 24.0, 23.7, 22.7, 21.4, 13.9. HRMS (ESI) calcd (found) for $C_{38}H_{50}AuN_2OS$ (MH^+): 779.3304 (779.3304).

[(IPr)AuCH(SPh_2)CO_2Et]$^+$$OTf^-$ (**3.4a**). A solution of (IPr)Au(OTf) (32 mg, 4.3×10^{-2} mmol) and Ph_2SCHCO_2Et (35 mg, 0.129 mmol) in CH_2Cl_2 (3 mL) was stirred at room temperature for 15 min. The resulting solution was concentrated under vacuum and layered with hexanes at room temperature to give **3.4a** (37 mg, 85%) as colorless crystals. ^{1}H NMR (500 MHz, CD_2Cl_2): δ 7.59−7.52 (m, 4H), 7.48 (d, *J* = 4.8 Hz, 4H), 7.35 (t, *J* = 7.8 Hz, 2H), 7.31−7.27 (m, 6H), 7.25 (s, 2H), 4.36 (s, 1H), 3.81 (dq, *J* = 10.1, 7.3 Hz, 1H), 3.61 (dq, *J* = 10.1, 7.3 Hz, 1H), 2.42 (sept, 4H), 1.19 (t, *J* = 7.8 Hz, 3H), 1.15 (d, *J* = 6.9 Hz, 6H), 0.94 (t, *J* = 7.2 Hz, 3H).^{13}C{^{1}H} NMR (126 MHz, CD_2Cl_2): δ 183.8, 168.7, 145.7, 145.7, 133.5, 133.4, 133.4, 131.5, 131.1, 130.9, 130.8, 129.1, 128.3, 127.6, 124.2, 124.1, 124.0, 61.5, 50.7,

28.7, 24.4, 24.3, 23.6, 23.5, 13.7. HRMS (ESI) calcd (found) for $C_{43}H_{52}AuN_2O_2S$ (M^+): 857.3410 (857.3417).

[(IPr)AuCH(SPh$_2$)C(O)(4-MeC$_6$H$_4$)]$^+$OTf$^-$ (**3.4b**). A solution of (IPr)Au(OTf) (25 mg, 3.4×10^{-2} mmol) and Ph$_2$SCHC(O)(4-MeC$_6$H$_4$) (11 mg, 3.4×10^{-2} mmol) in CH_2Cl_2 (2 mL) was stirred at 0 °C for 18 h. The resulting solution was concentrated under vacuum and layered with hexanes at −20 °C to give **3.4b** (18 mg, 49%) as a white solid. ^{1}H NMR (500 MHz, $CDCl_3$): δ 7.64 (dd, *J* = 7.9, 1.9 Hz, 2H), 7.59 (d, *J* = 8.1 Hz, 2H), 7.52 (d, *J* = 7.6 Hz, 2H), 7.49 (t, *J* = 7.7 Hz, 1H), 7.40−7.32 (m, 7H), 7.16 (dd, *J* = 7.7, 1.3 Hz, 2H), 7.14 (s, 2H), 7.02 (d, *J* = 8.0 Hz, 2H), 7.01 (d, *J* = 8.0 Hz, 2H), 6.03 (s, 1H), 2.40 (s, 3H), 2.36 (sept, *J* = 6.9 Hz, 2H), 2.28 (sept, *J* = 6.9 Hz, 2H), 1.23 (d, *J* = 6.9 Hz, 6H), 1.15 (d, *J* = 6.8 Hz, 6H), 1.10 (d, *J* = 6.9 Hz, 6H), 0.91 (d, *J* = 6.9 Hz, 6H). ^{13}C{^{1}H} NMR (126 MHz, CD_2Cl_2): δ 191.5, 184.5, 145.7, 144.4, 133.8, 133.4, 133.3, 131.5, 131.1, 131.0, 130.1, 129.8, 128.7, 128.1, 124.5, 124.4, 124.3, 61.0, 32.0, 29.1, 29.0, 24.8, 24.3, 24.1, 23.9, 23.1, 21.8, 14.3. HRMS (ESI) calcd (found) for $C_{48}H_{54}AuN_2OS$ (M^+): 903.3617 (903.3622).

3.5.2 Gold α,α-Dioxo Carbenoid Complexes

[(IPr)AuC(4-picoline)(CO$_2$Me)$_2$]$^+$OTf$^-$ (**3.5**). A solution of 4-picolinium bis(methoxycarbonyl)methylide (15 mg, 6.9×10^{-2} mmol) and (IPr)Au(OTf) (25 mg, 6.2×10^{-2} mmol) in CH_2Cl_2 (2 mL) was stirred at 25 °C for 18 h. The resulting solution was concentrated under vacuum and layered with hexanes to give **3.5** (51 mg, 70%) as off-

white crystals. ^{1}H NMR (500 MHz, $CDCl_3$): δ 7.94 (d, *J* = 6.4 Hz, 2H), 7.65 (t, *J* = 7.8 Hz, 2H), 7.56 (d, *J* = 6.3 Hz, 2H), 7.43 (s, 2H), 7.39 (d, *J* = 7.8 Hz, 4H), 3.41 (s, 6H), 2.66 (s, 3H), 2.47 (sept, *J* = 6.9 Hz, 4H), 1.25 (d, *J* = 6.8 Hz, 12H) 1.22 (d, *J* = 6.8 Hz, 12H). ^{13}C{^{1}H} NMR (126 MHz, $CDCl_3$): δ 181.0, 167.7, 161.1, 148.0, 146.0, 133.6, 131.3, 127.7, 124.5, 124.3, 91.0, 52.7, 28.9, 24.5, 24.1, 22.2.

[(IPr)AuC(SPh_2)(CO_2Me)$_2$]$^{+}$$OTf^{-}$ (**3.6**). A solution of diphenylsulfoxonium bis(methoxycarbonyl)methylide (22 mg, 6.9×10^{-2} mmol) in CH_2Cl_2 (1 mL) was added dropwise to a solution of (IPr)Au(OTf) (46 mg, 6.2×10^{-2} mmol) in CH_2Cl_2 (1 mL), and the mixture was stirred at 25 °C for 18 h. The resulting solution was concentrated under vacuum and layered with hexanes to give **3.6** (22 mg, 39%) as off-white crystals. ^{1}H NMR (500 MHz, CD_2Cl_2): δ 7.61 (t, *J* = 7.8 Hz, 2H), 7.57 (t, *J* = 6.8 Hz, 2H), 7.41 (d, *J* = 8.1 Hz, 4H), 7.38–7.33 (m, 8H), 7.31 (s, 2H), 3.38 (s, 3H), 3.37 (s, 3H), 2.47 (sept, *J* = 7.0 Hz, 4H), 1.23 (d, *J* = 6.9 Hz, 12H), 1.19 (d, *J* = 6.8 Hz, 12H). ^{13}C{^{1}H} NMR (126 MHz, CD_2Cl_2): δ 180.0, 166.6, 146.2, 134.0, 133.7, 131.5, 131.4, 130.8, 127.4, 124.8, 124.7, 71.0, 54.3, 54.1, 53.8, 53.6, 53.5, 53.4, 29.2, 24.5, 24.0.

3.5.3 Gold to Alkene Carbene Transfer

Compound 3.7. A suspension of **3.1b** (15 mg, 1.7×10^{-2} mmol) in cyclohexene (1 mL) was heated at 75 °C for 18 h. As the mixture heated, **3.1b** dissolved, followed by the slow precipitation of IPrAuOTf as the reaction progressed. The resulting mixture was

filtered through a plug of silica gel and concentrated under vacuum. ^{1}H NMR analysis of the oily residue established the formation of **3.7** in 33% yield as determined by integration of the aromatic resonance of **3.7** at δ 7.87 relative to the resonance of CH_2Br_2 as an internal standard. The structure and *exo* configuration of **3.7** were established by comparison to an authentic sample synthesized employing the method of Takebayashi.[125,126] To this end, a solution of *p*-methyl-2-diazoacetophenone (250 mg, 1.6 mmol) and $Cu(acac)_2$ (5 mg, 1.9×10^{-2} mmol) in cyclohexene (8 mL) was heated at 75 °C for 30 min. The reaction mixture was cooled to room temperature, filtered through a plug of silica gel, and concentrated under vacuum. The resulting brown residue was chromatographed (SiO_2; 9:1 hexanes/EtOAc) to give *cis*-**3.7** (104 mg, 31%) as a yellow oil. ^{1}H NMR (500 MHz, $CDCl_3$): δ 7.91 (d, *J* = 7.9 Hz, 2H), 7.28 (d, *J* = 7.3 Hz, 2H), 2.47 (t, *J* = 4.2 Hz, 1H), 2.43 (s, 3H), 2.05−1.96 (m, 2H), 1.92−1.90 (m, 2H), 1.82−1.77 (m, 2H), 1.46−1.25 (m, 4H). ^{13}C{^{1}H} NMR (126 MHz, $CDCl_3$): δ 199.81, 143.1, 135.9, 129.1, 128.0, 31.3, 26.4, 23.3, 21.6, 21.2. HRMS (ESI) calcd (found) for $C_{15}H_{19}O$ (MH^+): 215.1436 (215.1434).

3.5.4 Kinetic Experiment Following Conversion of 3.1a to 3.2a

A solution of **3.1a** (20 mg, 2.4×10^{-2} mmol) in CD_2Cl_2 (500 μL) was made in an NMR tube with hexamethylbenzene (389 mg, 2.4×10^{-3} mmol) used as the internal standard. 4-Picoline (2.37 μL, 2.4×10^{-2} mmol) from a stock solution was added to the

gold solution and mixed thoroughly. The reaction progress was then monitored by ^{1}H NMR and ^{19}F NMR until three half-lives had passed (Figure 4).

3.5.5 Crystallographic Data

3.5.5.1 Molecular Structure of 3.2a

For X-ray analysis, crystals were formed via vapor diffusion of pentane into a concentrated CH_2Cl_2 solution of **3.2a** at -20 °C. A colorless plate-like crystal of molecular formula $C_{38}H_{49}AuF_3N_3O_5S$ with the approximate dimensions 0.082 mm × 0.123 mm × 0.232 mm was used for the X-ray crystallographic analysis. The X-ray intensity data were measured on a Bruker-Nonius X8 Kappa APEX II system equipped with a fine-focus sealed tube (MoKα, λ = 0.71073 Å) and a graphite monochromator, with a total exposure time of 6.78 hours. The frames were integrated with the Bruker SAINT software package using a narrow-frame algorithm. The integration of the data using a monoclinic unit cell yielded a total of 56063 reflections to a maximum θ angle of 36.48° (0.60 Å resolution), of which 19339 were independent (average redundancy 2.899, completeness = 99.6%, R_{int} = 4.53%, R_{sig} = 5.90%) and 16602 (85.85%) were greater than $2\sigma(F^2)$. The final cell constants of $\underline{a}$ = 9.8186(4) Å, $\underline{b}$ = 17.7830(7) Å, $\underline{c}$ = 11.4302(4) Å, β = 95.7170(10)°, volume = 1985.83(13) $Å^3$, are based upon the refinement of the XYZ-centroids of 9856 reflections above 20 σ(I) with 4.581° < 2θ < 64.87°. Data were corrected for absorption effects using the Numerical Mu from Formula method (SADABS). The

ratio of minimum to maximum apparent transmission was 0.647. The calculated minimum and maximum transmission coefficients (based on crystal size) are 0.4710 and 0.7450. The structure was solved and refined using the Bruker SHELXTL Software Package using the space P 1 21 1, with Z = 2 for the formula unit $C_{38}H_{49}AuF_3N_3O_5S$. The final anisotropic full-matrix least-squares refinement on F^2 with 544 variables converged at R1 = 4.50%, for the observed data and wR2 = 10.50% for all data. The goodness-of-fit was 1.004. The largest peak in the final difference electron density synthesis was 11.359 $e^-/Å^3$ and the largest hole was –1.259 $e^-/Å^3$ with an RMS deviation of 0.199 $e^-/Å^3$. On the basis of the final model, the calculated density was 1.528 g/cm^3 and F(000), 920 e^-.

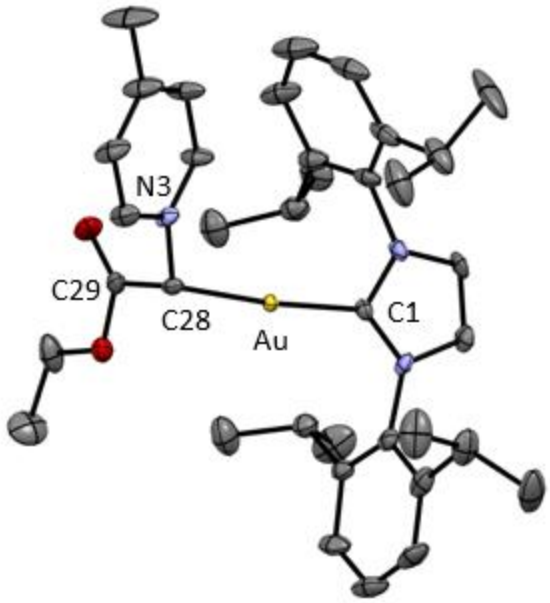

Figure 16. ORTEP diagram of gold(I) α-oxo carbenoid complex 3.2a with ellipsoids shown at 50% probability level and with counterion, solvent, and hydrogen atoms omitted.

Table 2. Bond lengths of complex 3.2a.

Bond	Length(Å)	Bond	Length(Å)
Au1-C1	2.016(5)	Au1-C28	2.081(6)
O1-C29	1.203(8)	O2-C29	1.349(8)
O2-C30	1.460(8)	N3-C36	1.332(8)
N3-C32	1.353(8)	N3-C28	1.491(8)
N2-C1	1.335(9)	N2-C3	1.408(10)
N2-C16	1.435(10)	N1-C1	1.349(7)
N1-C2	1.374(8)	N1-C4	1.464(11)
C4-C5	1.378(13)	C4-C9	1.432(14)
C34-C33	1.383(11)	C34-C35	1.391(10)
C34-C37	1.501(11)	C7-C8	1.357(15)
C7-C6	1.418(19)	C7-H7	0.95
C32-C33	1.380(10)	C32-H32	0.95
C19-C20	1.384(13)	C19-C18	1.385(12)
C19-H19	0.95	C33-H33	0.95
C23-C22	1.501(11)	C23-H23A	0.98
C23-H23B	0.98	C23-H23C	0.98
C37-H37A	0.98	C37-H37B	0.98
C37-H37C	0.98	C12-C10	1.533(12)
C12-H12A	0.98	C12-H12B	0.98
C12-H12C	0.98	C25-C21	1.519(13)
C25-C27	1.526(11)	C25-C26	1.528(12)
C25-H25	1	C14-C13	1.531(11)
C14-H14A	0.98	C14-H14B	0.98
C14-H14C	0.98	C24-C22	1.541(11)
C24-H24A	0.98	C24-H24B	0.98
C24-H24C	0.98	C27-H27A	0.98
C27-H27B	0.98	C27-H27C	0.98
C5-C6	1.379(14)	C5-C10	1.513(13)
C36-C35	1.382(9)	C36-H36	0.95
C13-C9	1.524(10)	C13-C15	1.529(10)
C13-H13	1	C29-C28	1.501(9)
C20-C21	1.377(13)	C20-H20	0.95
C35-H35	0.95	C26-H26A	0.98
C26-H26B	0.98	C26-H26C	0.98

C9-C8	1.385(12)	C15-H15A	0.98
C15-H15B	0.98	C15-H15C	0.98
C16-C21	1.414(11)	C16-C17	1.415(11)
C10-C11	1.545(13)	C10-H10	1
C11-H11A	0.98	C11-H11B	0.98
C11-H11C	0.98	C2-C3	1.366(14)
C2-H2	0.95	C3-H3	0.95
C17-C18	1.402(10)	C17-C22	1.500(11)
C18-H18	0.95	C22-H22	1
C8-H8	0.95	C6-H6	0.95
C28-H28	1	C30-C31	1.463(14)
C30-H30A	0.99	C30-H30B	0.99
C31-H31A	0.98	C31-H31B	0.98
C31-H31C	0.98	S1-O5	1.419(14)
S1-O4	1.437(14)	S1-O3	1.446(14)
S1-C38	1.796(16)	F1-C38	1.32(2)
F2-C38	1.347(14)	F3-C38	1.326(18)
S1A-O4A	1.430(12)	S1A-O5A	1.434(13)
S1A-O3A	1.438(12)	S1A-C38A	1.811(15)
F1A-C38A	1.319(19)	F2A-C38A	1.346(16)
F3A-C38A	1.35(2)		

Table 3. Bond angles of complex 3.2a.

Bond	Angle(°)	Bond	Angle(°)
C1-Au1-C28	174.4(2)	C29-O2-C30	115.1(6)
C36-N3-C32	119.8(5)	C36-N3-C28	121.7(5)
C32-N3-C28	118.2(5)	C1-N2-C3	111.1(7)
C1-N2-C16	127.6(7)	C3-N2-C16	121.1(6)
C1-N1-C2	112.9(6)	C1-N1-C4	123.2(6)
C2-N1-C4	123.2(7)	C5-C4-C9	123.4(8)
C5-C4-N1	120.1(9)	C9-C4-N1	116.1(8)
C33-C34-C35	117.3(6)	C33-C34-C37	121.1(7)
C35-C34-C37	121.6(7)	C8-C7-C6	118.3(9)
C8-C7-H7	120.8	C6-C7-H7	120.8
N3-C32-C33	120.2(6)	N3-C32-H32	119.9

C33-C32-H32	119.9	C20-C19-C18	120.7(7)
C20-C19-H19	119.6	C18-C19-H19	119.6
C32-C33-C34	121.1(6)	C32-C33-H33	119.5
C34-C33-H33	119.5	C22-C23-H23A	109.5
C22-C23-H23B	109.5	H23A-C23-H23B	109.5
C22-C23-H23C	109.5	H23A-C23-H23C	109.5
H23B-C23-H23C	109.5	C34-C37-H37A	109.5
C34-C37-H37B	109.5	H37A-C37-H37B	109.5
C34-C37-H37C	109.5	H37A-C37-H37C	109.5
H37B-C37-H37C	109.5	C10-C12-H12A	109.5
C10-C12-H12B	109.5	H12A-C12-H12B	109.5
C10-C12-H12C	109.5	H12A-C12-H12C	109.5
H12B-C12-H12C	109.5	C21-C25-C27	112.8(9)
C21-C25-C26	109.1(7)	C27-C25-C26	111.6(8)
C21-C25-H25	107.7	C27-C25-H25	107.7
C26-C25-H25	107.7	C13-C14-H14A	109.5
C13-C14-H14B	109.5	H14A-C14-H14B	109.5
C13-C14-H14C	109.5	H14A-C14-H14C	109.5
H14B-C14-H14C	109.5	C22-C24-H24A	109.5
C22-C24-H24B	109.5	H24A-C24-H24B	109.5
C22-C24-H24C	109.5	H24A-C24-H24C	109.5
H24B-C24-H24C	109.5	C25-C27-H27A	109.5
C25-C27-H27B	109.5	H27A-C27-H27B	109.5
C25-C27-H27C	109.5	H27A-C27-H27C	109.5
H27B-C27-H27C	109.5	C4-C5-C6	116.9(10)
C4-C5-C10	122.6(8)	C6-C5-C10	120.5(8)
N3-C36-C35	121.9(6)	N3-C36-H36	119.1
C35-C36-H36	119.1	C9-C13-C15	110.8(6)
C9-C13-C14	111.5(6)	C15-C13-C14	110.6(7)
C9-C13-H13	108	C15-C13-H13	108
C14-C13-H13	108	O1-C29-O2	125.0(6)
O1-C29-C28	125.3(6)	O2-C29-C28	109.7(5)
C21-C20-C19	121.4(7)	C21-C20-H20	119.3
C19-C20-H20	119.3	C36-C35-C34	119.6(7)
C36-C35-H35	120.2	C34-C35-H35	120.2
C25-C26-H26A	109.5	C25-C26-H26B	109.5

H26A-C26-H26B	109.5	C25-C26-H26C	109.5
H26A-C26-H26C	109.5	H26B-C26-H26C	109.5
C8-C9-C4	115.8(8)	C8-C9-C13	121.6(8)
C4-C9-C13	122.5(7)	C13-C15-H15A	109.5
C13-C15-H15B	109.5	H15A-C15-H15B	109.5
C13-C15-H15C	109.5	H15A-C15-H15C	109.5
H15B-C15-H15C	109.5	C21-C16-C17	122.2(7)
C21-C16-N2	119.9(7)	C17-C16-N2	117.8(6)
C5-C10-C12	111.5(10)	C5-C10-C11	109.6(7)
C12-C10-C11	110.4(8)	C5-C10-H10	108.4
C12-C10-H10	108.4	C11-C10-H10	108.4
C10-C11-H11A	109.5	C10-C11-H11B	109.5
H11A-C11-H11B	109.5	C10-C11-H11C	109.5
H11A-C11-H11C	109.5	H11B-C11-H11C	109.5
N2-C1-N1	104.4(5)	N2-C1-Au1	134.3(5)
N1-C1-Au1	121.2(4)	C3-C2-N1	105.4(6)
C3-C2-H2	127.3	N1-C2-H2	127.3
C2-C3-N2	106.1(5)	C2-C3-H3	126.9
N2-C3-H3	126.9	C18-C17-C16	117.0(7)
C18-C17-C22	119.7(7)	C16-C17-C22	123.3(7)
C20-C21-C16	117.7(9)	C20-C21-C25	121.7(8)
C16-C21-C25	120.6(9)	C19-C18-C17	120.8(8)
C19-C18-H18	119.6	C17-C18-H18	119.6
C17-C22-C23	111.3(7)	C17-C22-C24	110.7(7)
C23-C22-C24	110.8(8)	C17-C22-H22	108
C23-C22-H22	108	C24-C22-H22	108
C7-C8-C9	123.3(11)	C7-C8-H8	118.4
C9-C8-H8	118.4	C5-C6-C7	122.1(10)
C5-C6-H6	119	C7-C6-H6	119
N3-C28-C29	105.9(5)	N3-C28-Au1	115.3(4)
C29-C28-Au1	106.5(4)	N3-C28-H28	109.7
C29-C28-H28	109.7	Au1-C28-H28	109.7
O2-C30-C31	106.4(7)	O2-C30-H30A	110.4
C31-C30-H30A	110.4	O2-C30-H30B	110.4
C31-C30-H30B	110.4	H30A-C30-H30B	108.6
C30-C31-H31A	109.5	C30-C31-H31B	109.5

H31A-C31-H31B	109.5	C30-C31-H31C	109.5
H31A-C31-H31C	109.5	H31B-C31-H31C	109.5
O5-S1-O4	114.5(11)	O5-S1-O3	114.1(13)
O4-S1-O3	113.8(13)	O5-S1-C38	104.3(10)
O4-S1-C38	104.8(10)	O3-S1-C38	103.7(13)
F1-C38-F3	107.3(14)	F1-C38-F2	107.8(17)
F3-C38-F2	106.0(14)	F1-C38-S1	111.7(11)
F3-C38-S1	112.8(14)	F2-C38-S1	110.9(9)
O4A-S1A-O5A	115.0(12)	O4A-S1A-O3A	116.4(14)
O5A-S1A-O3A	114.0(13)	O4A-S1A-C38A	102.5(9)
O5A-S1A-C38A	102.4(10)	O3A-S1A-C38A	103.9(13)
F1A-C38A-F2A	108.3(15)	F1A-C38A-F3A	110.0(15)
F2A-C38A-F3A	106.5(14)	F1A-C38A-S1A	110.6(11)
F2A-C38A-S1A	110.9(10)	F3A-C38A-S1A	110.4(13)

Table 4. Dihedral angles of complex 3.2a.

Bond	Angle(°)	Bond	Angle(°)
C1-N1-C4-C5	95.8(9)	C2-N1-C4-C5	-94.8(9)
C1-N1-C4-C9	-77.0(9)	C2-N1-C4-C9	92.5(9)
C36-N3-C32-C33	0.3(11)	C28-N3-C32-C33	-173.8(7)
N3-C32-C33-C34	-0.3(13)	C35-C34-C33-C32	1.0(14)
C37-C34-C33-C32	-179.5(10)	C9-C4-C5-C6	-2.9(12)
N1-C4-C5-C6	-175.1(7)	C9-C4-C5-C10	175.9(7)
N1-C4-C5-C10	3.7(12)	C32-N3-C36-C35	-1.0(12)
C28-N3-C36-C35	172.8(7)	C30-O2-C29-O1	2.5(9)
C30-O2-C29-C28	-175.6(5)	C18-C19-C20-C21	0.3(11)
N3-C36-C35-C34	1.8(14)	C33-C34-C35-C36	-1.7(14)
C37-C34-C35-C36	178.8(10)	C5-C4-C9-C8	2.9(12)
N1-C4-C9-C8	175.4(7)	C5-C4-C9-C13	-179.8(7)
N1-C4-C9-C13	-7.4(11)	C15-C13-C9-C8	64.4(10)
C14-C13-C9-C8	-59.2(10)	C15-C13-C9-C4	-112.7(8)
C14-C13-C9-C4	123.7(8)	C1-N2-C16-C21	-100.1(9)
C3-N2-C16-C21	85.2(9)	C1-N2-C16-C17	83.5(10)
C3-N2-C16-C17	-91.3(8)	C4-C5-C10-C12	136.7(9)
C6-C5-C10-C12	-44.6(10)	C4-C5-C10-C11	-100.8(10)

C6-C5-C10-C11	77.9(10)	C3-N2-C1-N1	0.5(8)
C16-N2-C1-N1	-174.6(7)	C3-N2-C1-Au1	177.5(5)
C16-N2-C1-Au1	2.3(12)	C2-N1-C1-N2	0.0(7)
C4-N1-C1-N2	170.5(5)	C2-N1-C1-Au1	-177.4(4)
C4-N1-C1-Au1	-7.0(9)	C1-N1-C2-C3	-0.6(7)
C4-N1-C2-C3	-171.0(7)	N1-C2-C3-N2	0.9(7)
C1-N2-C3-C2	-0.9(8)	C16-N2-C3-C2	174.6(6)
C21-C16-C17-C18	-3.1(10)	N2-C16-C17-C18	173.3(7)
C21-C16-C17-C22	178.5(7)	N2-C16-C17-C22	-5.1(10)
C19-C20-C21-C16	-3.2(11)	C19-C20-C21-C25	175.8(7)
C17-C16-C21-C20	4.7(10)	N2-C16-C21-C20	-171.6(7)
C17-C16-C21-C25	-174.3(7)	N2-C16-C21-C25	9.4(10)
C27-C25-C21-C20	37.8(11)	C26-C25-C21-C20	-86.9(10)
C27-C25-C21-C16	-143.2(8)	C26-C25-C21-C16	92.1(9)
C20-C19-C18-C17	1.4(11)	C16-C17-C18-C19	0.0(11)
C22-C17-C18-C19	178.5(7)	C18-C17-C22-C23	59.4(10)
C16-C17-C22-C23	-122.2(8)	C18-C17-C22-C24	-64.2(10)
C16-C17-C22-C24	114.1(9)	C6-C7-C8-C9	3.7(15)
C4-C9-C8-C7	-3.4(13)	C13-C9-C8-C7	179.4(8)
C4-C5-C6-C7	3.1(13)	C10-C5-C6-C7	-175.7(8)
C8-C7-C6-C5	-3.5(14)	C36-N3-C28-C29	-81.1(7)
C32-N3-C28-C29	92.8(7)	C36-N3-C28-Au1	36.3(8)
C32-N3-C28-Au1	-149.8(5)	O1-C29-C28-N3	20.5(8)
O2-C29-C28-N3	-161.4(5)	O1-C29-C28-Au1	-102.7(7)
O2-C29-C28-Au1	75.4(5)	C29-O2-C30-C31	-163.8(7)
O5-S1-C38-F1	63.8(15)	O4-S1-C38-F1	-175.5(14)
O3-S1-C38-F1	-55.9(17)	O5-S1-C38-F3	-175.2(13)
O4-S1-C38-F3	-54.5(15)	O3-S1-C38-F3	65.1(17)
O5-S1-C38-F2	-56.4(18)	O4-S1-C38-F2	64.3(18)
O3-S1-C38-F2	-176.1(18)	O4A-S1A-C38A-F1A	-62.6(15)
O5A-S1A-C38A-F1A	177.8(14)	O3A-S1A-C38A-F1A	58.9(18)
O4A-S1A-C38A-F2A	57.6(16)	O5A-S1A-C38A-F2A	-61.9(17)
O3A-S1A-C38A-F2A	179.1(17)	O4A-S1A-C38A-F3A	175.4(12)
O5A-S1A-C38A-F3A	55.9(15)	O3A-S1A-C38A-F3A	-63.0(17)

3.5.5.2 Molecular Structure of 3.2b

An oily residue of **3.2b** was dissolved in diethyl ether containing one drop of CH_2Cl_2 and cooled to -20 °C to give colorless crystals suitable for X-ray analysis. A colorless plate-like crystal of molecular formula $C_{47}H_{61}AuF_3N_3O_5S$ with the approximate dimensions 0.064 mm × 0.159 mm × 0.346 mm was used for the X-ray crystallographic analysis. The X-ray intensity data were measured on a Bruker-Nonius X8 Kappa APEX II system equipped with a fine-focus sealed tube (MoKα, λ = 0.71073 Å) and a graphite monochromator, with a total exposure time of 16.67 hours. The frames were integrated with the Bruker SAINT software package using a narrow-frame algorithm. The integration of the data using a triclinic unit cell yielded a total of 496165 reflections to a maximum θ angle of 30.03° (0.71 Å resolution), of which 56218 were independent (average redundancy 8.826, completeness = 100.0%, R_{int} = 6.06%, R_{sig} = 3.65%) and 42981 (76.45%) were greater than $2\sigma(F^2)$. The final cell constants of a = 16.8791(5) Å, b = 23.8263(7) Å, c = 26.7619(8) Å, α = 72.4940(10)°, β = 78.6610(10)°, γ = 70.2010(10)°, volume = 9603.6(5) $Å^3$, are based upon the refinement of the XYZ-centroids of 2885 reflections above 20 σ(I) with 3.509° < 2θ < 57.42°. Data were corrected for absorption effects using the numerical method (SADABS). The ratio of minimum to maximum apparent transmission was 0.607. The calculated minimum and maximum transmission coefficients (based on crystal size) are 0.4070 and 0.8230. The structure was solved and

refined using the Bruker SHELXTL Software Package using the space P -1, with Z = 8 for the formula unit $C_{47}H_{61}AuF_3N_3O_5S$. The final anisotropic full-matrix least-squares refinement on F^2 with 2209 variables converged at R1 = 3.58%, for the observed data and wR2 = 7.58% for all data. The goodness-of-fit was 1.059. The largest peak in the final difference electron density synthesis was 3.319 $e^-/Å^3$ and the largest hole was –1.376 $e^-/Å^3$ with an RMS deviation of 0.113 $e^-/Å^3$. On the basis of the final model, the calculated density was 1.430 g/cm^3 and F(000), 4208 e^-.

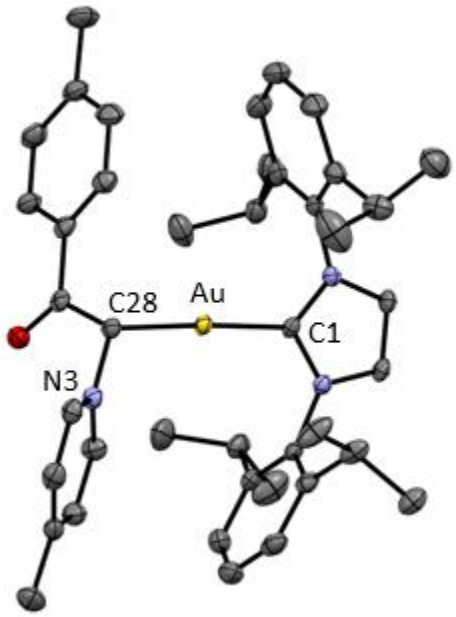

Figure 17. ORTEP diagram of gold(I) α-oxo carbenoid complex 3.2b with ellipsoids shown at 50% probability level and with counterion, solvent, and hydrogen atoms omitted.

Table 5. Bond lengths of complex 3.2b.

Bond	Length(Å)	Bond	Length(Å)

Au1-C1	2.013(3)	Au1-C28	2.087(3)
O1-C29	1.226(4)	N1-C1	1.350(4)
N1-C2	1.382(4)	N1-C4	1.445(4)
N2-C1	1.350(4)	N2-C3	1.389(4)
N2-C16	1.448(4)	N3-C41	1.345(4)
N3-C37	1.348(4)	N3-C28	1.484(4)
C2-C3	1.349(4)	C2-H2	0.95
C3-H3	0.95	C4-C9	1.396(4)
C4-C5	1.398(4)	C5-C6	1.391(5)
C5-C10	1.515(5)	C6-C7	1.377(5)
C6-H6	0.95	C7-C8	1.384(5)
C7-H7	0.95	C8-C9	1.403(5)
C8-H8	0.95	C9-C13	1.507(5)
C10-C11	1.531(5)	C10-C12	1.535(5)
C10-H10	1	C11-H11A	0.98
C11-H11B	0.98	C11-H11C	0.98
C12-H12A	0.98	C12-H12B	0.98
C12-H12C	0.98	C13-C15	1.538(4)
C13-C14	1.538(4)	C13-H13	1
C14-H14A	0.98	C14-H14B	0.98
C14-H14C	0.98	C15-H15A	0.98
C15-H15B	0.98	C15-H15C	0.98
C16-C21	1.396(4)	C16-C17	1.397(5)
C17-C18	1.400(5)	C17-C22	1.520(5)
C18-C19	1.377(5)	C18-H18	0.95
C19-C20	1.375(6)	C19-H19	0.95
C20-C21	1.397(5)	C20-H20	0.95
C21-C25	1.515(5)	C22-C24	1.505(5)
C22-C23	1.526(5)	C22-H22	1
C23-H23A	0.98	C23-H23B	0.98
C23-H23C	0.98	C24-H24A	0.98
C24-H24B	0.98	C24-H24C	0.98
C25-C27	1.529(5)	C25-C26	1.529(5)
C25-H25	1	C26-H26A	0.98
C26-H26B	0.98	C26-H26C	0.98
C27-H27A	0.98	C27-H27B	0.98

C27-H27C	0.98	C28-C29	1.491(4)
C28-H28	1	C29-C30	1.496(4)
C30-C31	1.382(5)	C30-C35	1.396(4)
C31-C32	1.388(5)	C31-H31	0.95
C32-C33	1.379(5)	C32-H32	0.95
C33-C34	1.401(5)	C33-C36	1.511(5)
C34-C35	1.388(5)	C34-H34	0.95
C35-H35	0.95	C36-H36A	0.98
C36-H36B	0.98	C36-H36C	0.98
C37-C38	1.376(4)	C37-H37	0.95
C38-C39	1.384(4)	C38-H38	0.95
C39-C40	1.382(5)	C39-C42	1.501(5)
C40-C41	1.377(5)	C40-H40	0.95
C41-H41	0.95	C42-H42A	0.98
C42-H42B	0.98	C42-H42C	0.98

Table 6. Bond angles of complex 3.2b.

Bond	Angle(°)	Bond	Angle(°)
C1-Au1-C28	176.89(11)	C1-N1-C2	110.9(2)
C1-N1-C4	122.0(2)	C2-N1-C4	127.0(2)
C1-N2-C3	110.7(2)	C1-N2-C16	123.0(2)
C3-N2-C16	126.1(2)	C41-N3-C37	119.5(3)
C41-N3-C28	120.7(3)	C37-N3-C28	119.8(2)
N1-C1-N2	105.1(2)	N1-C1-Au1	124.5(2)
N2-C1-Au1	130.4(2)	C3-C2-N1	106.7(2)
C3-C2-H2	126.6	N1-C2-H2	126.6
C2-C3-N2	106.5(3)	C2-C3-H3	126.7
N2-C3-H3	126.7	C9-C4-C5	122.7(3)
C9-C4-N1	118.4(3)	C5-C4-N1	118.8(3)
C6-C5-C4	117.7(3)	C6-C5-C10	120.2(3)
C4-C5-C10	122.1(3)	C7-C6-C5	121.0(3)
C7-C6-H6	119.5	C5-C6-H6	119.5
C6-C7-C8	120.6(3)	C6-C7-H7	119.7
C8-C7-H7	119.7	C7-C8-C9	120.6(3)
C7-C8-H8	119.7	C9-C8-H8	119.7

C4-C9-C8	117.4(3)	C4-C9-C13	122.4(3)
C8-C9-C13	120.2(3)	C5-C10-C11	111.6(3)
C5-C10-C12	110.7(3)	C11-C10-C12	111.2(3)
C5-C10-H10	107.7	C11-C10-H10	107.7
C12-C10-H10	107.7	C10-C11-H11A	109.5
C10-C11-H11B	109.5	H11A-C11-H11B	109.5
C10-C11-H11C	109.5	H11A-C11-H11C	109.5
H11B-C11-H11C	109.5	C10-C12-H12A	109.5
C10-C12-H12B	109.5	H12A-C12-H12B	109.5
C10-C12-H12C	109.5	H12A-C12-H12C	109.5
H12B-C12-H12C	109.5	C9-C13-C15	111.0(3)
C9-C13-C14	110.6(3)	C15-C13-C14	110.4(3)
C9-C13-H13	108.3	C15-C13-H13	108.3
C14-C13-H13	108.3	C13-C14-H14A	109.5
C13-C14-H14B	109.5	H14A-C14-H14B	109.5
C13-C14-H14C	109.5	H14A-C14-H14C	109.5
H14B-C14-H14C	109.5	C13-C15-H15A	109.5
C13-C15-H15B	109.5	H15A-C15-H15B	109.5
C13-C15-H15C	109.5	H15A-C15-H15C	109.5
H15B-C15-H15C	109.5	C21-C16-C17	123.8(3)
C21-C16-N2	117.8(3)	C17-C16-N2	118.5(3)
C16-C17-C18	116.5(3)	C16-C17-C22	122.7(3)
C18-C17-C22	120.8(3)	C19-C18-C17	121.0(4)
C19-C18-H18	119.5	C17-C18-H18	119.5
C20-C19-C18	121.0(3)	C20-C19-H19	119.5
C18-C19-H19	119.5	C19-C20-C21	120.8(3)
C19-C20-H20	119.6	C21-C20-H20	119.6
C16-C21-C20	117.0(3)	C16-C21-C25	122.2(3)
C20-C21-C25	120.9(3)	C24-C22-C17	112.7(3)
C24-C22-C23	110.7(3)	C17-C22-C23	110.4(3)
C24-C22-H22	107.6	C17-C22-H22	107.6
C23-C22-H22	107.6	C22-C23-H23A	109.5
C22-C23-H23B	109.5	H23A-C23-H23B	109.5
C22-C23-H23C	109.5	H23A-C23-H23C	109.5
H23B-C23-H23C	109.5	C22-C24-H24A	109.5
C22-C24-H24B	109.5	H24A-C24-H24B	109.5

C22-C24-H24C	109.5	H24A-C24-H24C	109.5
H24B-C24-H24C	109.5	C21-C25-C27	112.5(3)
C21-C25-C26	110.7(3)	C27-C25-C26	110.5(3)
C21-C25-H25	107.6	C27-C25-H25	107.6
C26-C25-H25	107.6	C25-C26-H26A	109.5
C25-C26-H26B	109.5	H26A-C26-H26B	109.5
C25-C26-H26C	109.5	H26A-C26-H26C	109.5
H26B-C26-H26C	109.5	C25-C27-H27A	109.5
C25-C27-H27B	109.5	H27A-C27-H27B	109.5
C25-C27-H27C	109.5	H27A-C27-H27C	109.5
H27B-C27-H27C	109.5	N3-C28-C29	110.0(2)
N3-C28-Au1	112.56(18)	C29-C28-Au1	104.73(18)
N3-C28-H28	109.8	C29-C28-H28	109.8
Au1-C28-H28	109.8	O1-C29-C28	121.8(3)
O1-C29-C30	121.1(3)	C28-C29-C30	116.9(3)
C31-C30-C35	119.1(3)	C31-C30-C29	123.1(3)
C35-C30-C29	117.7(3)	C30-C31-C32	120.1(3)
C30-C31-H31	119.9	C32-C31-H31	119.9
C33-C32-C31	121.6(3)	C33-C32-H32	119.2
C31-C32-H32	119.2	C32-C33-C34	118.3(3)
C32-C33-C36	121.1(3)	C34-C33-C36	120.6(3)
C35-C34-C33	120.5(3)	C35-C34-H34	119.7
C33-C34-H34	119.7	C34-C35-C30	120.3(3)
C34-C35-H35	119.8	C30-C35-H35	119.8
C33-C36-H36A	109.5	C33-C36-H36B	109.5
H36A-C36-H36B	109.5	C33-C36-H36C	109.5
H36A-C36-H36C	109.5	H36B-C36-H36C	109.5
N3-C37-C38	121.3(3)	N3-C37-H37	119.3
C38-C37-H37	119.3	C37-C38-C39	120.2(3)
C37-C38-H38	119.9	C39-C38-H38	119.9
C40-C39-C38	117.3(3)	C40-C39-C42	121.4(3)
C38-C39-C42	121.3(3)	C41-C40-C39	121.0(3)
C41-C40-H40	119.5	C39-C40-H40	119.5
N3-C41-C40	120.6(3)	N3-C41-H41	119.7
C40-C41-H41	119.7	C39-C42-H42A	109.5
C39-C42-H42B	109.5	H42A-C42-H42B	109.5

C39-C42-H42C	109.5	H42A-C42-H42C	109.5
H42B-C42-H42C	109.5		

Table 7. Dihedral angles of complex 3.2b.

Bond	Angle(°)	Bond	Angle(°)
C2-N1-C1-N2	-0.4(3)	C4-N1-C1-N2	-179.2(2)
C2-N1-C1-Au1	179.6(2)	C4-N1-C1-Au1	0.7(4)
C3-N2-C1-N1	0.4(3)	C16-N2-C1-N1	176.0(3)
C3-N2-C1-Au1	-179.5(2)	C16-N2-C1-Au1	-3.9(4)
C1-N1-C2-C3	0.2(3)	C4-N1-C2-C3	179.0(3)
N1-C2-C3-N2	0.1(3)	C1-N2-C3-C2	-0.3(3)
C16-N2-C3-C2	-175.7(3)	C1-N1-C4-C9	-84.7(3)
C2-N1-C4-C9	96.6(3)	C1-N1-C4-C5	91.7(3)
C2-N1-C4-C5	-87.0(4)	C9-C4-C5-C6	1.7(4)
N1-C4-C5-C6	-174.6(3)	C9-C4-C5-C10	-178.1(3)
N1-C4-C5-C10	5.6(4)	C4-C5-C6-C7	-0.5(5)
C10-C5-C6-C7	179.3(3)	C5-C6-C7-C8	-0.3(5)
C6-C7-C8-C9	0.0(5)	C5-C4-C9-C8	-1.9(4)
N1-C4-C9-C8	174.3(3)	C5-C4-C9-C13	179.0(3)
N1-C4-C9-C13	-4.7(4)	C7-C8-C9-C4	1.1(4)
C7-C8-C9-C13	-179.9(3)	C6-C5-C10-C11	56.0(4)
C4-C5-C10-C11	-124.2(3)	C6-C5-C10-C12	-68.4(4)
C4-C5-C10-C12	111.4(4)	C4-C9-C13-C15	-122.6(3)
C8-C9-C13-C15	58.4(4)	C4-C9-C13-C14	114.5(3)
C8-C9-C13-C14	-64.5(4)	C1-N2-C16-C21	-89.8(4)
C3-N2-C16-C21	85.1(4)	C1-N2-C16-C17	89.2(4)
C3-N2-C16-C17	-96.0(4)	C21-C16-C17-C18	2.1(5)
N2-C16-C17-C18	-176.7(3)	C21-C16-C17-C22	-176.8(3)
N2-C16-C17-C22	4.3(4)	C16-C17-C18-C19	-1.1(5)
C22-C17-C18-C19	177.9(3)	C17-C18-C19-C20	-0.8(6)
C18-C19-C20-C21	1.7(6)	C17-C16-C21-C20	-1.2(5)
N2-C16-C21-C20	177.6(3)	C17-C16-C21-C25	-179.5(3)
N2-C16-C21-C25	-0.7(4)	C19-C20-C21-C16	-0.7(5)
C19-C20-C21-C25	177.6(3)	C16-C17-C22-C24	134.7(3)
C18-C17-C22-C24	-44.2(5)	C16-C17-C22-C23	-101.0(4)

C18-C17-C22-C23	80.1(4)	C16-C21-C25-C27	-133.2(3)
C20-C21-C25-C27	48.6(4)	C16-C21-C25-C26	102.6(4)
C20-C21-C25-C26	-75.6(4)	C41-N3-C28-C29	-111.4(3)
C37-N3-C28-C29	67.3(3)	C41-N3-C28-Au1	132.3(2)
C37-N3-C28-Au1	-49.1(3)	N3-C28-C29-O1	-14.6(4)
Au1-C28-C29-O1	106.6(3)	N3-C28-C29-C30	170.0(2)
Au1-C28-C29-C30	-68.8(3)	O1-C29-C30-C31	171.4(3)
C28-C29-C30-C31	-13.1(4)	O1-C29-C30-C35	-10.7(4)
C28-C29-C30-C35	164.8(3)	C35-C30-C31-C32	-1.1(5)
C29-C30-C31-C32	176.8(3)	C30-C31-C32-C33	0.1(5)
C31-C32-C33-C34	1.0(5)	C31-C32-C33-C36	-178.5(3)
C32-C33-C34-C35	-1.2(5)	C36-C33-C34-C35	178.4(3)
C33-C34-C35-C30	0.2(5)	C31-C30-C35-C34	1.0(5)
C29-C30-C35-C34	-177.1(3)	C41-N3-C37-C38	1.0(5)
C28-N3-C37-C38	-177.6(3)	N3-C37-C38-C39	-1.5(5)
C37-C38-C39-C40	0.1(5)	C37-C38-C39-C42	179.2(3)
C38-C39-C40-C41	1.8(5)	C42-C39-C40-C41	-177.3(3)
C37-N3-C41-C40	0.9(4)	C28-N3-C41-C40	179.6(3)
C39-C40-C41-N3	-2.4(5)		

3.5.5.3 Molecular Structure of 3.3a

A concentrated solution of **3.3a** was layered with toluene at room temperature give colorless crystals suitable for X-ray analysis. A colorless block-like crystal of molecular formula $C_{34}H_{48}AuF_3N_2O_5S_2$ with the approximate dimensions 0.110 mm × 0.133 mm × 0.285 mm was used for the X-ray crystallographic analysis. The X-ray intensity data were measured on a Bruker-Nonius X8 Kappa APEX II system equipped with a fine-focus sealed tube (MoKα, λ = 0.71073 Å) and a graphite monochromator, with a total exposure time of 5.49 hours. The frames were integrated with the Bruker

SAINT software package using a narrow-frame algorithm. The integration of the data using a monoclinic unit cell yielded a total of 128883 reflections to a maximum θ angle of 36.50° (0.60 Å resolution), of which 18063 were independent (average redundancy 7.135, completeness = 99.7%, R_{int} = 4.71%, R_{sig} = 3.15%) and 15183 (84.06%) were greater than $2\sigma(F^2)$. The final cell constants of a = 9.4745(6) Å, b = 18.0071(11) Å, c = 21.6308(13) Å, β = 91.6085(14)°, volume = 3688.9(4) $Å^3$, are based upon the refinement of the XYZ-centroids of 9757 reflections above 20 σ(I) with 4.900° < 2θ < 69.44°. Data were corrected for absorption effects using the Numerical Mu from Formula method (SADABS). The ratio of minimum to maximum apparent transmission was 0.703. The calculated minimum and maximum transmission coefficients (based on crystal size) are 0.4969 and 0.7069. The final anisotropic full-matrix least-squares refinement on F^2 with 435 variables converged at R1 = 5.61%, for the observed data and wR2 = 14.26% for all data. The goodness-of-fit was 1.040. The largest peak in the final difference electron density synthesis was 22.173 $e^-/Å^3$ and the largest hole was –1.773 $e^-/Å^3$ with an RMS deviation of 0.261 $e^-/Å^3$. On the basis of the final model, the calculated density was 1.590 g/cm^3 and F(000), 1776 e^-.

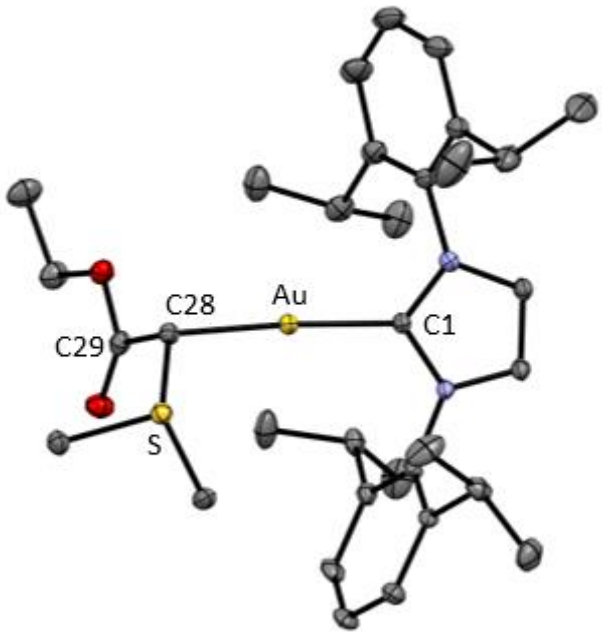

Figure 18. ORTEP diagram of gold(I) α-oxo carbenoid complex 3.3a with ellipsoids shown at 50% probability level and with counterion, solvent, and hydrogen atoms omitted.

Table 8. Bond lengths of complex 3.3a.

Bond	Length(Å)	Bond	Length(Å)
Au1-C1	2.012(3)	Au1-C28	2.088(4)
S1-C28	1.782(4)	S1-C32	1.788(4)
S1-C33	1.790(4)	O1-C29	1.209(5)
O2-C29	1.342(5)	O2-C30	1.454(5)
N1-C1	1.354(4)	N1-C2	1.385(5)
N1-C4	1.443(4)	N2-C1	1.351(4)
N2-C3	1.391(5)	N2-C16	1.444(5)
C2-C3	1.348(5)	C2-H2	0.95
C3-H3	0.95	C4-C9	1.404(5)
C4-C5	1.406(5)	C5-C6	1.402(5)
C5-C10	1.515(6)	C6-C7	1.376(6)
C6-H6	0.95	C7-C8	1.396(5)
C7-H7	0.95	C8-C9	1.395(5)

C8-H8	0.95	C9-C13	1.508(5)
C10-C11	1.523(6)	C10-C12	1.523(6)
C10-H10	1	C11-H11A	0.98
C11-H11B	0.98	C11-H11C	0.98
C12-H12A	0.98	C12-H12B	0.98
C12-H12C	0.98	C13-C15	1.528(6)
C13-C14	1.528(7)	C13-H13	1
C14-H14A	0.98	C14-H14B	0.98
C14-H14C	0.98	C15-H15A	0.98
C15-H15B	0.98	C15-H15C	0.98
C16-C17	1.395(6)	C16-C21	1.399(6)
C17-C18	1.396(6)	C17-C22	1.527(7)
C18-C19	1.370(8)	C18-H18	0.95
C19-C20	1.388(8)	C19-H19	0.95
C20-C21	1.401(6)	C20-H20	0.95
C21-C25	1.514(6)	C22-C23	1.524(9)
C22-C24	1.524(7)	C22-H22	1
C23-H23A	0.98	C23-H23B	0.98
C23-H23C	0.98	C24-H24A	0.98
C24-H24B	0.98	C24-H24C	0.98
C25-C26	1.524(6)	C25-C27	1.529(7)
C25-H25	1	C26-H26A	0.98
C26-H26B	0.98	C26-H26C	0.98
C27-H27A	0.98	C27-H27B	0.98
C27-H27C	0.98	C28-C29	1.492(5)
C28-H28	1	C30-C31	1.498(6)
C30-H30A	0.99	C30-H30B	0.99
C31-H31A	0.98	C31-H31B	0.98
C31-H31C	0.98	C32-H32A	0.98
C32-H32B	0.98	C32-H32C	0.98
C33-H33A	0.98	C33-H33B	0.98
C33-H33C	0.98	S2-O5	1.435(4)
S2-O3	1.438(4)	S2-O4	1.451(3)
S2-C34	1.827(4)	F1-C34	1.333(5)
F2-C34	1.331(5)	F3-C34	1.336(5)

Table 9. Bond angles of complex 3.3a.

Bond	Angle(°)	Bond	Angle(°)
C1-Au1-C28	175.42(14)	C28-S1-C32	106.01(18)
C28-S1-C33	107.12(18)	C32-S1-C33	100.57(19)
C29-O2-C30	114.8(3)	C1-N1-C2	110.9(3)
C1-N1-C4	123.6(3)	C2-N1-C4	124.8(3)
C1-N2-C3	110.5(3)	C1-N2-C16	125.5(3)
C3-N2-C16	123.9(3)	N2-C1-N1	105.1(3)
N2-C1-Au1	130.4(3)	N1-C1-Au1	124.4(2)
C3-C2-N1	106.6(3)	C3-C2-H2	126.7
N1-C2-H2	126.7	C2-C3-N2	106.9(3)
C2-C3-H3	126.6	N2-C3-H3	126.6
C9-C4-C5	123.2(3)	C9-C4-N1	119.3(3)
C5-C4-N1	117.6(3)	C6-C5-C4	117.1(3)
C6-C5-C10	120.3(3)	C4-C5-C10	122.5(3)
C7-C6-C5	120.7(3)	C7-C6-H6	119.6
C5-C6-H6	119.6	C6-C7-C8	121.1(4)
C6-C7-H7	119.4	C8-C7-H7	119.4
C9-C8-C7	120.5(4)	C9-C8-H8	119.8
C7-C8-H8	119.8	C8-C9-C4	117.3(3)
C8-C9-C13	121.2(3)	C4-C9-C13	121.5(3)
C5-C10-C11	112.4(3)	C5-C10-C12	110.0(4)
C11-C10-C12	110.3(4)	C5-C10-H10	108
C11-C10-H10	108	C12-C10-H10	108
C10-C11-H11A	109.5	C10-C11-H11B	109.5
H11A-C11-H11B	109.5	C10-C11-H11C	109.5
H11A-C11-H11C	109.5	H11B-C11-H11C	109.5
C10-C12-H12A	109.5	C10-C12-H12B	109.5
H12A-C12-H12B	109.5	C10-C12-H12C	109.5
H12A-C12-H12C	109.5	H12B-C12-H12C	109.5
C9-C13-C15	113.6(3)	C9-C13-C14	109.7(3)
C15-C13-C14	109.5(4)	C9-C13-H13	108
C15-C13-H13	108	C14-C13-H13	108
C13-C14-H14A	109.5	C13-C14-H14B	109.5
H14A-C14-H14B	109.5	C13-C14-H14C	109.5
H14A-C14-H14C	109.5	H14B-C14-H14C	109.5

C13-C15-H15A	109.5	C13-C15-H15B	109.5
H15A-C15-H15B	109.5	C13-C15-H15C	109.5
H15A-C15-H15C	109.5	H15B-C15-H15C	109.5
C17-C16-C21	123.1(4)	C17-C16-N2	118.5(3)
C21-C16-N2	118.3(4)	C16-C17-C18	117.1(4)
C16-C17-C22	122.5(4)	C18-C17-C22	120.3(4)
C19-C18-C17	121.6(5)	C19-C18-H18	119.2
C17-C18-H18	119.2	C18-C19-C20	120.2(4)
C18-C19-H19	119.9	C20-C19-H19	119.9
C19-C20-C21	120.9(4)	C19-C20-H20	119.5
C21-C20-H20	119.5	C16-C21-C20	117.0(4)
C16-C21-C25	122.2(4)	C20-C21-C25	120.8(4)
C23-C22-C24	111.6(6)	C23-C22-C17	109.1(4)
C24-C22-C17	112.4(5)	C23-C22-H22	107.9
C24-C22-H22	107.9	C17-C22-H22	107.9
C22-C23-H23A	109.5	C22-C23-H23B	109.5
H23A-C23-H23B	109.5	C22-C23-H23C	109.5
H23A-C23-H23C	109.5	H23B-C23-H23C	109.5
C22-C24-H24A	109.5	C22-C24-H24B	109.5
H24A-C24-H24B	109.5	C22-C24-H24C	109.5
H24A-C24-H24C	109.5	H24B-C24-H24C	109.5
C21-C25-C26	113.5(4)	C21-C25-C27	110.9(4)
C26-C25-C27	110.6(4)	C21-C25-H25	107.2
C26-C25-H25	107.2	C27-C25-H25	107.2
C25-C26-H26A	109.5	C25-C26-H26B	109.5
H26A-C26-H26B	109.5	C25-C26-H26C	109.5
H26A-C26-H26C	109.5	H26B-C26-H26C	109.5
C25-C27-H27A	109.5	C25-C27-H27B	109.5
H27A-C27-H27B	109.5	C25-C27-H27C	109.5
H27A-C27-H27C	109.5	H27B-C27-H27C	109.5
C29-C28-S1	114.9(3)	C29-C28-Au1	106.5(2)
S1-C28-Au1	108.67(18)	C29-C28-H28	108.9
S1-C28-H28	108.9	Au1-C28-H28	108.9
O1-C29-O2	123.4(4)	O1-C29-C28	125.7(3)
O2-C29-C28	110.9(3)	O2-C30-C31	107.8(4)
O2-C30-H30A	110.1	C31-C30-H30A	110.1

O2-C30-H30B	110.1	C31-C30-H30B	110.1
H30A-C30-H30B	108.5	C30-C31-H31A	109.5
C30-C31-H31B	109.5	H31A-C31-H31B	109.5
C30-C31-H31C	109.5	H31A-C31-H31C	109.5
H31B-C31-H31C	109.5	S1-C32-H32A	109.5
S1-C32-H32B	109.5	H32A-C32-H32B	109.5
S1-C32-H32C	109.5	H32A-C32-H32C	109.5
H32B-C32-H32C	109.5	S1-C33-H33A	109.5
S1-C33-H33B	109.5	H33A-C33-H33B	109.5
S1-C33-H33C	109.5	H33A-C33-H33C	109.5
H33B-C33-H33C	109.5	O5-S2-O3	115.7(2)
O5-S2-O4	114.9(2)	O3-S2-O4	114.9(2)
O5-S2-C34	103.76(19)	O3-S2-C34	103.0(2)
O4-S2-C34	102.11(19)	F2-C34-F1	107.4(3)
F2-C34-F3	107.7(3)	F1-C34-F3	107.2(3)
F2-C34-S2	111.0(3)	F1-C34-S2	111.3(3)
F3-C34-S2	112.1(3)		

Table 10. Dihedral angles of complex 3.3a.

Bond	Angle(°)	Bond	Angle(°)
C3-N2-C1-N1	-0.9(4)	C16-N2-C1-N1	174.7(3)
C3-N2-C1-Au1	-178.5(3)	C16-N2-C1-Au1	-2.9(6)
C2-N1-C1-N2	0.7(4)	C4-N1-C1-N2	-169.6(3)
C2-N1-C1-Au1	178.5(3)	C4-N1-C1-Au1	8.2(5)
C1-N1-C2-C3	-0.2(4)	C4-N1-C2-C3	169.9(3)
N1-C2-C3-N2	-0.3(4)	C1-N2-C3-C2	0.7(4)
C16-N2-C3-C2	-174.9(3)	C1-N1-C4-C9	-102.3(4)
C2-N1-C4-C9	88.7(4)	C1-N1-C4-C5	77.1(5)
C2-N1-C4-C5	-91.8(4)	C9-C4-C5-C6	2.0(5)
N1-C4-C5-C6	-177.4(3)	C9-C4-C5-C10	-176.7(3)
N1-C4-C5-C10	3.9(5)	C4-C5-C6-C7	-0.9(6)
C10-C5-C6-C7	177.8(4)	C5-C6-C7-C8	-0.3(6)
C6-C7-C8-C9	0.6(6)	C7-C8-C9-C4	0.4(6)
C7-C8-C9-C13	178.8(4)	C5-C4-C9-C8	-1.7(5)
N1-C4-C9-C8	177.7(3)	C5-C4-C9-C13	179.8(3)

N1-C4-C9-C13	-0.7(5)	C6-C5-C10-C11	56.2(5)
C4-C5-C10-C11	-125.2(4)	C6-C5-C10-C12	-67.2(5)
C4-C5-C10-C12	111.4(4)	C8-C9-C13-C15	35.7(5)
C4-C9-C13-C15	-145.9(4)	C8-C9-C13-C14	-87.1(5)
C4-C9-C13-C14	91.2(5)	C1-N2-C16-C17	108.6(4)
C3-N2-C16-C17	-76.4(5)	C1-N2-C16-C21	-73.4(5)
C3-N2-C16-C21	101.6(4)	C21-C16-C17-C18	-2.2(6)
N2-C16-C17-C18	175.7(4)	C21-C16-C17-C22	173.9(4)
N2-C16-C17-C22	-8.2(6)	C16-C17-C18-C19	0.6(7)
C22-C17-C18-C19	-175.6(5)	C17-C18-C19-C20	1.0(7)
C18-C19-C20-C21	-1.1(7)	C17-C16-C21-C20	2.0(6)
N2-C16-C21-C20	-175.9(4)	C17-C16-C21-C25	-179.4(4)
N2-C16-C21-C25	2.7(6)	C19-C20-C21-C16	-0.3(6)
C19-C20-C21-C25	-178.9(4)	C16-C17-C22-C23	-99.4(6)
C18-C17-C22-C23	76.6(6)	C16-C17-C22-C24	136.3(5)
C18-C17-C22-C24	-47.7(6)	C16-C21-C25-C26	149.6(4)
C20-C21-C25-C26	-31.9(6)	C16-C21-C25-C27	-85.2(5)
C20-C21-C25-C27	93.3(5)	C32-S1-C28-C29	65.9(3)
C33-S1-C28-C29	-40.8(3)	C32-S1-C28-Au1	-53.3(2)
C33-S1-C28-Au1	-160.07(18)	C30-O2-C29-O1	1.7(6)
C30-O2-C29-C28	179.8(3)	S1-C28-C29-O1	-27.4(5)
Au1-C28-C29-O1	93.0(4)	S1-C28-C29-O2	154.5(3)
Au1-C28-C29-O2	-85.1(3)	C29-O2-C30-C31	167.6(4)
O5-S2-C34-F2	-175.0(3)	O3-S2-C34-F2	64.1(3)
O4-S2-C34-F2	-55.3(3)	O5-S2-C34-F1	-55.4(3)
O3-S2-C34-F1	-176.3(3)	O4-S2-C34-F1	64.3(3)
O5-S2-C34-F3	64.6(3)	O3-S2-C34-F3	-56.4(4)
O4-S2-C34-F3	-175.7(3)		

3.5.5.4 Molecular Structure of 3.3b

An oily residue of **3.3b** was dissolved in diethyl ether containing one drop of CH_2Cl_2 and cooled to -20 °C to give colorless crystals suitable for X-ray analysis. A colorless tablet-like crystal of molecular formula $C_{43}H_{60}AuF_3N_2O_5S_2$ with the

approximate dimensions 0.116 mm × 0.151 mm × 0.289 mm was used for the X-ray crystallographic analysis. The X-ray intensity data were measured on a Bruker-Nonius X8 Kappa APEX II system equipped with a fine-focus sealed tube (MoKα, λ = 0.71073 Å) and a graphite monochromator, with a total exposure time of 10.88 hours. The frames were integrated with the Bruker SAINT software package using a narrow-frame algorithm. The integration of the data using a triclinic unit cell yielded a total of 225246 reflections to a maximum θ angle of 37.94° (0.58 Å resolution), of which 24809 were independent (average redundancy 9.079, completeness = 99.5%, R_{int} = 4.72%, R_{sig} = 2.91%) and 21952 (88.48%) were greater than $2\sigma(F^2)$. The final cell constants of a = 10.5055(9) Å, b = 14.9092(12) Å, c = 16.1332(13) Å, α = 70.640(2)°, β = 78.647(2)°, γ = 76.645(2)°, volume = 2299.6(3) $Å^3$, are based upon the refinement of the XYZ-centroids of 810 reflections above 20 σ(I) with 4.558° < 2θ < 68.09°. Data were corrected for absorption effects using the numerical method (SADABS). The ratio of minimum to maximum apparent transmission was 0.627. The calculated minimum and maximum transmission coefficients (based on crystal size) are 0.4450 and 0.6980. The final anisotropic full-matrix least-squares refinement on F^2 with 518 variables converged at R1 = 2.30%, for the observed data and wR2 = 4.86% for all data. The goodness-of-fit was 1.049. The largest peak in the final difference electron density synthesis was 1.302 $e^-/Å^3$ and the largest

hole was –0.856 $e^-/Å^3$ with an RMS deviation of 0.106 $e^-/Å^3$. On the basis of the final model, the calculated density was 1.449 g/cm^3 and F(000), 1020 e^-.

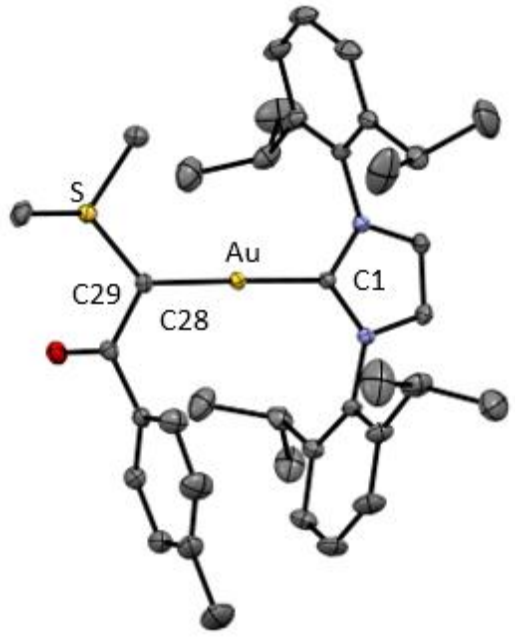

Figure 19. ORTEP diagram of gold(I) α-oxo carbenoid complex 3.3b with ellipsoids shown at 50% probability level and with counterion, solvent, and hydrogen atoms omitted.

Table 11. Bond lengths of complex 3.3b.

Bond	Length(Å)	Bond	Length(Å)
Au1-C1	2.0045(11)	Au1-C28	2.0836(12)
S1-C28	1.7853(12)	S1-C37	1.7911(14)
S1-C38	1.7928(14)	O1-C29	1.2287(15)
N1-C1	1.3494(15)	N1-C2	1.3823(15)
N1-C4	1.4422(15)	N2-C1	1.3519(14)
N2-C3	1.3827(15)	N2-C16	1.4375(15)
C2-C3	1.3489(17)	C2-H2	0.95
C3-H3	0.95	C4-C9	1.3964(18)
C4-C5	1.3975(18)	C5-C6	1.3976(19)

C5-C10	1.518(2)	C6-C7	1.375(2)
C6-H6	0.95	C7-C8	1.390(2)
C7-H7	0.95	C8-C9	1.3983(19)
C8-H8	0.95	C9-C13	1.512(2)
C10-C11	1.521(3)	C10-C12	1.526(2)
C10-H10	1	C11-H11A	0.98
C11-H11B	0.98	C11-H11C	0.98
C12-H12A	0.98	C12-H12B	0.98
C12-H12C	0.98	C13-C15	1.523(2)
C13-C14	1.532(2)	C13-H13	1
C14-H14A	0.98	C14-H14B	0.98
C14-H14C	0.98	C15-H15A	0.98
C15-H15B	0.98	C15-H15C	0.98
C16-C17	1.3954(18)	C16-C21	1.3981(18)
C17-C18	1.3957(19)	C17-C22	1.513(2)
C18-C19	1.380(2)	C18-H18	0.95
C19-C20	1.386(2)	C19-H19	0.95
C20-C21	1.3952(19)	C20-H20	0.95
C21-C25	1.516(2)	C22-C24	1.519(2)
C22-C23	1.528(2)	C22-H22	1
C23-H23A	0.98	C23-H23B	0.98
C23-H23C	0.98	C24-H24A	0.98
C24-H24B	0.98	C24-H24C	0.98
C25-C26	1.506(3)	C25-C27	1.516(2)
C25-H25	1	C26-H26A	0.98
C26-H26B	0.98	C26-H26C	0.98
C27-H27A	0.98	C27-H27B	0.98
C27-H27C	0.98	C28-C29	1.4856(17)
C28-H28	1	C29-C30	1.4936(17)
C30-C31	1.390(2)	C30-C35	1.3927(19)
C31-C32	1.393(2)	C31-H31	0.95
C32-C33	1.393(3)	C32-H32	0.95
C33-C34	1.387(2)	C33-C36	1.502(2)
C34-C35	1.3873(19)	C34-H34	0.95
C35-H35	0.95	C36-H36A	0.98
C36-H36B	0.98	C36-H36C	0.98

C37-H37A	0.98	C37-H37B	0.98
C37-H37C	0.98	C38-H38A	0.98
C38-H38B	0.98	C38-H38C	0.98
S2-O3	1.4285(13)	S2-O2	1.4373(13)
S2-O4	1.4386(14)	S2-C39	1.8172(16)
F1-C39	1.3355(18)	F2-C39	1.3287(18)
F3-C39	1.3246(19)	O1S-C3S	1.415(2)
O1S-C1S	1.420(3)	C1S-C2S	1.502(3)
C1S-H1SA	0.99	C1S-H1SB	0.99
C2S-H2SA	0.98	C2S-H2SB	0.98
C2S-H2SC	0.98	C3S-C4S	1.502(3)
C3S-H3SA	0.99	C3S-H3SB	0.99
C4S-H4SA	0.98	C4S-H4SB	0.98
C4S-H4SC	0.98		

Table 12. Bond angles of complex 3.3b.

Bond	Angle(°)	Bond	Angle(°)
C1-Au1-C28	179.01(5)	C28-S1-C37	102.47(6)
C28-S1-C38	103.33(6)	C37-S1-C38	100.67(7)
C1-N1-C2	110.96(10)	C1-N1-C4	124.83(10)
C2-N1-C4	124.14(10)	C1-N2-C3	111.25(10)
C1-N2-C16	123.93(10)	C3-N2-C16	124.62(10)
N1-C1-N2	104.63(10)	N1-C1-Au1	128.04(8)
N2-C1-Au1	127.31(8)	C3-C2-N1	106.88(11)
C3-C2-H2	126.6	N1-C2-H2	126.6
C2-C3-N2	106.28(10)	C2-C3-H3	126.9
N2-C3-H3	126.9	C9-C4-C5	124.21(11)
C9-C4-N1	118.28(11)	C5-C4-N1	117.51(11)
C4-C5-C6	116.94(13)	C4-C5-C10	122.52(12)
C6-C5-C10	120.51(13)	C7-C6-C5	120.55(14)
C7-C6-H6	119.7	C5-C6-H6	119.7
C6-C7-C8	121.06(13)	C6-C7-H7	119.5
C8-C7-H7	119.5	C7-C8-C9	120.88(14)
C7-C8-H8	119.6	C9-C8-H8	119.6
C4-C9-C8	116.28(13)	C4-C9-C13	122.10(11)

C8-C9-C13	121.55(12)	C5-C10-C11	110.74(15)
C5-C10-C12	112.30(14)	C11-C10-C12	111.59(15)
C5-C10-H10	107.3	C11-C10-H10	107.3
C12-C10-H10	107.3	C10-C11-H11A	109.5
C10-C11-H11B	109.5	H11A-C11-H11B	109.5
C10-C11-H11C	109.5	H11A-C11-H11C	109.5
H11B-C11-H11C	109.5	C10-C12-H12A	109.5
C10-C12-H12B	109.5	H12A-C12-H12B	109.5
C10-C12-H12C	109.5	H12A-C12-H12C	109.5
H12B-C12-H12C	109.5	C9-C13-C15	113.00(13)
C9-C13-C14	110.80(13)	C15-C13-C14	109.98(13)
C9-C13-H13	107.6	C15-C13-H13	107.6
C14-C13-H13	107.6	C13-C14-H14A	109.5
C13-C14-H14B	109.5	H14A-C14-H14B	109.5
C13-C14-H14C	109.5	H14A-C14-H14C	109.5
H14B-C14-H14C	109.5	C13-C15-H15A	109.5
C13-C15-H15B	109.5	H15A-C15-H15B	109.5
C13-C15-H15C	109.5	H15A-C15-H15C	109.5
H15B-C15-H15C	109.5	C17-C16-C21	123.95(11)
C17-C16-N2	118.45(11)	C21-C16-N2	117.60(11)
C16-C17-C18	116.75(13)	C16-C17-C22	121.95(11)
C18-C17-C22	121.30(12)	C19-C18-C17	121.00(14)
C19-C18-H18	119.5	C17-C18-H18	119.5
C18-C19-C20	120.72(13)	C18-C19-H19	119.6
C20-C19-H19	119.6	C19-C20-C21	120.83(14)
C19-C20-H20	119.6	C21-C20-H20	119.6
C20-C21-C16	116.74(13)	C20-C21-C25	120.95(13)
C16-C21-C25	122.31(11)	C17-C22-C24	112.13(15)
C17-C22-C23	111.08(13)	C24-C22-C23	112.01(16)
C17-C22-H22	107.1	C24-C22-H22	107.1
C23-C22-H22	107.1	C22-C23-H23A	109.5
C22-C23-H23B	109.5	H23A-C23-H23B	109.5
C22-C23-H23C	109.5	H23A-C23-H23C	109.5
H23B-C23-H23C	109.5	C22-C24-H24A	109.5
C22-C24-H24B	109.5	H24A-C24-H24B	109.5
C22-C24-H24C	109.5	H24A-C24-H24C	109.5

H24B-C24-H24C	109.5	C26-C25-C27	111.99(18)
C26-C25-C21	111.76(13)	C27-C25-C21	111.73(14)
C26-C25-H25	107	C27-C25-H25	107
C21-C25-H25	107	C25-C26-H26A	109.5
C25-C26-H26B	109.5	H26A-C26-H26B	109.5
C25-C26-H26C	109.5	H26A-C26-H26C	109.5
H26B-C26-H26C	109.5	C25-C27-H27A	109.5
C25-C27-H27B	109.5	H27A-C27-H27B	109.5
C25-C27-H27C	109.5	H27A-C27-H27C	109.5
H27B-C27-H27C	109.5	C29-C28-S1	107.95(8)
C29-C28-Au1	106.15(8)	S1-C28-Au1	111.27(6)
C29-C28-H28	110.5	S1-C28-H28	110.5
Au1-C28-H28	110.5	O1-C29-C28	122.15(11)
O1-C29-C30	120.11(11)	C28-C29-C30	117.72(10)
C31-C30-C35	119.13(12)	C31-C30-C29	122.47(12)
C35-C30-C29	118.26(11)	C30-C31-C32	119.66(15)
C30-C31-H31	120.2	C32-C31-H31	120.2
C33-C32-C31	121.48(15)	C33-C32-H32	119.3
C31-C32-H32	119.3	C34-C33-C32	118.20(14)
C34-C33-C36	120.89(17)	C32-C33-C36	120.89(16)
C33-C34-C35	120.85(14)	C33-C34-H34	119.6
C35-C34-H34	119.6	C34-C35-C30	120.62(13)
C34-C35-H35	119.7	C30-C35-H35	119.7
C33-C36-H36A	109.5	C33-C36-H36B	109.5
H36A-C36-H36B	109.5	C33-C36-H36C	109.5
H36A-C36-H36C	109.5	H36B-C36-H36C	109.5
S1-C37-H37A	109.5	S1-C37-H37B	109.5
H37A-C37-H37B	109.5	S1-C37-H37C	109.5
H37A-C37-H37C	109.5	H37B-C37-H37C	109.5
S1-C38-H38A	109.5	S1-C38-H38B	109.5
H38A-C38-H38B	109.5	S1-C38-H38C	109.5
H38A-C38-H38C	109.5	H38B-C38-H38C	109.5
O3-S2-O2	117.28(10)	O3-S2-O4	114.87(10)
O2-S2-O4	113.11(8)	O3-S2-C39	102.33(8)
O2-S2-C39	103.52(7)	O4-S2-C39	103.18(9)
F3-C39-F2	107.31(13)	F3-C39-F1	107.90(14)

F2-C39-F1	106.89(13)	F3-C39-S2	111.14(12)
F2-C39-S2	111.63(11)	F1-C39-S2	111.73(11)
C3S-O1S-C1S	112.77(16)	O1S-C1S-C2S	108.34(18)
O1S-C1S-H1SA	110	C2S-C1S-H1SA	110
O1S-C1S-H1SB	110	C2S-C1S-H1SB	110
H1SA-C1S-H1SB	108.4	C1S-C2S-H2SA	109.5
C1S-C2S-H2SB	109.5	H2SA-C2S-H2SB	109.5
C1S-C2S-H2SC	109.5	H2SA-C2S-H2SC	109.5
H2SB-C2S-H2SC	109.5	O1S-C3S-C4S	109.00(17)
O1S-C3S-H3SA	109.9	C4S-C3S-H3SA	109.9
O1S-C3S-H3SB	109.9	C4S-C3S-H3SB	109.9
H3SA-C3S-H3SB	108.3	C3S-C4S-H4SA	109.5
C3S-C4S-H4SB	109.5	H4SA-C4S-H4SB	109.5
C3S-C4S-H4SC	109.5	H4SA-C4S-H4SC	109.5
H4SB-C4S-H4SC	109.5		

Table 13. Dihedral angles of complex 3.3b.

Bond	Angle(°)	Bond	Angle(°)
C2-N1-C1-N2	0.25(13)	C4-N1-C1-N2	177.19(11)
C2-N1-C1-Au1	178.79(9)	C4-N1-C1-Au1	-4.27(17)
C3-N2-C1-N1	-0.01(13)	C16-N2-C1-N1	-174.92(11)
C3-N2-C1-Au1	-178.56(9)	C16-N2-C1-Au1	6.53(17)
C1-N1-C2-C3	-0.40(15)	C4-N1-C2-C3	-177.37(11)
N1-C2-C3-N2	0.38(14)	C1-N2-C3-C2	-0.24(15)
C16-N2-C3-C2	174.63(12)	C1-N1-C4-C9	94.35(15)
C2-N1-C4-C9	-89.11(15)	C1-N1-C4-C5	-86.79(15)
C2-N1-C4-C5	89.75(15)	C9-C4-C5-C6	2.9(2)
N1-C4-C5-C6	-175.88(13)	C9-C4-C5-C10	-175.20(14)
N1-C4-C5-C10	6.0(2)	C4-C5-C6-C7	-1.5(2)
C10-C5-C6-C7	176.60(16)	C5-C6-C7-C8	-0.6(3)
C6-C7-C8-C9	1.7(3)	C5-C4-C9-C8	-1.9(2)
N1-C4-C9-C8	176.86(12)	C5-C4-C9-C13	175.12(13)
N1-C4-C9-C13	-6.11(19)	C7-C8-C9-C4	-0.4(2)
C7-C8-C9-C13	-177.47(15)	C4-C5-C10-C11	118.04(18)
C6-C5-C10-C11	-60.0(2)	C4-C5-C10-C12	-116.46(17)

C6-C5-C10-C12	65.5(2)	C4-C9-C13-C15	136.12(15)
C8-C9-C13-C15	-47.0(2)	C4-C9-C13-C14	-99.94(16)
C8-C9-C13-C14	76.94(18)	C1-N2-C16-C17	-92.70(15)
C3-N2-C16-C17	93.06(15)	C1-N2-C16-C21	87.33(15)
C3-N2-C16-C21	-86.91(15)	C21-C16-C17-C18	0.14(19)
N2-C16-C17-C18	-179.82(11)	C21-C16-C17-C22	-178.92(12)
N2-C16-C17-C22	1.11(18)	C16-C17-C18-C19	0.3(2)
C22-C17-C18-C19	179.36(14)	C17-C18-C19-C20	-0.6(2)
C18-C19-C20-C21	0.4(2)	C19-C20-C21-C16	0.0(2)
C19-C20-C21-C25	179.76(14)	C17-C16-C21-C20	-0.29(19)
N2-C16-C21-C20	179.68(11)	C17-C16-C21-C25	179.97(12)
N2-C16-C21-C25	-0.06(18)	C16-C17-C22-C24	-126.92(16)
C18-C17-C22-C24	54.1(2)	C16-C17-C22-C23	106.90(15)
C18-C17-C22-C23	-72.12(17)	C20-C21-C25-C26	68.8(2)
C16-C21-C25-C26	-111.42(18)	C20-C21-C25-C27	-57.5(2)
C16-C21-C25-C27	122.20(17)	C37-S1-C28-C29	-179.61(9)
C38-S1-C28-C29	76.08(10)	C37-S1-C28-Au1	-63.51(8)
C38-S1-C28-Au1	-167.82(7)	S1-C28-C29-O1	11.69(15)
Au1-C28-C29-O1	-107.70(12)	S1-C28-C29-C30	-170.02(9)
Au1-C28-C29-C30	70.59(12)	O1-C29-C30-C31	-145.86(14)
C28-C29-C30-C31	35.82(18)	O1-C29-C30-C35	29.90(18)
C28-C29-C30-C35	-148.42(12)	C35-C30-C31-C32	-1.6(2)
C29-C30-C31-C32	174.13(15)	C30-C31-C32-C33	1.9(3)
C31-C32-C33-C34	-0.3(3)	C31-C32-C33-C36	178.32(18)
C32-C33-C34-C35	-1.6(2)	C36-C33-C34-C35	179.77(16)
C33-C34-C35-C30	1.9(2)	C31-C30-C35-C34	-0.3(2)
C29-C30-C35-C34	-176.19(12)	O3-S2-C39-F3	55.86(14)
O2-S2-C39-F3	178.20(12)	O4-S2-C39-F3	-63.70(13)
O3-S2-C39-F2	-63.91(14)	O2-S2-C39-F2	58.43(13)
O4-S2-C39-F2	176.53(11)	O3-S2-C39-F1	176.45(13)
O2-S2-C39-F1	-61.21(13)	O4-S2-C39-F1	56.89(13)
C3S-O1S-C1S-C2S	-177.07(18)	C1S-O1S-C3S-C4S	178.10(17)

4. Direct Observation and Characterization of Cyclized Gold(I)-Alkenoxysulfonium Intermediate.

4.1 Background

The oxidation of alkynes utilizing gold(I) catalysts have attracted considerable attention over the past decade owing to cationic gold(I) complexes relevant ability for the functionalization of C-C multiple bonds.[3,29,80,81] Specifically, a variety of reactions have been recorded using sulfoxides, heterocyclic *N*-oxides, and similar nucleophilic oxidants containing an oxygen atom bound to a leaving group as the oxygen transfer agent in cationic gold(I)-catalyzed alkyne oxidation reactions.[53-56,59,127,128] It is common in these reactions for the oxidant to be tethered to the alkyne. Although interest and applications surrounding cationic gold(I) complexes in organic synthesis has risen, there is still little known regarding the mechanism intermediates formed in these transformations.

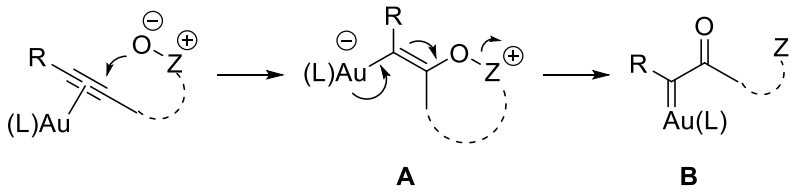

Scheme 18. Generation of *N*-alkenoxypyridinium/sulfonium species (A) and carbene (B) with a tethered oxygen source and leaving group (Z).

Currently, there are two proposed mechanisms for oxygen atom transfer reactions. First, the nucleophilic oxidant attacks a carbon of an activated gold π-alkyne

complex to form a gold alkenoxysulfonium/pyridinium intermediate (**A**) followed by heterolytic cleavage of the oxygen bound leaving group to form a reactive α-oxo gold carbene complex (**B**) (Scheme 18). Alternatively, after formation of gold alkenoxysulfonium/pyridinium complex (**A**), the reaction may completely bypass the α-oxo gold carbene complex (**B**) in favor of alternate lower energy non-carbene pathways.[56,58,62,92] There is also research to support formation of a gold-oxide bond forming first before forming an gold alkenoxysulfonium/pyridinium complex (**A**).[59,137] Despite the many applications of these oxygen atom transfer reagent in gold(I) catalysis, direct observation of key gold alkenoxysulfonium/pyridinium species has yet to be achieved, resulting in significant gaps in our understanding of the structure and reactivities of these intermediates and their role in the mechanism of gold(I)-catalyzed alkyne oxidation transformations.

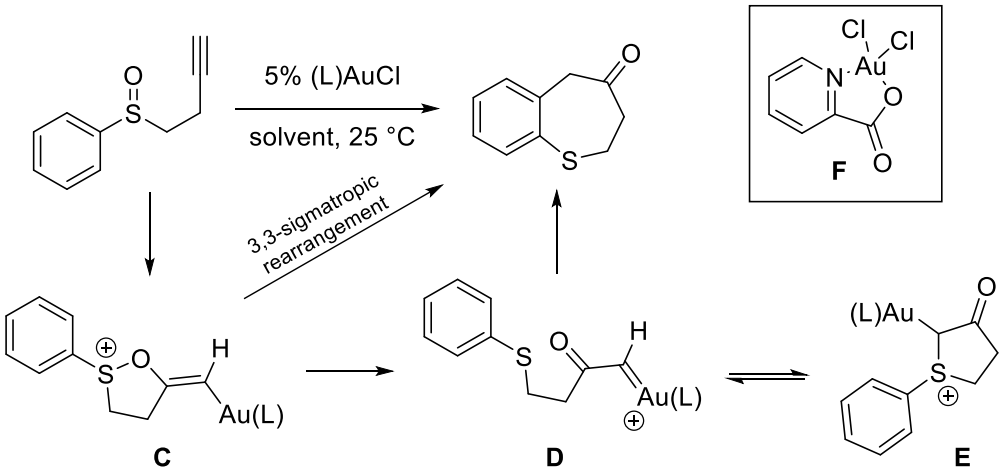

Scheme 19. Reported intramolecular rearrangement of alkynyl sulfoxides. Toste conditions: (IMes)AuCl/AgSbF$_6$ (5 mol %), CH$_2$Cl$_2$.[75] Zhang conditions: Catalyst F (5 mol %), 1,2-dichloroethane.[76]

Recently, gold(I)-catalysis has been reported to synthesize dihydrobenzothiephinones from sulfoxides tethered to alkynes (Scheme 19).[75,76] After treatment of homopropargyl sulfoxides with a gold catalyst, these reported reactions often evoke a 5-*exo*-dig cyclization (**C**), gold alkenoxysulfonium complex, that has yet to be observed. Toste then proposes the mechanism progresses to a gold α-oxo carbene intermediate (**D**)(Scheme 19).[75] In addition to the formation of **D** being unfavored by DFT calculations,[56,60,76] Zhang hypothesizes that formation of **D** would result in the sulfonium ion resting state, **E**. Instead, Zhang proposed **C** undergoes a [3,3]-sigmatropic rearrangement to form the dihydrobenzothiephinone product.[60] As none of these intermediates have been observed within the confines of these oxygen atom transfer reactions, there remains much debate surrounding the mechanism of these

transformations. Herein we report the observation and characterization of cyclized intermediate **C**, observed in stoichiometric low temperature conditions.

4.2 Characterization of N-Alkenoxysulfonium Species

4.2.1 Low-Temperature Characterization

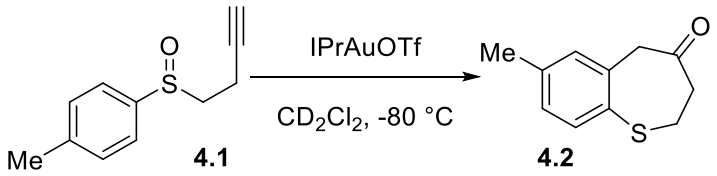

Figure 20. Stoichiometric reaction studied at low temperatures to observe intermediates.

Toward detection of intermediate **C**, we investigated the gold(I)-catalyzed conversion of but-1-yn-4-yl(*p*-tolyl)sulfoxide (**4.1**) into 1-benzothiepin-4-one (**4.2**) (Figure 20). In an initial experiment, a 1:1 mixture of alkynyl sulfoxide (9.2 mg, 4.8 x 10^{-2} mmol) and (IPr)AuOTf (36 mg, 4.8 x 10^{-2} mmol) in CD_2Cl_2 was mixed thoroughly at -78 °C. ^{1}H NMR analysis at -80 °C showed formation of an intermediate with a diagnostic peak at δ 5.50, which was attributed to species **4.4**, which constituted 40 % yield from the initial starting material **4.1** (Scheme 20). Complex **4.4** was thermally unstable and characterized at or below -60 °C by NMR spectroscopy. When this solution was warmed at -20 °C for 2 h, **4.1** was consumed to form 1-benzothiepin-4-one bound to gold (**4.3**) at 100 % yield from **4.4** (determined via ^{1}H NMR spectroscopy). Throughout complete conversion of **4.4** to **4.3**, no observed peaks were observed that could be assigned to α-oxo carbene

intermediate (**B**) or any other organometallic species. Upon recrystallization of the reaction mixture at room temperature, the gold bound 1-benzothiepin-4-one complex **4.3** converted entirely to **4.2** and (IPr)AuOTf.

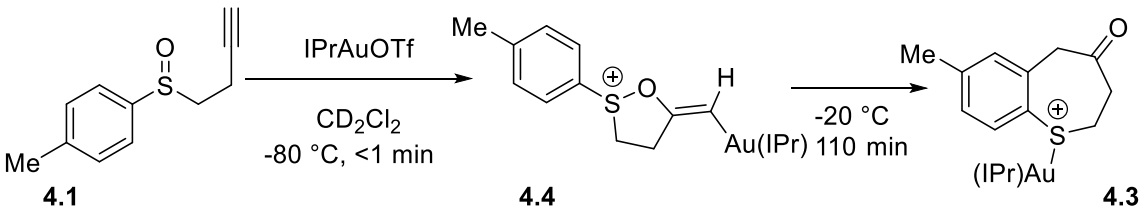

Scheme 20. Generation of proposed N-alkenoxysulfonium intermediate (4.4) at low temperatures.

4.2.2 Isotopic Labeling Experiments

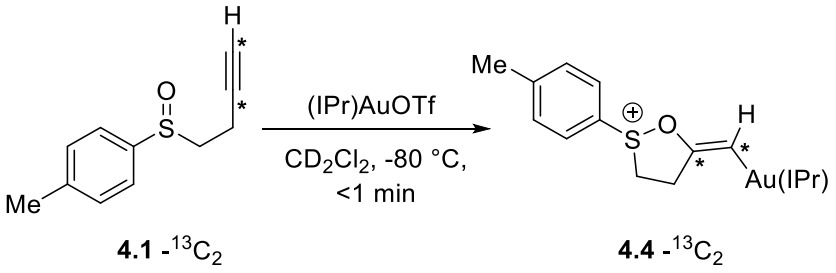

Figure 21. Isotopic labeling experiment with carbon-13 to identify vinyl carbons via NMR.

To further characterize complex **4.4**, isotopically labeled **4.1**-$^{13}C_2$ (25% $^{13}C_2$) and treated with (IPr)AuOTf in a 1:1 mixture in CD_2Cl_2 at -78 °C (<1 min) to identify the alkene carbons in the ^{13}C NMR spectra of **4.4**-$^{13}C_2$ (Figure 21). The proton-decoupled ^{13}C NMR spectrum of **4.4**-$^{13}C_2$ (at -60 °C) displayed doublets at δ 156.8 (d, J_{CC} = 81.6 Hz) and δ 102.7 (d, J_{CC} = 81.6 Hz) assigned to the alkenyl carbon atoms α- and β-to gold,

respectively. When compared to similar reported enol ether compounds, such as (E)-2-ethylidene-tetrahydrofuran, the alkene carbon labeled atoms in the ^{13}C NMR spectra of **4.4**-$^{13}C_2$ align with the reported alkene enol ether peaks.[154] Additionally, ^{1}H NMR analysis of **4.4**-$^{13}C_2$ (at -60 °C) displayed a doublet of doublets at δ 5.49 (dd, J_{CH} = 149.0, 6.2 Hz, 1H) assigned to the vinylic proton of **4.4**-$^{13}C_2$ that was superimposed on a singlet at δ 5.50 corresponding the vinylic resonance of unlabeled **4.4**.

In a second set of experiments, isotopically-labelled **4.1**-d_1 bearing an C(sp)–D bond was treated with (IPr)AuOTf yielded **4.4**-d_1 at -78 °C (time) and analyzed without isolation by ^{1}H and ^{13}C NMR spectroscopy. The ^{1}H NMR spectra of **4.4**-d_1 also showed decreased intensity of the singlet at δ 5.50 relative to the intensity of the singlet at δ 5.50 in the unlabeled 4.4 ^{1}H NMR spectrum, which supports the assignment of the resonance at δ 5.50 as the vinylic proton of 4.4. The ^{13}C NMR spectrum of **4.4**-d_1 displayed significant attenuation of the intensity of the vinylic resonance at δ 102.7 relative to that of unlabeled **4.4** owing to the one-bond carbon-deuterium coupling and absence of NOE enhancement. In comparison the vinylic resonance of **4.4**-d_1 at δ 156.8 was not significantly attenuated relative to that of unlabeled **4.4.** Taken together, these observations indicate that the resonance at δ 102.7 corresponds to the α-H and the δ 156.8 peak corresponds to the β-H, and that 5-*exo*-dig intermediate forms, as opposed to the 6-*endo*-dig (**4.5**-d_1). It was then confirmed that **4.4** (5-*exo*-dig) was the observed

intermediate as opposed to the 6-*endo*-dig intermediate via deuterium labeling experiments (Figure 22).

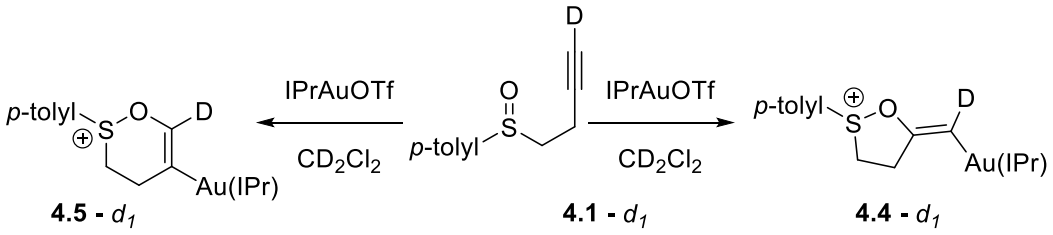

Figure 22. Isotopic labeling experiment to determine whether the 6-*endo*-dig (4.5) intermediate or the 5-*exo*-dig (4.4) intermediate forms.

4.2.2.1 Treatment of *N*-alkenoxysulfonium species with a nucleophile

In an attempt to trap and observe other potential intermediates, specifically a gold α-oxo carbenoid intermediate, nucleophiles, such as 4-picoline, were introduced to the reaction mixture after the generation of compound **4.4** (Figure 2). To this end, a solution of **4.4** was generated with but-1-yn-4-yl(p-tolyl)sulfoxide (**4.1**) (5.5 mg, 2.9 x 10^{-2} mmol) and (IPr)AuOTf (21 mg, 2.9 x 10^{-2} mmol) in CD_2Cl_2 at -78 °C, then was treated with 4-picoline (1 equiv) in at -78 °C and promptly (~3 min) analyzed by ^{1}H NMR spectroscopy, which revealed the disappearance of the vinylic resonance of **4.4** at δ 5.50 and the appearance of a singlet of equal intensity at δ 5.88 without significant perturbation of any of the other peaks in the ^{1}H NMR spectrum. ^{1}H NMR analysis of the solution generated via addition of picoline to the ^{13}C-labeled isotopomer **4.4**-$^{13}C_2$ at -78

°C immediately displayed a doublet of doublets at δ 5.88 (dd, J_{CH} = 149.0, 6.2 Hz, 1H) assigned to the vinylic resonance. Importantly, both the one-bond and two-bond carbon-hydrogen coupling constants were not significantly different from $^{1}J_{CH}$ and $^{2}J_{CH}$ for **4.4**-$^{13}C_2$. In the ^{13}C NMR spectrum of a solution of **4.4**-$^{13}C_2$ and picoline the labeled alkene peaks were only slightly affected in the ^{13}C NMR spectra, located at resonances δ 157.7(d, J_{CC} = 81.6 Hz) and δ 103.8 (d, J_{CC} = 81.6 Hz).

Addition of either tetrahydrothiophene or trimethyl phosphite to a solution of **4.4** in CD_2Cl_2 at -78 °C also led to a shift in the chemical shift of the vinylic proton of **4.4** from δ 5.50 to δ 5.88. In comparison, weaker Lewis bases, such as diphenyl sulfide and triphenyl phosphine did not cause a α-H shift. These observations are attributed to a hydrogen bonding effect due to the addition of the nucleophile (Figure 23).

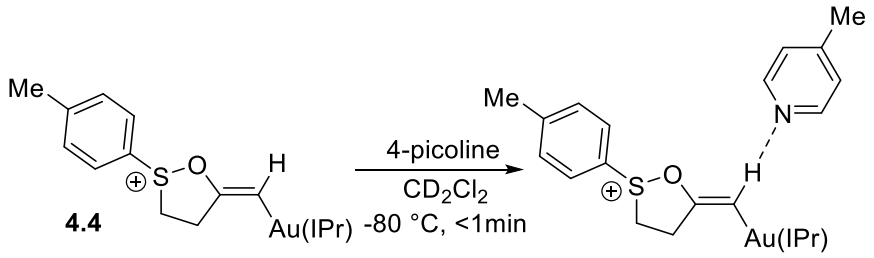

Figure 23. Hypothesized hydrogen bonding structure when 4.4 is treated with 4-picoline.

While hydrogen bonding commonly results in increased shielding of a proton, the adjacent alkene could explain as to why and increase in chemical shift is observed from δ 5.50 to δ 5.88. The resulting pull of electron density away from the oxygen and

towards the hydrogen as a result of hydrogen bonding, could also explained the increased stability of **4.4** in the presence of 4-picoline, which was discovered during kinetic studies.

4.3 Kinetic Analysis of the conversion of 4.4 to 4.3

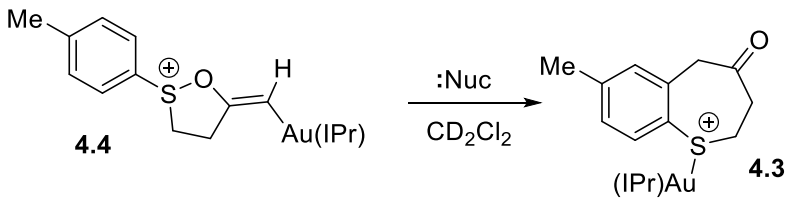

Figure 24. Decomposition of 4.4 studied for kinetic data.

Temperature (°C)	Nucleophile	Time (min)	k ($M^{-1}s^{-1}$)
-20	none	110	0.113 ± 0.002
-15	none	60	0.224 ± 0.002
-10	none	100	0.207 ± 0.005
-5	none	40	0.507 ± 0.01
0	none	30	0.735 ± 0.05
-20	4-picoline[a]	280	0.023 ± 0.0004

Table 14. Observed rate constants from second order reactions of 4.4 (17 mM) at varying temperatures in CD_2Cl_2. [a]With 4-picoline present, the reaction yields 4.2.

The kinetics of the conversion of **4.4** to **4.3** were analyzed employing ^{1}H NMR analysis. When a solution of **4.4** (17 mM) was generated at -80 °C in CD_2Cl_2 and warmed to -20 °C, disappearance of **4.4** displayed second-order decay to 3 half-lives with a second-order rate constant of 0.113 ± 0.002 M–1 s–1 (Figures 26-31) with the formation of **4.3** (Figure 24). Second-order rate constants for the disappearance of **4.4** were determined as a function of temperature from –20 to 0 °C (Table 14). Eyring analysis of

the resulting data provided activation parameters: $\Delta H^{\ddagger}$ = 12.1 kcal and $\Delta S^{\ddagger}$ = -14.9 kcal/mol K (Figure 25), indicating a distinct ring opening step, suggesting **4.4** does not undergo a [3,3}-sigmatropic rearrangement as hypothesized by Zhang.[60] It was also observed that addition of 4-picoline to **4.4** decreased the rate constant for disappearance of **4.4** by a factor of ~5, from k = 0.113 ± 0.002 $M^{-1}s^{-1}$ to k = 0.023 ± 0.0004 $M^{-1}s^{-1}$ at -20 °C. This decrease in reactivity of **4.4** in the presence of picoline can be attributed to the hydrogen bonding pulling the electronegativity of the double bond away from the oxygen, thereby slowing down the formation of the carbonyl needed for a ring opening step.

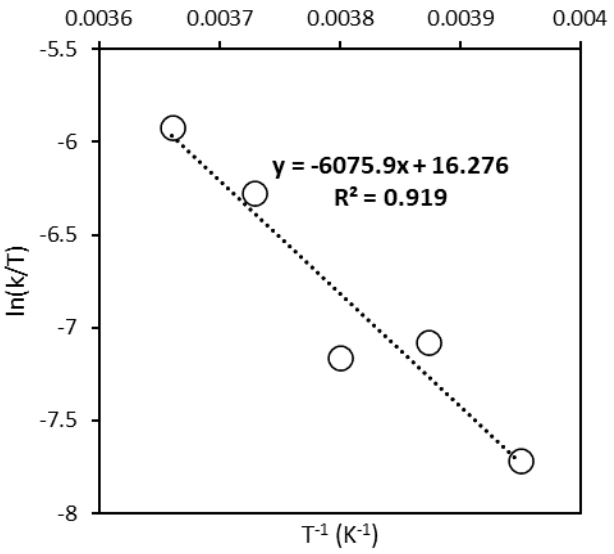

Figure 25. Eyring plot of transformation from complex 4.4 to 4.2 at temperatures ranging from -20 to 0°C. Calculated $\Delta H^{\ddagger}$ = 12.1 kcal and $\Delta S^{\ddagger}$ = -14.9 kcal/molK.

4.4 Synthesis of Gold N-Oxides and Sulfoxides

4.4.1 Isolation of Gold-Oxides

Previously, Fiksdahl[137] has reported a series of gold-nitrone complexes, proving the gold-oxygen bond is strong enough to form stable gold-oxide compounds. To expand on the series of known gold-oxide compounds, three gold-oxide compounds were characterized following the reported procedure for synthesis of gold-nitrone complexes (Scheme 21).

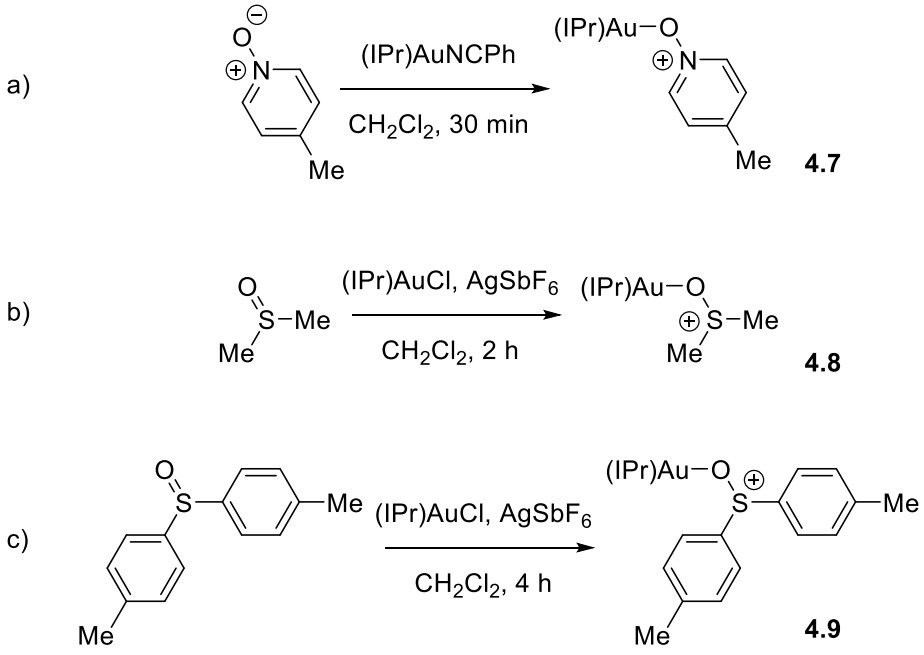

Scheme 21. Synthesis of gold-oxide complexes 4.7-4.9.

A solution of gold complex (1 equivalent) was combined with an excess of appropriate oxide and dissolved in dichloromethane. When required, 1 equivalent of $AgSbF_6$ was added to perform an anion exchange. Synthesis of gold picoline N-oxide

(**4.7**) could be carried out with either (IPr)AuNCPh, (IPr)AuOTf,, or (IPr)AuCl/$AgSbF_6$ with similar yields. Compounds **4.7-4.9** were isolated via filtration of reaction mixture through Celite and recrystallization.

4.4.2 Reactions of Gold(I) *N*-Oxides and Sulfoxides with Alkynes

The synthesized gold-oxides complexes (**4.7-4.9**) were then treated with 3-hexyne and *p*-tolylacetylene in a series of displacement reactions. Gold π-alkyne complexes were also synthesized using reported procedures[30,133-135] and treated with *N*-oxides and sulfoxides to further test the reactivity.

4.4.2.1 Gold (I) Picoline *N*-Oxide with Alkynes

Complex **4.7** (10 mg, 1.4 x 10^{-2} mmol) was treated with one equivalent terminal alkyne *p*-tolylacetylene in CD_2Cl_2 at room temperature and immediately to yield σ,π-acetylide complex {[(IPr)Au]$_2$(η^1,η^2-C≡C(4-C_6H_4Me))} *in situ*, which has been reported to form from [(IPr)Au(η^2-HC≡C(4-C_6H_4Me))]$^+SbF_6^-$ at in 1 hour at temperatures above 0 °C.[134] When **4.7** (15 mg, 2.2 x 10^{-2} mmol) was treated with 3-hexyne, (2.44 μL, 2.2 x 10^{-2} mmol) and CH_2Br_2 (1.5 μL, 2.2 x 10^{-2} mmol), as an internal standard, in CD_2Cl_2 at room temperature, and was immediately analyzed by ^{1}H NMR, finding 4-hexen-3-one (23 % ^{1}H NMR yield) and (IPr)Au-(4-picoline) were obtained (Scheme 22). When [(IPr)Au(η^2-EtC≡CEt)]$^+SbF_6^-$ (15 mg, 1.7 x 10^{-2} mmol) was treated with PNO (1.8 mg, 1.7 x 10^{-2} mmol) and CH_2Br_2 (1.2 μL, 1.7 x 10^{-2} mmol), as an internal standard, in CD_2Cl_2 at room

temperature, again, immediately yielding 4-hexen-3-one (23 % ^{1}H NMR yield) and (IPr)Au-(4-picoline). The products, 4-hexen-3-one and (IPr)Au(4-picoline), confirmed by reported NMR spectra.[114,136] As the spectra of 4-hexen-3-one and (IPr)Au(4-picoline) *in situ* matched the reported NMR spectra for each compound, they reaction mixture was not further worked up. As starting with either compound **4.7** or [(IPr)Au(η^2-EtC≡CEt)]$^{+}$SbF$_6^{-}$ results in the same product mixture, it can be concluded that both reactions are going through the same intermediate, likely an N-alkenoxypyridinium species (Scheme 22, intermediate **I**).

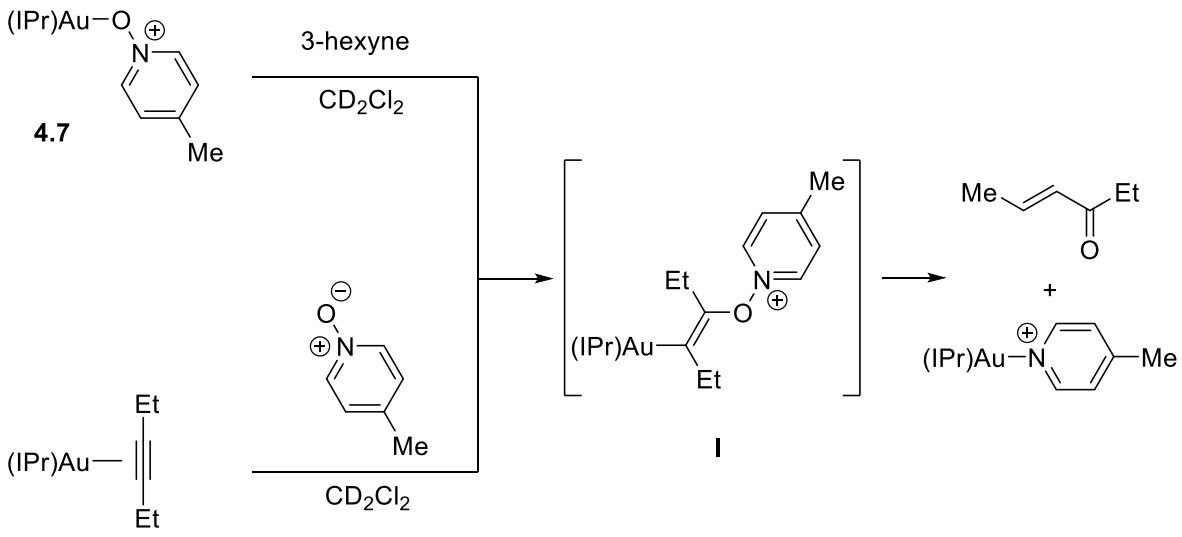

Scheme 22. Oxygen atom transfer reaction resulted in the same products whether starting with the gold-*N*-oxide or the gold π-alkyne complex. This indicates both pathways form intermediate I.

4.4.2.2 Gold (I) Sulfoxides with Alkynes

Sulfoxide complexes **4.8** and **4.9** were treated with terminal alkyne *p*-tolylacetylene and internal alkyne 3-hexyne (Scheme 23). Complex **4.8** (25 mg, 3.0 x 10^{-2} mmol) was dissolved in an NMR tube with CD_2Cl_2 (600 μL), then treated with *p*-tolylacetylene (3.9 μL, 3.0 x 10^{-2} mmol). Complex **4.9** (25 mg, 2.4 x 10^{-2} mmol) was dissolved in an NMR tube with CD_2Cl_2 (600 μL), then treated with *p*-tolylacetylene (3.0 μL, 2.4 x 10^{-2} mmol). After addition of the alkyne, the NMR tube was inverted three times and the reaction mixture was immediately analyzed by ^{1}H NMR spectroscopy to yield {[(IPr)Au]$_2$(η^1,η^2-C≡C(4-C_6H_4Me))} (75 % yield)(Scheme 23, bottom), which has been demonstrated to readily form from [(IPr)Au(η^2-HC≡C(4-C_6H_4Me))]$^+SbF_6^-$ in 1 hour at temperatures above 0 °C. [134]

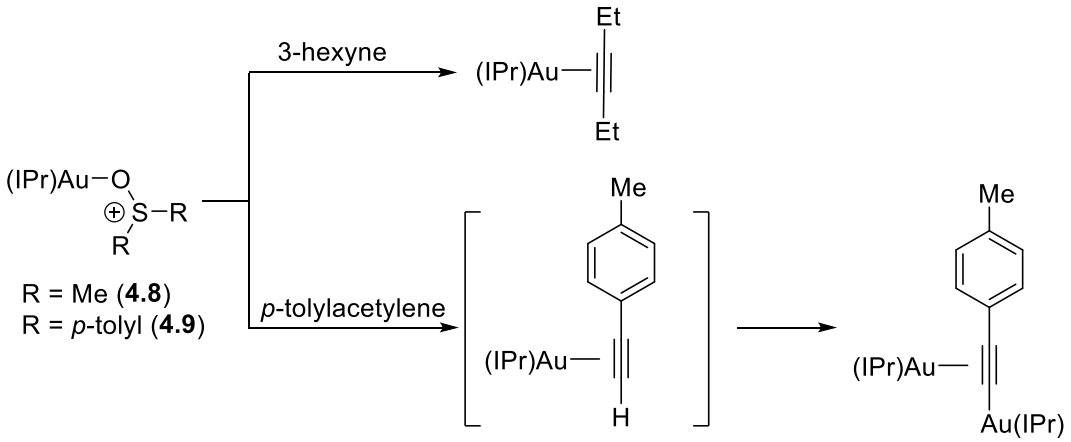

Scheme 23. Gold sulfoxide complexes were readily displaced by alkynes to form the gold π-alkyne complex.

Similarly, complex **4.8** (15 mg, 1.7 x 10^{-2} mmol) was dissolved in an NMR tube with CD_2Cl_2 (600 μL), then treated with 3-hexyne (1.2 μL, 1.7 x 10^{-2} mmol). Complex **4.9** (20 mg, 1.9 x 10^{-2} mmol) was dissolved in an NMR tube with CD_2Cl_2 (600 μL), then treated with 3-hexyne (2.16 μL, 1.9 x 10^{-2} mmol). After addition of the alkyne, the NMR tube was inverted three times and the reaction mixture was immediately analyzed by ^1H NMR spectroscopy to quantitatively yield $[(IPr)Au(\eta^2\text{-}EtC{\equiv}CEt)]^+SbF_6^-$ (Scheme 46, top).

When starting with $[(IPr)Au(\eta^2\text{-}EtC{\equiv}CEt)]^+SbF_6^-$ (15 mg, 1.7 x 10^{-2} mmol) dissolved in CD_2Cl_2 (600 μL) then adding dimethyl sulfoxide (1.2 μL, 1.7 x 10^{-2} mmol) at room temperature, no reaction was initially observed via ^1H NMR analysis. The reaction mixture was left at room temperature for 1 week, but there still only starting material present. When excess sulfoxide (10 equivalents) was added and the mixture left at room temperature for another 24 hours, there was still no reaction observed. These observations indicate that the gold π-alkyne bond is more stable than the gold-oxygen bond when the gold-oxide is a sulfoxide complex.

4.5 Summary

In summary, the stoichiometric reaction of alkynyl sulfoxide 4.**1** with (IPr)AuOTf at -80 °C led to 5-*exo*-dig cyclization to form the *N*-alkenoxysulfonium complex **4.4**. Using isotopic labeling experiments, the structure was confirmed to be the 5-*exo*-dig intermediate as opposed to the 6-*endo*-dig intermediate. A series of kinetic studies was

conducted to show complex **4.4** undergoes conversion to gold-bound bicyclic product **4.3** in 110 min at -20 °C, which, upon workup, forms **4.2**. When a nucleophile such as 4-picoline is introduced, there is an observed α-H shift in the ^{1}H NMR spectrum from δ 5.50 to δ 5.88, and complex **4.4** goes directly to product **4.2** in 280 min at -20 °C. The observation of **4.4** confirms that *N*-alkenoxysulfonium species are key intermediates in the gold(I)-catalyzed alkyne oxidation transformation. Failure to observe an α-oxo carbenoid intermediate when **4.4** was treated with 4-picoline indicates a carbenoid species is not evoked in these transformations. The experiments with gold-oxides and alkynes indicate that gold N-oxides will form instead of a gold π-alkyne, and a gold π-alkyne will form instead of a gold sulfoxide. This supports the hypothesis that the gold-catalyzed rearrangement of alkynyl sulfoxide mechanism first has the gold bind to the alkyne as opposed to the oxygen.

4.6 Experimental Data

4.6.1 General Methods

Reactions were carried out under a nitrogen atmosphere in flame dried glassware using standard glovebox and Schlenk techniques. NMR Spectra were obtained on a 400 MHz Varian Inova spectrometer, a 500 MHz Bruker spectrometer, a 500 MHz Bruker spectrometer, and a 700 MHz Varian spectrometer. ^{13}C NMR spectra were referenced to residual $CDCl_3$ (δ 77.2) or CH_2Cl_2 (δ 53.8). The ^{1}H NMR spectra was

referenced to residual $CDCl_3$ (δ 7.26) or CH_2Cl_2 (δ 5.32). Diethyl ether, CH_2Cl_2, and THF were purified by passage through columns of activated alumina under nitrogen. Silver-free (IPr)AuOTf was synthesized employing published procedures.[119,120] All other reagents were obtained through major chemical suppliers and used as received. But-1-yn-4-yl(p-tolyl)sulfoxide (**4.1**) was synthesized employing known procedures.[129] The synthesis of carbon labeled but-1-yn-4-yl(p-tolyl)sulfoxide was guided by reported procedures of the synthesis of similar unlabeled compounds.[130,131]

4.6.2 Synthesis of But-1-yn-4-yl(p-tolyl)sulfoxide-$^{13}C_2$ (4.1-$^{13}C_2$).

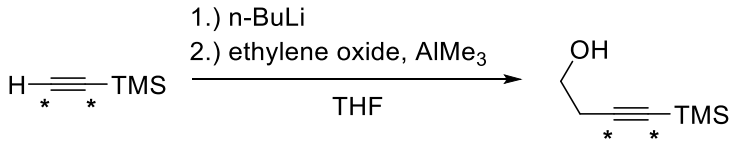

4.10

Scheme 24. Synthesis of 4.10.

Trimethylsilylacetylene-$^{13}C_2$ (100 mg, 1.0 mmol) and trimethylsilylacetylene (300 mg, 3.0 mmol) were dissolved in THF (6 mL) and cooled to -78 °C, followed by the addition of n-BuLi (2.0 mL, 5.0 mmol) and stirred for 45 min. The reaction mixture was then warmed to 0 °C and stirred for 15 min before the addition of $AlMe_3$ (2.0 mL, 5.0 mmol). The reaction mixture was then brought to 25 °C and stirred for 24 h. The reaction mixture was then quenched with H_2O (2 mL), extracted with Et_2O (20 mL), and washed with 10% HCl (20 mL). The organic layer was then dried over MgSO4, then filtered and

concentrated to yield **4.10** (560 mg, 98 %). ^{1}H NMR (400 MHz, $CDCl_3$): δ 3.66 (t, *J* = 6.8 Hz, 2H), 2.46 (t, *J* = 6.8 Hz, 2H), 0.14 (s, 9H).

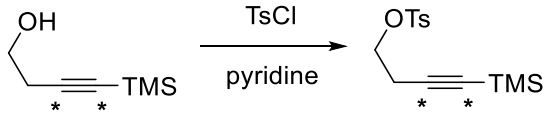

4.10 **4.11**

Scheme 25. Synthesis of 4.11.

4.10 (100 mg, 3.9 mmol) was dissolved in pyridine (5 mL) and cooled to 0 °C, followed by the addition of 4-toluenesulfonyl chloride (990 mg, 5.2 mmol). The mixture was stirred at 0 °C for 12 hours. The reaction mixture was then washed with $NaHCO_3$ (10 mL) and extracted with chloroform (3 x 10 mL). The organic layers were combined, dried over $MgSO_4$, then filtered and concentrated to yield **4.10** (173 mg, 15 %). ^{1}H NMR (500 MHz, $CDCl_3$): δ 7.80 (d, *J* = 7.3 Hz, 2H), 7.35 (d, *J* = 7.3 Hz, 2H), 4.08 (t, *J* = 7.6 Hz, 2H), 2.59 (t, *J* = 7.6 Hz, 2H), 2.45 (s, 3H), 0.13 (s, 9H).

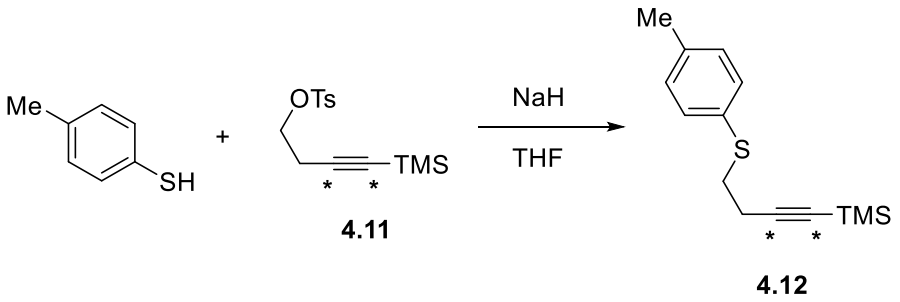

Scheme 26. Synthesis of 4.12.

4-methylbenzenethiol (75 mg, 0.60 mmol) and NaH (60% in mineral oil, 32 mg) were dissolved in THF (4 mL), cooled to 0 °C, and stirred for 30 minutes. **4.11** (173 mg, 0.59 mmol) was dissolved in THF (1 mL) and cooled to 0 °C and then added to the reaction mixture. The solution was then brought to 25 °C and stirred for 12 hours. The mixture was then quenched with H_2O (10 mL) and the product extracted with Et_2O (2 x 10 mL). The organic layers were then combined, washed with brine (10 mL), dried over $MgSO_4$, then filtered and concentrated to afford **4.12** (136 mg, 92 %). ^{1}H NMR (400 MHz, $CDCl_3$): δ 7.29 (d, *J* = 7.8 Hz, 2H), 7.10 (d, *J* = 7.8 Hz, 2H), 3.00 (t, *J* = 7.6 Hz, 2H), 2.49 (t, *J* = 7.6 Hz, 2H), 2.32 (s, 3H), 0.14 (s, 9H).

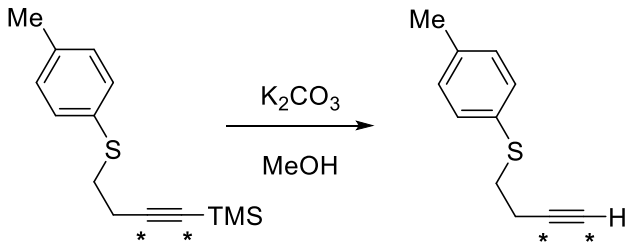

Scheme 27. Synthesis of 4.13.

4.12 (136 mg, 0.55 mmol) was combined with K_2CO_3 (10 mg, 7.0 x 10^{-2} mmol) and dissolved in methanol (6 mL), then stirred at 25 °C for 24 hours. The mixture was then filtered through a pad of Celite and concentrated under vacuum to yield **4.13** (55 mg, 57 %) which was used immediately for the following reaction.

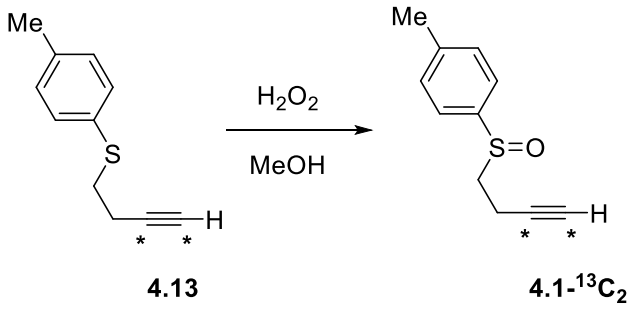

Scheme 28. Synthesis of 4.1-$^{13}C_2$.

4.13 (55 mg, 0.31 mmol) was dissolved in methanol (2 mL) and H_2O_2 (30 %, 0.15 mL) was added dropwise. The mixture was stirred at 25 °C for 24 hours, then quenched with H_2O (5 mL) and the product extracted with Et_2O (3 x 5 mL). The organic layers were then combined, washed with brine (5 mL), dried over $MgSO_4$, then filtered and

concentrated to afford yellow solids. The solids were purified via column chromatography (SiO_2, hexanes/EtOAc = 1/1) and yielded a yellow solid, **4.1-$^{13}C_2$** (48 mg, 81 %). $^{13}C\{^1H\}$ NMR (126 MHz, $CDCl_3$): δ 80.81 (d, *J* = 174 Hz), 71.1 (d, *J* = 174 Hz).

4.6.3 Synthesis of But-1-yn-4-yl(p-tolyl)sulfoxide-d_1 (4.1-d_1).

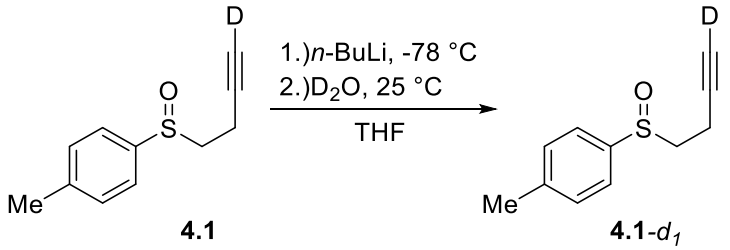

4.1 **4.1-d_1**

Scheme 29. Synthesis of 4.1-d_1.

4.1 (150 mg, 0.78 mmol) was dissolved in THF (2 mL) and cooled to 0 °C, followed by the addition of *n*-BuLi (0.47 mL, 1.17 mmol) and stirred for 1 hour. D_2O (1 mL) was then added, and the mixture was warmed to 25 °C, and stirred for 24 hours. The product was then extracted with Et_2O (5 mL), then concentrated under vacuum to afford **4.1-d_1** (143 mg, 95 %). Product was confirmed by missing alkynyl proton resonance at δ 2.03 in the ^1H NMR spectra with 75% deuterium incorporation.

4.6.4 Generation of Complex 4.4

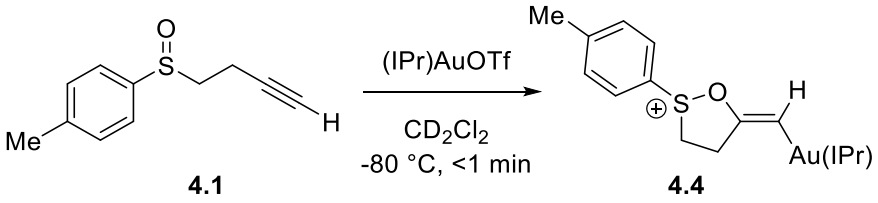

Scheme 30. Synthesis of 4.4.

But-1-yn-4-yl(p-tolyl)sulfoxide (**4.1**) (9.2 mg, 4.8 x 10^{-2} mmol) from a stock solution was added to a solution of (IPr)AuOTf (36 mg, 4.8 x 10^{-2} mmol) in CD_2Cl_2 (0.6 mL) and CH_2Br_2 (4.2 mg, 2.4 x 10^{-2} mmol) in an NMR tube under nitrogen cooled to -78 °C in a bath. The resulting pale-yellow solution was then analyzed without isolation by NMR spectroscopy. The yield of 40 % for the conversion of (IPr)AuOTf to Intermediate **4.4** was determined by integrating the α-H resonance of **4.4** at δ 5.50 relative to the resonance of CH_2Br_2 at δ 4.94 in the ^{1}H NMR spectrum. ^{1}H NMR (500 MHz, CD_2Cl_2; - 60 °C): δ 8.05 (s, 1H), 7.59 (t, *J* = 7.8 Hz, 2H), 7.42 (s, 2H), 7.37 (d, *J* = 7.8 Hz, 2H), 7.26 (d, *J* = 7.8 Hz, 2H), 6.83 (s, 1H), 6.67 (s, 2H), 5.50 (s, 1H), 3.30 – 3.11 (m, 2H), 2.47 – 2.30 (m, 6H), 2.26 (s, 3H),1.20 (d, *J* = 6.6 Hz, 6H), 1.18 (d, *J* = 6.6 Hz, 6H), 1.16 (d, *J* = 6.6 Hz, 6H), 1.01 (d, *J* = 6.6 Hz, 6H).^{13}C {^{1}H} (126 MHz, CD_2Cl_2; - 60 °C): δ 175.7, 156.9, 145.1, 145.1, 140.9, 138.9, 132.6, 131.7, 131.4, 130.9, 129.9, 125.7, 124.3, 124.1, 124.1, 102.7, 38.9, 34.3, 28.5, 28.4, 24.5, 24.3, 23.4, 23.2, 20.8.

4.6.4.1 Generation of Complex 4.4-$^{13}C_2$

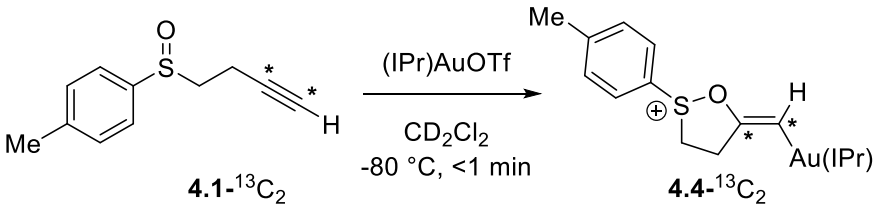

Scheme 31. Synthesis of 4.4-$^{13}C_2$.

4.1-$^{13}C_2$ (9.3 mg, 4.8 x 10^{-2} mmol) from a stock solution was added to a solution of (IPr)AuOTf (36 mg, 4.8 x 10^{-2} mmol) in CD_2Cl_2 (0.6 mL) and CH_2Br_2 (4.2 mg, 2.4 x 10^{-2} mmol) in an NMR tube under nitrogen cooled to -78 °C in a bath. The resulting pale-yellow solution was then analyzed without isolation by NMR spectroscopy. ^{1}H NMR (500 MHz, CD_2Cl_2; - 60 °C): δ 5.50 (dd, J_{CH} = 149.0, 6.2 Hz, 1H). $^{13}C\{^1H\}$ (126 MHz, CD_2Cl_2; - 60 °C): δ 156.8 (d, J = 81.6 Hz), 102.7 (d, J = 81.6 Hz).

4.6.4.2 Generation of deuterium labeled intermediate

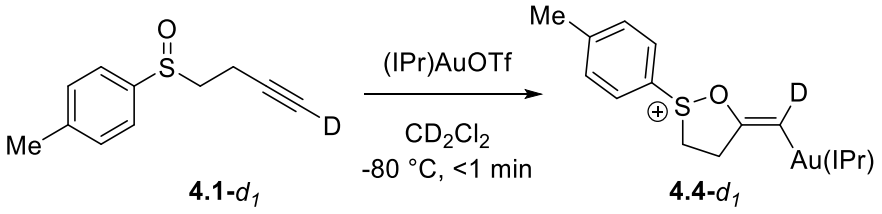

Scheme 32. Synthesis of 4.4-d_1.

(IPr)AuOTf (22 mg, 3.0 x 10^{-2} mmol) was dissolved in CD_2Cl_2 in an NMR tube and cooled to -78°C. From stock solutions, CH_2Br_2 (2.5 mg, 1.5 x 10^{-2} mmol) and **4.1**-d_1 (5.8 mg, 3.0 x 10^{-2} mmol) was added to the cooled gold solution. The NMR tube was then

placed into an NMR probe cooled to -80 °C to observe and characterize **4.4**- d_1 without further isolation. The α-H peak at δ 5.50 in the ^{1}H NMR spectra decreased in intensity due to deuterium labeling. The α-C peak in the ^{13}C NMR spectra decreased in intensity due to carbon-deuterium splitting and was no longer visible at δ 102.7. ^{1}H NMR (500 MHz, CD_2Cl_2; - 60 °C): δ 5.50 (s, 1H). ^{13}C{^{1}H} (126 MHz, CD_2Cl_2; - 60 °C): δ 156.8.

4.6.5 Synthesis of 1-benzothiepin-4-one (4.2) and derivatives

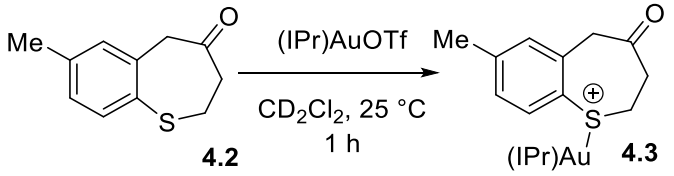

Scheme 33. Synthesis of 4.3.

The solution of Intermediate **4.4** (23 mg, 2.9 x 10^{-2} mmol) was warmed to -20 °C to form **4.3** (40 % from **4.1**, 100 % from **4.4** – *determined via NMR*) in 110 minutes. Compound **4.3** was synthesized independently via reaction of (IPr)AuOTf (35 mg, 4.8 x 10^{-2} mmol) and 4.**2** (9.16 mg, 4.8 x 10^{-2} mmol) in CD_2Cl_2 (0.6 mL) at 25 °C for 1 hour (yield here). The NMR tube was then placed into probe to analyze **4.3**, *in situ*. ^{1}H NMR (500 MHz, CD_2Cl_2): δ 7.63 (t, *J* = 8.0 Hz, 2H), 7.52 (s, 2H), 7.39 (d, *J* = 7.8 Hz, 4H), 7.10 (s, 1H), 6.99 (s, 1H), 3.58 (s, 2H), 3.20 (dd, *J* = 7.7, 5.0 Hz, 2H), 2.70 (dd, *J* = 7.6, 5.1 Hz, 2H), 2.50 (sept, *J* = 6.8 Hz, 4H), 2.36 (s, 3H), 1.26 (d, *J* = 6.8 Hz, 12H), 1.20 (d, *J* = 6.8 Hz, 12H). ^{13}C {^{1}H} (126 MHz, CD_2Cl_2): δ 201.1, 176.3, 146.2, 144.3, 136.9, 133.9, 133.5, 133.2, 131.8, 129.7, 125.5, 125.1, 51.0, 45.7, 38.7, 29.3, 24.8, 24.1, 21.3.

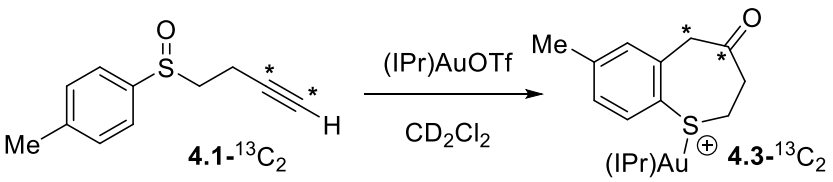

Scheme 34. Synthesis of 4.3-$^{13}C_2$.

4.3-$^{13}C_2$ (9.3 mg, 4.8 x 10^{-2} mmol) from a stock solution was added to a solution of (IPr)AuOTf (36 mg, 4.8 x 10^{-2} mmol) in CD_2Cl_2 (0.6 mL) and CH_2Br_2 (4.2 mg, 2.4 x 10^{-2} mmol) in an NMR tube under nitrogen cooled to -78 °C in a bath. The resulting pale-yellow solution of **4.3-**$^{13}C_2$ was then analyzed without isolation by NMR spectroscopy. ^{1}H NMR (500 MHz, CD_2Cl_2): δ 3.58 (dd, J_{CH} = 130.5, 6.5 Hz, 2H). $^{13}C\{^1H\}$ (126 MHz, CD_2Cl_2): δ 201.1 (d, J = 37.8 Hz), 50.9 (d, J = 37.8 Hz).

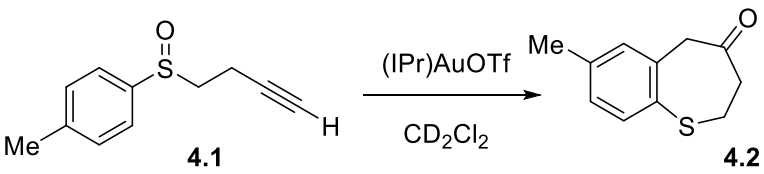

Scheme 35. Synthesis of 4.2.

4.2. A solution of **4.3** (23 mg, 2.9 x 10^{-2} mmol) in CD_2Cl_2 was passed through a pad of Celite and concentrated under vacuum. The resulting residue was dissolved in methylene chloride, layered with pentane, and cooled at 4 °C for 24 h. The mother liquor was removed from the white solids and was concentrated to yield **2** (1.0 mg, 18 %). Compound **4.2** was also synthesized independently by dissolving **4.1** (94 mg, 0.5 mmol)

in methylene chloride (5 mL) and stirring with (IPr)AuOTf (18.2 mg, 2.5 x 10^{-2} mmol) for 1 h. The solution was then concentrated under vacuum and dissolved in methylene chloride and layered with pentane, then cooled to 4 °C for 24 hours. The mother liquor was then decanted and concentrated to yield **4.2** (77 mg, 80 %) ^{1}H NMR (500 MHz, $CDCl_3$) δ 7.39 (d, *J* = 7.8 Hz, 1H), 7.09 (s, 1H), 6.99 (d, *J* = 7.8 Hz, 1H), 3.93 (s, 2H), 3.04 – 2.96 (m, 2H), 2.86 – 2.80 (m, 2H), 2.30 (s, 3H). ^{13}C {^{1}H} (126 MHz, CD_2Cl_2): δ 206.6, 139.5, 138.7, 134.1, 132.0, 131.3, 128.7, 51.5, 45.7, 32.5, 21.1. HRMS (ESI) calcd. (found) for $C_{11}H_{12}OS$ ([M+H]$^{+}$): 193.0682 (193.0683).

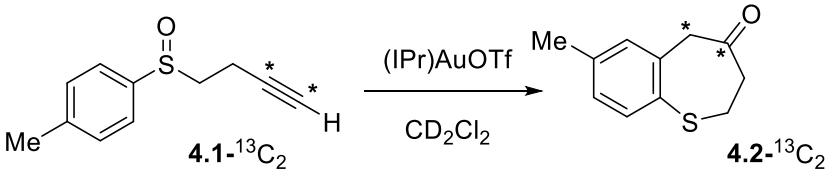

Scheme 36. Synthesis of 4.2-$^{13}C_2$.

4.2-$^{13}C_2$. **4.1**-$^{13}C_2$ (9.3 mg, 4.8 x 10^{-2} mmol) from a stock solution was added to a solution of (IPr)AuOTf (36 mg, 4.8 x 10^{-2} mmol) in CD_2Cl_2 (0.6 mL) and CH_2Br_2 (4.2 mg, 2.4 x 10^{-2} mmol) in an NMR tube under nitrogen cooled to -78 °C in a bath. The resulting pale-yellow solution of **4.1-$^{13}C_2$** was then analyzed without isolation by NMR spectroscopy. ^{1}H NMR (500 MHz, CD_2Cl_2): δ 3.92 (dd, J_{CH} = 130.1, 6.7 Hz, 2H). ^{13}C {^{1}H} (126 MHz, CD_2Cl_2): δ 206.5 (d, *J* = 37.8 Hz), 51.4 (d, *J* = 37.8 Hz).

4.6.6 Treatment of 4.4 with a nucleophile

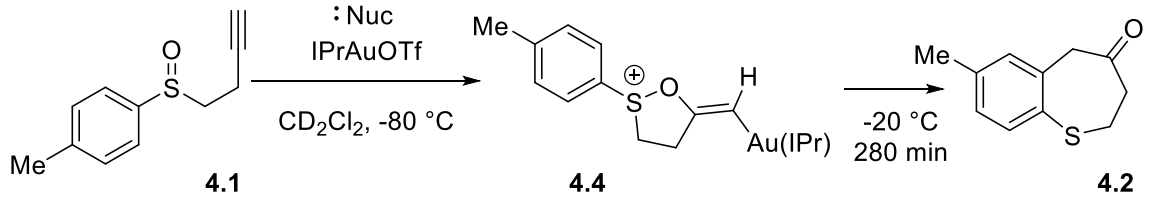

Scheme 37. Generating complex 4.4 at low temperature, then treating with a nucleophile before conversion to product (4.2).

Reaction of 4.4 with picoline. But-1-yn-4-yl(p-tolyl)sulfoxide (**4.1**) (5.5 mg, 2.9 x 10^{-2} mmol) was taken from a stock solution and added to a solution of (IPr)AuOTf (21 mg, 2.9 x 10^{-2} mmol) in CD_2Cl_2 (0.6 mL) and CH_2Br_2 (2.5 mg, 1.4 x 10^{-2} mmol) in an NMR tube under nitrogen cooled to -96 °C in a bath. After 5 minutes, 4-picoline (2.7 mg, 2.9 x 10^{-2} mmol) was added, and the sample placed into an NMR probe cooled to -80 °C. When monitored with ^{1}H NMR spectroscopy, the previously observed δ 5.50 α-H peak is immediately gone, and instead a δ 5.88 α-H is observed. This shift in peak is attributed to and effect of hydrogen bonding from the addition of the 4-picoline. The same proton shift was observed when 1 equivalent of THT or $P(OMe)_3$ was used as the nucleophile. Carbon Labeled peaks of **4.4** in the presence of 4-picoline: ^{1}H NMR (700 MHz, CD_2Cl_2; -60 °C): δ 5.50 (dd, J_{CH} = 149.0, 6.2 Hz, 1H). ^{13}C {^{1}H} NMR (176 MHz, CD_2Cl_2; -60 °C): δ 157.7(d, J = 81.6 Hz), 103.8 (d, J = 81.6 Hz).

4.5.6.1 Kinetics experiment of 4.4 to 4.2 in the presence of 4-picoline

The same mixture used to generate **4.4** in the presence of 4-picoline was used for kinetic analysis. The probe was warmed to -20 °C and the solution monitored periodically by ^{1}H NMR spectroscopy. The concentration of **4** was determined by integrating the α-H peak at δ 5.88 relative to the resonance for CH_2Br_2 at δ 4.94. After 280 minutes, a plot of 1/[**4.4**] versus time was linear to >3 half-lives with a second-order rate constant of 2.15 x 10^{-2} $M^{-1}s^{-1}$. When 2 equivalents of 4-picoline were used, the conversion to product was complete in <5 minutes and -20 °C.

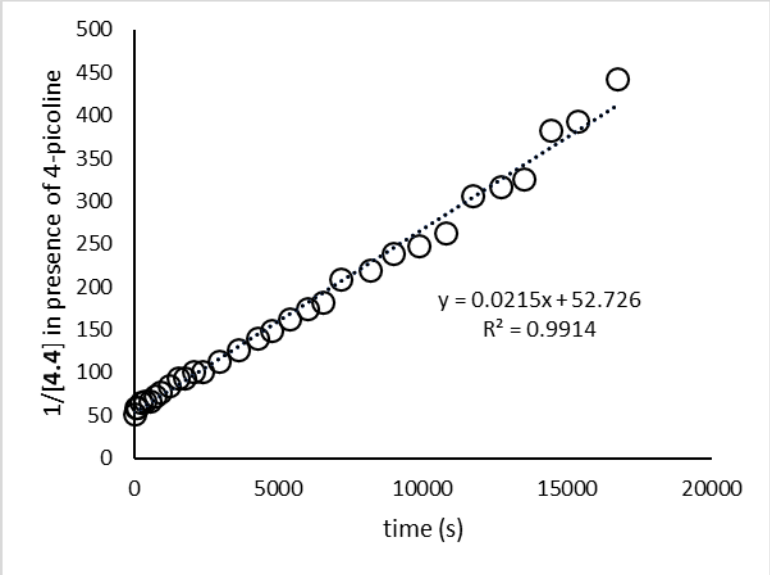

Figure 26. Second order kinetics of conversion of 4.4 to 4.1 in the presence of 4-picoline at -20 °C.

Table 15. Kinetic data for decomposition of 4.4 in the presence of 4-picoline at -20 °C.

Time (s)	[**4.4**]	1/[**4.4**]

0	0.0193	51.94
57	0.0170	58.79
110	0.0169	59.25
224	0.0154	64.80
360	0.0151	66.07
544	0.0148	67.51
725	0.0139	72.02
898	0.0129	77.24
1200	0.0118	84.54
1533	0.0107	93.32
1762	0.0107	93.62
2078	0.0099	100.84
2350	0.0098	101.92
2951	0.0089	112.65
3627	0.0079	126.41
4257	0.0071	140.29
4774	0.0067	149.14
5392	0.0061	163.31
6005	0.0057	175.39
6549	0.0055	181.58
7154	0.0048	208.82
8176	0.0045	220.14
8983	0.0042	238.71
9861	0.0040	248.24
10801	0.0038	262.58
11726	0.0033	306.01
12676	0.0031	317.61
13475	0.0031	326.09
14411	0.0026	382.32
15341	0.0025	392.95
16166	0.0022	454.55
16744	0.0023	443.64

4.6.7 Kinetics Experiments of Decomposition of Complex 4.4

A solution of Intermediate **4.4** was generated *in situ* at -78 °C by treating (IPr)AuOTf (18 mg, 2.5 x 10^{-2} mmol) with but-1-yn-4-yl(p-tolyl)sulfoxide (**4.1**) (4.7 mg, 2.5 x 10^{-2} mmol) and CH_2Br_2 in CD_2Cl_2 (0.6 mL) and placed in the probe of an NMR spectrometer at -80 °C. The spectrometer was warmed to -20 °C and the reaction was monitored periodically with ^1H NMR spectroscopy. The concentration of **4.4** was determined by integration of the α-H resonance at δ 5.50 relative to the resonance of CH_2Br_2 at δ 4.94. A plot of 1/[**4.4**] versus time was linear to >3 half-lives with a second order rate constant of 0.112 $M^{-1}s^{-1}$. The experiment was repeated at temperature -15 °C, -10 °C, -5 °C and 0 °C. Eyring analysis of the second-order rate constants for the decomposition of **4.4** as a function of temperature (-20 °C to 0 °C) was linear where $\ln(k/T) = (-6076)/T + 16.28$.

Table 16. Values used to produce Eyring Plot.

Temp (K)	k (M-1s-1)	1/T (1/K)	ln(k/T)
253.15	0.1129	0.00395	-7.715
258.15	0.2172	0.00387	-7.080
263.15	0.2037	0.00380	-7.164
268.15	0.5067	0.00373	-6.271
273.15	0.7317	0.00366	-5.922

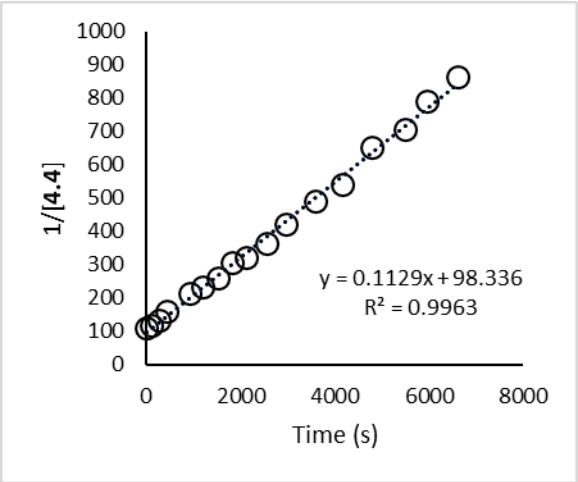

Figure 27: Second-order plot for the elimination of 4.4 in CD_2Cl_2 at -20 °C.

Table 17. Kinetics data for decomposition of 4.4 at -20 °C.

Time (s)	[**4.4**]	1/[**4.4**]
0	0.00908	110.13
104	0.00835	119.75
280	0.00756	132.22
420	0.00627	159.43
913	0.00470	212.77
1205	0.00427	234.35
1512	0.00387	258.70
1821	0.00325	308.04
2107	0.00312	320.34
2556	0.00275	364.07
2960	0.00238	420.80
3578	0.00203	493.30
4158	0.00185	540.31
4784	0.00153	652.58
5483	0.00141	707.94
5950	0.00126	791.23
6620	0.00116	863.82
7184	0.00106	942.09
7803	0.00083	1198.14

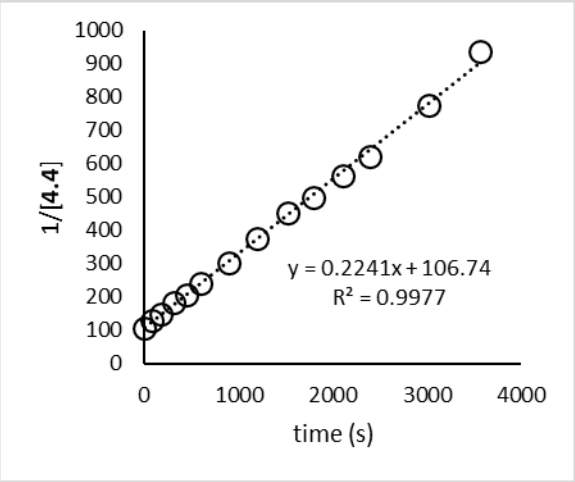

Figure 28: Second-order plot for the elimination of 4.4 in CD_2Cl_2 at -15 °C.

Table 18. Kinetics data for decomposition of 4.4 at -15 °C.

Time (s)	[**4.4**]	1/[**4.4**]
0	0.00924	108.26
75	0.00777	128.63
181	0.00665	150.48
312	0.00542	184.61
442	0.00485	206.18
594	0.00411	243.24
890	0.00331	301.68
1198	0.00267	374.36
1525	0.00221	452.52
1790	0.00200	499.14
2112	0.00177	566.29
2387	0.00161	621.41
3024	0.00129	774.74
3564	0.00107	938.11
4141	0.00093	1075.61
4780	0.00076	1309.48
5373	0.00070	1421.42

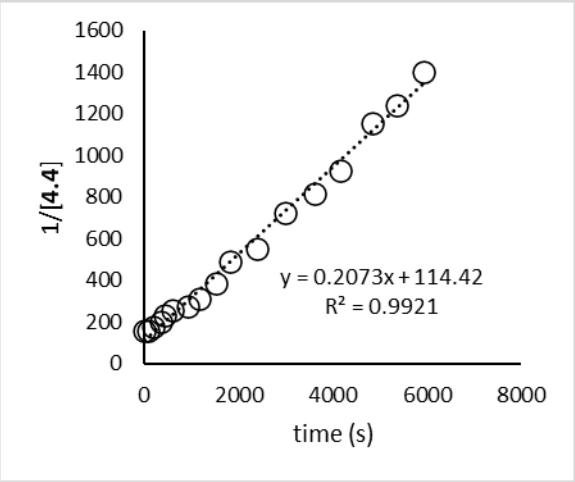

Figure 29: Second-order plot for the elimination of 4.4 in CD_2Cl_2 at -10 °C.

Table 19. Kinetics data for decomposition of 4.4 at -10 °C.

Time (s)	[**4.4**]	1/[**4.4**]
0	0.00624	160.34
71	0.00639	156.48
195	0.00558	179.14
354	0.00495	201.92
434	0.00434	230.51
590	0.00388	257.64
915	0.00360	277.98
1179	0.00321	311.73
1511	0.00258	387.72
1831	0.00204	490.70
2385	0.00181	553.06
2990	0.00138	722.56
3606	0.00122	818.78
4150	0.00108	929.46
4840	0.00087	1155.63
5360	0.00081	1240.60
5925	0.00071	1402.49

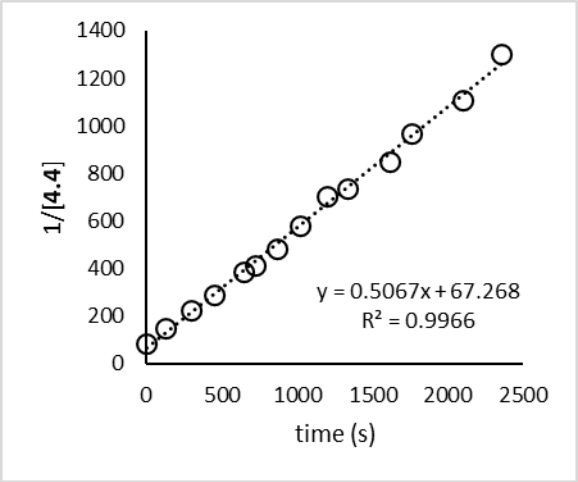

Figure 30: Second-order plot for the elimination of 4.4 in CD_2Cl_2 at -5 °C.

Table 20. Kinetics data for decomposition of 4.4 at -5 °C.

Time (s)	[**4.4**]	1/[**4.4**]
0	0.01175	85.10
126	0.00665	150.36
295	0.00450	222.08
452	0.00347	287.87
644	0.00259	386.28
720	0.00243	411.41
870	0.00206	486.05
1017	0.00173	578.08
1201	0.00142	705.11
1331	0.00135	739.26
1612	0.00118	850.92
1760	0.00103	966.22
2100	0.00090	1108.28
2357	0.00077	1304.02

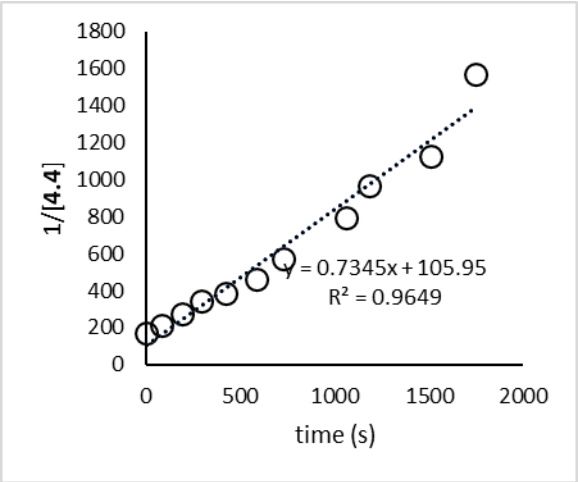

Figure 31: Second-order plot for the elimination of 4.4 in CD_2Cl_2 at 0 °C.

Table 21. Kinetics data for decomposition of 4.4 at -0 °C.

Time (s)	[**4.4**]	1/[**4.4**]
0	0.00582	171.78
79	0.00472	212.02
191	0.00362	276.30
293	0.00292	342.67
418	0.00257	388.59
585	0.00217	460.04
724	0.00175	572.14
898	0.00155	643.39
1058	0.00126	792.00
1183	0.00103	970.22
1509	0.00089	1125.97
1744	0.00064	1571.11

4.6.8 Characterization of Gold *N*-Oxide and Sulfoxides

$[(IPr)AuO(4\text{-}MeC_5H_4N)]^+$ $NCPh^-$ (4.7). (IPr)AuNCPh(20 mg, 2.9 x 10^{-2} mmol) and picoline *N*-oxide (4 mg, 3.5 x 10^{-2} mmol) (PNO) were combined in a vial and brought

into a glovebox. The mixture was dissolved in dichloromethane (3 mL), then stirred for 30 minutes (Scheme 42). The vial was then removed from the glovebox and the mixture was filtered through Celite, then concentrated under vacuum. The resulting oil was dissolved in minimal dichloromethane and layered with hexanes and cooled to -20 °C overnight to afford **4.7**(17 mg, 86 %) as white crystals (Figure 32). When attempted with a silver salt, no increase in yield was observed. Alternatively, the reaction would be carried out with (IPr)AuCl and $AgSbF_6$ with similar yields. ^{1}H NMR (500 MHz, CD_2Cl_2): δ 7.82 (d, *J* = 6.7 Hz, 2H), 7.64 (t, *J* = 7.8 Hz, 2H), 7.41 (s, 2H), 7.40 (d, *J* = 7.4 Hz, 4H), 7.26 (d, *J* = 6.3 Hz, 2H), 2.53 (sept, *J* = 6.9 Hz, 4H), 2.48 (s, 3H), 1.29 (d, *J* = 6.9 Hz, 12H), 1.26 (d, *J* = 6.9 Hz, 12H). ^{13}C NMR (126 MHz, CD_2Cl_2): δ 162.9, 146.4, 137.8, 134.0, 131.6, 128.1, 124.9, 124.8, 29.3, 24.6, 24.2, 21.1. When **B.1** analyzed by mass spectroscopy, the *N*-oxide ligand readily was removed and only fragments were observed. This was observed for all gold-oxide species.

$[(IPr)AuO(SMe_2)]^+$ SbF_6^- (4.8). (IPr)AuCl (25 mg, 4.0 x 10^{-2} mmol) was added to a vial and brought into a glovebox and mixed with $AgSbF_6$ (14 mg, 4.0 x 10^{-2} mmol). The solids were dissolved in dichloromethane (2 mL), then dimethyl sulfoxide (50 mg, 8.1 x 10^{-2} mmol) was added to the solution and stirred at room temperature for 2 hours (Scheme 44). The mixture was then removed from the glovebox and filtered through Celite, then concentrated under vacuum. The oily residue was then dissolved minimal

diethyl ether, then cooled to -20 °C for 24 hours to yield **4.8** (22 mg, 80 %) as a white solid. ^{1}H NMR (500 MHz, CD_2Cl_2): δ 7.59 (t, *J* = 7.8 Hz, 2H), 7.39 (s, 2H), 7.38 (d, *J* = 7.8 Hz, 4H), 2.52 (s, 7H), 2.50 – 2.45 (m, 3H), 1.32 (d, *J* = 6.9 Hz, 12H), 1.25 (d, *J* = 6.9 Hz, 12H).

[(IPr)AuO(S(4-MeC$_6$H$_4$)$_2$)]$^+$ SbF$_6^-$ (4.9). (IPr)AuCl (50 mg, 8.1 x 10^{-2} mmol) and *p*-tolyl sulfoxide (56 mg, 0.24 mmol) were combined and brought into a glovebox in a vial. $AgSbF_6$ (28 mg, 8.1 x 10^{-2} mmol) was added to the mixture, then the solids were dissolved in dichloromethane (2 mL). The mixture was stirred at room temperature for 4 hours, then brought out of the box, filtered through Celite, the concentrated under vacuum. The residue was then dissolved in minimal diethyl ether and cooled to -20 °C for 48 hours to yield **4.9** (65.3 mg, 99 %) as a white solid. ^{1}H NMR (500 MHz, $CDCl_3$): δ 7.56 (t, *J* = 7.8 Hz, 2H), 7.34 (s, 2H), 7.28 (d, *J* = 7.8 Hz, 4H), 7.23 (broad s, 6H), 2.41 (sept, *J* = 6.9 Hz, 4H), 2.39 (s, 6H), 1.20 (d, *J* = 6.9 Hz, 12H), 1.15 (d, *J* = 6.9 Hz, 12H). ^{13}C NMR (126 MHz, $CDCl_3$): δ 160.3, 145.7, 133.4, 131.2, 131.0, 126.3, 125.8, 124.7, 124.4, 28.8, 24.5, 23.9, 21.6.

4.6.9 Crystallographic Data

4.6.9.1 Molecular Structure of 4.7

For X-ray analysis, crystals were formed via diffusion of hexane into a concentrated CH_2Cl_2 solution of **4.7** at -20 °C. A clear, colorless blocks-like crystal of

molecular formula $C_{33}H_{43}AuF_6N_3OSb$ with the approximate dimensions 0.097 mm × 0.149 mm × 0.189 mm was used for the X-ray crystallographic analysis. The X-ray intensity data were measured on a Bruker APEX II system equipped with a fine-focus sealed tube (MoKα, λ = 0.71073 Å) and a graphite monochromator, with a total exposure time of 5.36 hours. The frames were integrated with the Bruker SAINT software package using a narrow-frame algorithm. The integration of the data using a triclinic unit cell yielded a total of 29990 reflections to a maximum θ angle of 29.57° (0.72 Å resolution), of which 9948 were independent (average redundancy 3.015, completeness = 99.7%, R_{int} = 1.89%, R_{sig} = 2.12%) and 9265 (93.13%) were greater than $2\sigma(F^2)$. The final cell constants of $\underline{a}$ = 8.6902(12) Å, $\underline{b}$ = 14.433(2) Å, $\underline{c}$ = 14.816(2) Å, β = 92.764(2)°, γ = 98.232(2)°, volume = 1780.0(4) $Å^3$, are based upon the refinement of the XYZ-centroids of 2968 reflections above 20 σ(I) with 2.929° < 2θ < 62.21°. Data were corrected for absorption effects using the Numerical Mu from Formula method (SADABS). The ratio of minimum to maximum apparent transmission was 0.618. The calculated minimum and maximum transmission coefficients (based on crystal size) are 0.4560 and 0.6460. The final anisotropic full-matrix least-squares refinement on F^2 with 415 variables converged at R1 = 1.91%, for the observed data and wR2 = 4.26% for all data. The goodness-of-fit was 1.032. The largest peak in the final difference electron density synthesis was 1.806 $e^-/Å^3$

and the largest hole was –1.712 $e^-/Å^3$ with an RMS deviation of 0.083 $e^-/Å^3$. On the basis of the final model, the calculated density was 1.736 g/cm^3 and F(000), 908 e^-.

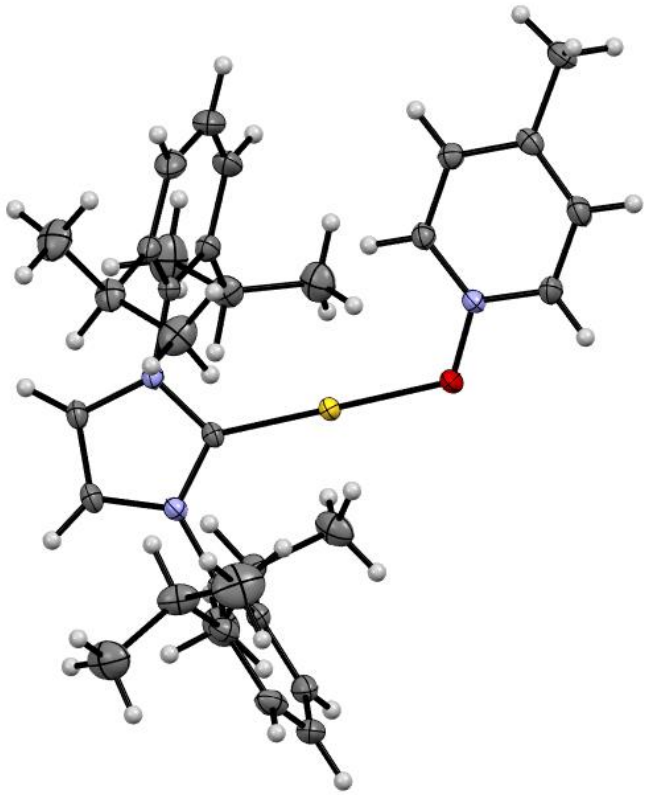

Figure 32. ORTEP diagram of gold(I) α-oxo carbenoid complex 4.7 with ellipsoids shown at 50% probability level and with counterion, solvent, and hydrogen atoms omitted.

Table 22. Bond lengths of complex 4.7.

Bond	Length(Å)	Bond	Length(Å)
Au1-C1	1.9585(19)	Au1-O1	2.0388(14)
O1-N3	1.357(2)	N1-C1	1.345(2)
N1-C2	1.387(3)	N1-C4	1.447(3)
N2-C1	1.349(3)	N2-C3	1.387(2)
N2-C16	1.445(3)	N3-C28	1.344(3)

N3-C32	1.346(3)	C2-C3	1.350(3)
C2-H2	0.95	C3-H3	0.95
C4-C9	1.395(3)	C4-C5	1.398(3)
C5-C6	1.395(3)	C5-C10	1.522(3)
C6-C7	1.380(3)	C6-H6	0.95
C7-C8	1.383(3)	C7-H7	0.95
C8-C9	1.390(3)	C8-H8	0.95
C9-C13	1.517(3)	C10-C11	1.525(4)
C10-C12	1.529(4)	C10-H10	1
C11-H11A	0.98	C11-H11B	0.98
C11-H11C	0.98	C12-H12A	0.98
C12-H12B	0.98	C12-H12C	0.98
C13-C15	1.526(3)	C13-C14	1.534(3)
C13-H13	1	C14-H14A	0.98
C14-H14B	0.98	C14-H14C	0.98
C15-H15A	0.98	C15-H15B	0.98
C15-H15C	0.98	C16-C17	1.396(3)
C16-C21	1.402(3)	C17-C18	1.401(3)
C17-C22	1.519(3)	C18-C19	1.376(4)
C18-H18	0.95	C19-C20	1.379(4)
C19-H19	0.95	C20-C21	1.395(3)
C20-H20	0.95	C21-C25	1.513(3)
C22-C24	1.525(3)	C22-C23	1.531(3)
C22-H22	1	C23-H23A	0.98
C23-H23B	0.98	C23-H23C	0.98
C24-H24A	0.98	C24-H24B	0.98
C24-H24C	0.98	C25-C27	1.528(3)
C25-C26	1.529(3)	C25-H25	1
C26-H26A	0.98	C26-H26B	0.98
C26-H26C	0.98	C27-H27A	0.98
C27-H27B	0.98	C27-H27C	0.98
C28-C29	1.377(3)	C28-H28	0.95
C29-C30	1.388(3)	C29-H29	0.95
C30-C31	1.392(3)	C30-C33	1.498(3)
C31-C32	1.372(3)	C31-H31	0.95
C32-H32	0.95	C33-H33A	0.98

C33-H33B	0.98	C33-H33C	0.98
Sb1-F4	1.842(2)	Sb1-F5	1.843(2)
Sb1-F6	1.8534(19)	Sb1-F3	1.8541(18)
Sb1-F1	1.8626(18)	Sb1-F2	1.8737(17)

Table 23. Bond angles of complex 4.7.

Bond	Angle(°)	Bond	Angle(°)
C1-Au1-O1	179.20(8)	N3-O1-Au1	119.48(12)
C1-N1-C2	110.37(17)	C1-N1-C4	122.86(16)
C2-N1-C4	126.75(16)	C1-N2-C3	110.26(17)
C1-N2-C16	122.35(16)	C3-N2-C16	127.38(17)
C28-N3-C32	121.58(17)	C28-N3-O1	122.66(16)
C32-N3-O1	115.75(17)	N1-C1-N2	105.89(16)
N1-C1-Au1	129.84(15)	N2-C1-Au1	124.24(14)
C3-C2-N1	106.75(17)	C3-C2-H2	126.6
N1-C2-H2	126.6	C2-C3-N2	106.73(18)
C2-C3-H3	126.6	N2-C3-H3	126.6
C9-C4-C5	123.46(19)	C9-C4-N1	118.06(18)
C5-C4-N1	118.46(18)	C6-C5-C4	116.9(2)
C6-C5-C10	120.7(2)	C4-C5-C10	122.4(2)
C7-C6-C5	120.7(2)	C7-C6-H6	119.6
C5-C6-H6	119.6	C6-C7-C8	121.0(2)
C6-C7-H7	119.5	C8-C7-H7	119.5
C7-C8-C9	120.6(2)	C7-C8-H8	119.7
C9-C8-H8	119.7	C8-C9-C4	117.3(2)
C8-C9-C13	120.4(2)	C4-C9-C13	122.27(19)
C5-C10-C11	111.4(2)	C5-C10-C12	110.4(2)
C11-C10-C12	111.4(2)	C5-C10-H10	107.8
C11-C10-H10	107.8	C12-C10-H10	107.8
C10-C11-H11A	109.5	C10-C11-H11B	109.5
H11A-C11-H11B	109.5	C10-C11-H11C	109.5
H11A-C11-H11C	109.5	H11B-C11-H11C	109.5
C10-C12-H12A	109.5	C10-C12-H12B	109.5
H12A-C12-H12B	109.5	C10-C12-H12C	109.5
H12A-C12-H12C	109.5	H12B-C12-H12C	109.5

C9-C13-C15	111.45(19)	C9-C13-C14	110.66(19)
C15-C13-C14	110.71(19)	C9-C13-H13	108
C15-C13-H13	108	C14-C13-H13	108
C13-C14-H14A	109.5	C13-C14-H14B	109.5
H14A-C14-H14B	109.5	C13-C14-H14C	109.5
H14A-C14-H14C	109.5	H14B-C14-H14C	109.5
C13-C15-H15A	109.5	C13-C15-H15B	109.5
H15A-C15-H15B	109.5	C13-C15-H15C	109.5
H15A-C15-H15C	109.5	H15B-C15-H15C	109.5
C17-C16-C21	123.51(19)	C17-C16-N2	118.39(18)
C21-C16-N2	118.02(18)	C16-C17-C18	117.1(2)
C16-C17-C22	122.91(19)	C18-C17-C22	120.0(2)
C19-C18-C17	120.9(2)	C19-C18-H18	119.6
C17-C18-H18	119.6	C18-C19-C20	120.5(2)
C18-C19-H19	119.7	C20-C19-H19	119.7
C19-C20-C21	121.6(2)	C19-C20-H20	119.2
C21-C20-H20	119.2	C20-C21-C16	116.4(2)
C20-C21-C25	121.8(2)	C16-C21-C25	121.77(19)
C17-C22-C24	109.8(2)	C17-C22-C23	112.4(2)
C24-C22-C23	111.0(2)	C17-C22-H22	107.8
C24-C22-H22	107.8	C23-C22-H22	107.8
C22-C23-H23A	109.5	C22-C23-H23B	109.5
H23A-C23-H23B	109.5	C22-C23-H23C	109.5
H23A-C23-H23C	109.5	H23B-C23-H23C	109.5
C22-C24-H24A	109.5	C22-C24-H24B	109.5
H24A-C24-H24B	109.5	C22-C24-H24C	109.5
H24A-C24-H24C	109.5	H24B-C24-H24C	109.5
C21-C25-C27	113.2(2)	C21-C25-C26	110.43(19)
C27-C25-C26	109.4(2)	C21-C25-H25	107.9
C27-C25-H25	107.9	C26-C25-H25	107.9
C25-C26-H26A	109.5	C25-C26-H26B	109.5
H26A-C26-H26B	109.5	C25-C26-H26C	109.5
H26A-C26-H26C	109.5	H26B-C26-H26C	109.5
C25-C27-H27A	109.5	C25-C27-H27B	109.5
H27A-C27-H27B	109.5	C25-C27-H27C	109.5
H27A-C27-H27C	109.5	H27B-C27-H27C	109.5

N3-C28-C29	119.64(18)	N3-C28-H28	120.2
C29-C28-H28	120.2	C28-C29-C30	121.0(2)
C28-C29-H29	119.5	C30-C29-H29	119.5
C29-C30-C31	117.06(19)	C29-C30-C33	122.0(2)
C31-C30-C33	120.98(19)	C32-C31-C30	121.0(2)
C32-C31-H31	119.5	C30-C31-H31	119.5
N3-C32-C31	119.7(2)	N3-C32-H32	120.1
C31-C32-H32	120.1	C30-C33-H33A	109.5
C30-C33-H33B	109.5	H33A-C33-H33B	109.5
C30-C33-H33C	109.5	H33A-C33-H33C	109.5
H33B-C33-H33C	109.5	F4-Sb1-F5	91.96(18)
F4-Sb1-F6	89.36(16)	F5-Sb1-F6	178.44(13)
F4-Sb1-F3	177.65(12)	F5-Sb1-F3	89.45(14)
F6-Sb1-F3	89.20(11)	F4-Sb1-F1	89.33(10)
F5-Sb1-F1	90.86(11)	F6-Sb1-F1	89.99(10)
F3-Sb1-F1	92.53(10)	F4-Sb1-F2	90.18(9)
F5-Sb1-F2	89.45(10)	F6-Sb1-F2	89.70(10)
F3-Sb1-F2	87.95(10)	F1-Sb1-F2	179.42(9)

Table 24. Dihedral angles of complex 4.7.

Bond	Angle(°)	Bond	Angle(°)
Au1-O1-N3-C28	-14.7(2)	Au1-O1-N3-C32	166.46(14)
C2-N1-C1-N2	0.0(2)	C4-N1-C1-N2	178.37(17)
C2-N1-C1-Au1	-177.98(15)	C4-N1-C1-Au1	0.4(3)
C3-N2-C1-N1	0.0(2)	C16-N2-C1-N1	-178.95(17)
C3-N2-C1-Au1	178.15(14)	C16-N2-C1-Au1	-0.8(3)
C1-N1-C2-C3	0.0(2)	C4-N1-C2-C3	-178.32(19)
N1-C2-C3-N2	0.0(2)	C1-N2-C3-C2	0.0(2)
C16-N2-C3-C2	178.85(19)	C1-N1-C4-C9	-86.6(2)
C2-N1-C4-C9	91.5(2)	C1-N1-C4-C5	91.8(2)
C2-N1-C4-C5	-90.1(2)	C9-C4-C5-C6	1.7(3)
N1-C4-C5-C6	-176.61(18)	C9-C4-C5-C10	-177.0(2)
N1-C4-C5-C10	4.6(3)	C4-C5-C6-C7	-0.7(3)
C10-C5-C6-C7	178.1(2)	C5-C6-C7-C8	-0.4(3)
C6-C7-C8-C9	0.6(3)	C7-C8-C9-C4	0.4(3)

C7-C8-C9-C13	-179.9(2)	C5-C4-C9-C8	-1.6(3)
N1-C4-C9-C8	176.76(18)	C5-C4-C9-C13	178.75(19)
N1-C4-C9-C13	-2.9(3)	C6-C5-C10-C11	57.9(3)
C4-C5-C10-C11	-123.4(2)	C6-C5-C10-C12	-66.4(3)
C4-C5-C10-C12	112.3(2)	C8-C9-C13-C15	53.3(3)
C4-C9-C13-C15	-127.0(2)	C8-C9-C13-C14	-70.4(3)
C4-C9-C13-C14	109.3(2)	C1-N2-C16-C17	77.3(2)
C3-N2-C16-C17	-101.4(2)	C1-N2-C16-C21	-99.5(2)
C3-N2-C16-C21	81.7(3)	C21-C16-C17-C18	0.2(3)
N2-C16-C17-C18	-176.42(18)	C21-C16-C17-C22	-178.0(2)
N2-C16-C17-C22	5.3(3)	C16-C17-C18-C19	0.0(3)
C22-C17-C18-C19	178.4(2)	C17-C18-C19-C20	-0.4(4)
C18-C19-C20-C21	0.5(4)	C19-C20-C21-C16	-0.2(3)
C19-C20-C21-C25	177.5(2)	C17-C16-C21-C20	-0.1(3)
N2-C16-C21-C20	176.53(18)	C17-C16-C21-C25	-177.9(2)
N2-C16-C21-C25	-1.2(3)	C16-C17-C22-C24	108.3(3)
C18-C17-C22-C24	-69.9(3)	C16-C17-C22-C23	-127.6(2)
C18-C17-C22-C23	54.2(3)	C20-C21-C25-C27	31.9(3)
C16-C21-C25-C27	-150.5(2)	C20-C21-C25-C26	-91.2(3)
C16-C21-C25-C26	86.5(2)	C32-N3-C28-C29	0.9(3)
O1-N3-C28-C29	-177.79(18)	N3-C28-C29-C30	-0.8(3)
C28-C29-C30-C31	0.1(3)	C28-C29-C30-C33	178.9(2)
C29-C30-C31-C32	0.6(3)	C33-C30-C31-C32	-178.2(2)
C28-N3-C32-C31	-0.3(3)	O1-N3-C32-C31	178.6(2)
C30-C31-C32-N3	-0.5(3)		

5. Conclusion

Cationic gold(I) α-oxo carbenes have often been invoked as the key reaction intermediate in many gold(I)-catalyzed reactions. This species of α-oxo carbenes has been proposed as the intermediate in gold(I)-catalyzed carbene transfer reactions of stabilized diazo compounds with alkenes, alkynes, and arenes, as well as in gold(I)-catalyzed oxidation of alkynes with aromatic and aliphatic oxidants (e.g., amine *N*-oxides, sulfoxides, nitrones, epoxides, and nitro groups) and subsequent carbene transfer. Despite α-oxo carbenes being the prominent hypothesized intermediate in these reactions, there is not experimental or computational evidence to support the formation of α-oxo carbenes in these transformations. Alternatively, computational studies and gas-phase experiments suggest that the mechanism progresses directly from an *N*-alkenoxysulfonium/pyridinium species to an α-oxo carbenoid species. Bot the *N*-alkenoxysulfonium/pyridinium complexes and α-oxo carbenoid complexes are supported by computational studies, but there is a gap in experimental evidence to support the formation of such compounds.

We first looked at the synthesis, structure, and reactivity, of α-oxo carbenoid complexes to gather experimental evidence on these compounds. Therefore, we have synthesized a series of gold α-oxo carbenoid complexes, such as trifluoromethanesulfonate, pyridinium, and sulfonium α-oxo carbenoid complexes, as

well as α,α-dioxo carbenoid complexes. All synthesized compounds were found to be stable at room temperature and in the solid state and was able to be characterized by crystal structure. The stability of these complexes varied depending on the ylide ligand or the leaving group. The trifluoromethanesulfonate complexes were able to carry out cyclopropanation reactions and was easily displaced by nucleophiles, such as 4-picoline and dimethyl sulfide. Alternatively, the entire ylide from the α,α-dioxo carbenoid complexes could be displaces with nucleophiles. Otherwise, these α-oxo carbenoid complexes displayed no reactivity. The low reactivity suggests these carbenoids may not participate in gold-catalyzed alkyne oxidation reactions but do suggest *N*-alkenoxypyridinium/sulfonium complexes as reactive intermediates.

To gain more insight on N-alkenoxysulfonium species, we looked at the rearrangement of alkynyl sulfoxides. Using low temperature NMR techniques and isotopic labeling experiments, an *N*-alkenoxysulfonium species was observed and characterized as the key intermediate in the transformation. Formation of the *N*-alkenoxysulfonium complex confirmed that the mechanism forms the 5-*exo*-dig compound as opposed to the 6-*endo*-dig compound. Kinetic data showed that the transformation from the *N*-alkenoxysulfonium intermediate to product was second order, which was slowed by the presence of a nucleophile. Other than slowing the rate of reaction and shifting the NMR peaks due to hydrogen bonding, the nucleophile had

no effect on the intermediate. At no point in low temperature analysis was an α-oxo carbene species observed.

Taken together, this work focused on the observation and characterization of key reaction intermediates opposes the formation of gold α-oxo carbenes in these transformations. We were able to conclude that gold α-oxo carbenoids are a stable species of compounds, although they may not be involved in the oxidation and carbene transfer reactions. Alternatively, the *N*-alkenoxysulfonium intermediate was shown to be the key intermediate in the gold-catalyzed alkyne oxidation reaction. This work helps fill the gap in knowledge surrounding the mechanism of gold(I)-catalyzed carbene transfer reactions of stabilized diazo compounds and oxidation of alkynes with aromatic and aliphatic oxidants and carbene transfer.

Appendix A: Synthesis of Thiophenium Complexes

A.1 Background

The following synthetic approached to synthesize thiophenium complexes were carried out with the intention to identify potential intermediates in the gold(I)-catalyzed rearrangement of alkynyl sulfoxides and further understand the mechanism of gold-catalyzed alkynyl sulfoxide rearrangements (refer to Chapter 4). Zhang and coworkers report that formation of a gold α-oxo carbene species (**A**) in the intramolecular sulfoxide rearrangement reaction would likely result in observation or trapping of thiophenium complex (**B**)(Scheme 38).

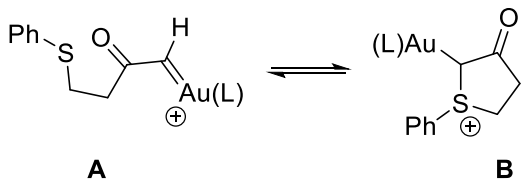

Scheme 38. Proposed isomerization of carbene (A) to gold-bound thiophenium complex (B).

Similarly, Davies[138,139] reported gold-catalyzed intramolecular alkyne oxidation and subsequent [2,3]-sigmatropic rearrangement to synthesize a series of heterocyclic rings. They propose that after initial formation an *N*-alkenoxysulfonium species (**C**), an α-oxo carbene species (**D**) forms and then cyclizes to a sulfur ylide (**E**), which then undergoes a [2,3]-sigmatropic rearrangement to yield the observed products (**F**) (Scheme 39). The proposed sulfur ylide intermediate (**E**) is similar to the predicted resting

cyclization intermediate (**B**). While Davies does not experimental observe intermediates **D** or **E**, the observed products support the sigmatropic rearrangement from **E**, which would form from either a carbene or perhaps a carbenoid complex. While progress synthesizing thiophenium complexes was achieved, these complexes were never observed when studying the gold(I)-catalyzed rearrangement of alkynyl sulfoxides reported in chapter four. Herein, we report the synthetic efforts to make thiophenium complexes.

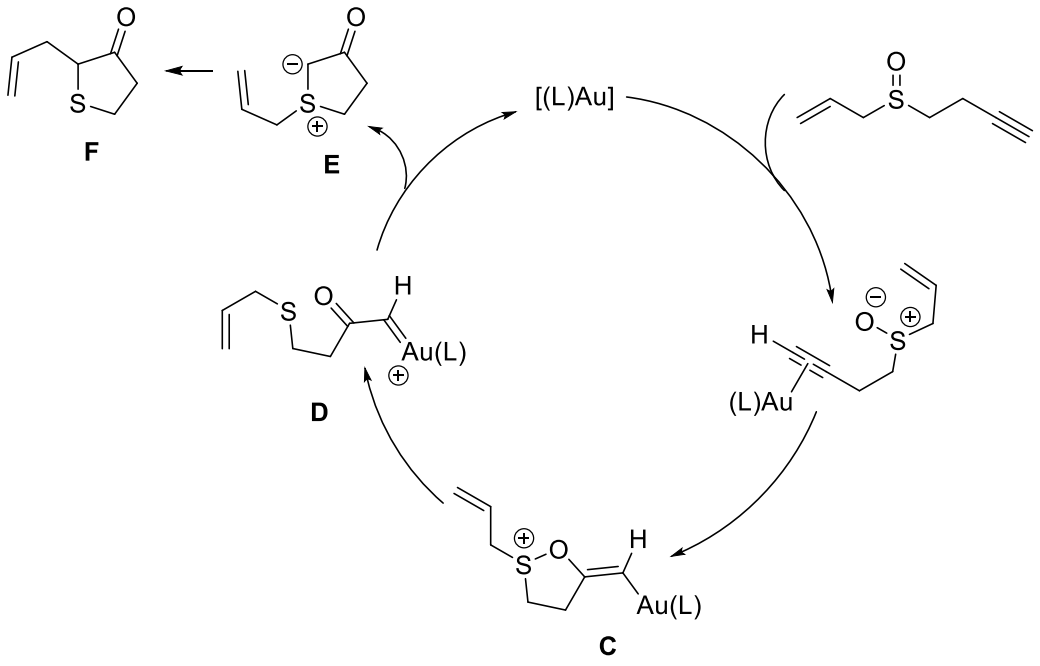

Scheme 39. Reaction mechanism wherein a thiophenium complex (E) is generated before undergoing sigmatropic rearrangement to achieve the observed products.[138]

A.2 Gold(I)-Catalyzed Rearrangement of Alkynyl Benzyl Sulfoxide

Instead of starting with but-1-yn-4-yl(p-tolyl)sulfoxide, the benzyl analog, 1-((but-3-yn-1-ylsulfinyl)methyl)-4-methylbenzene (**A.1**), was used. There have been reported thiophenium complexes synthesized featuring varying alkyl group attached to the sulfur (**G** and **H**) or stabilized with additional functional group on the five membered ring (**I** and **J**)(Figure 33).[140]

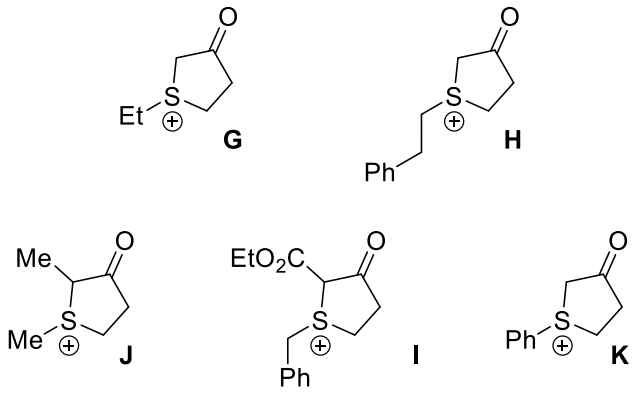

Figure 33. Reported thiophenium complexes.

In the hopes that the benzyl group would demonstrate similar stability to compounds **G**-**J**, 1-((but-3-yn-1-ylsulfinyl)methyl)-4-methylbenzene (17.2 mg, 8.3 x 10^{-2} mmol) was added to (IPr)AuOTf (61.2 mg, 8.3 x 10^{-2} mmol) in dichloromethane (4 mL) at room temperature. After two hours, an aliquot of the reaction mixture was analyzed by ^{1}H NMR, showing two prominent compounds in a 2:1 mixture (**A.2:A.3**). The spectrum features an ABq at δ 4.38 (J_{AB} = 11.2 Hz), which is a characteristic splitting pattern of

thiophenium complexes, indicating the formation of **A.2** *in situ* (Scheme 35). The spectrum also featured peaks at δ 6.29 (dd, *J* = 17.7, 10.5 Hz), 6.17 (d, *J* = 17.7 Hz), and 5.90 (d, *J* = 10.5 Hz), which has been attributed to the decomposition of **A.2** to **A.3**. Purkiss[132] has reported thiophenium complex (Figure 31, **K**) readily undergoing ring-opening to form vinyl ketones, which is what has appeared to have happened with **A.2** to **A.3** *in situ* (Scheme 40). Upon a recrystallization workup of the reaction, the thiophenium complex **A.2** and vinyl ketone **A.3** were no longer present. Instead, compound **A.4** was isolated as a yellow oil (31 %). While other organic fragments were observed to attribute to the loss in mass, they were not characterized and were not compound **A.2** or **A.3**.

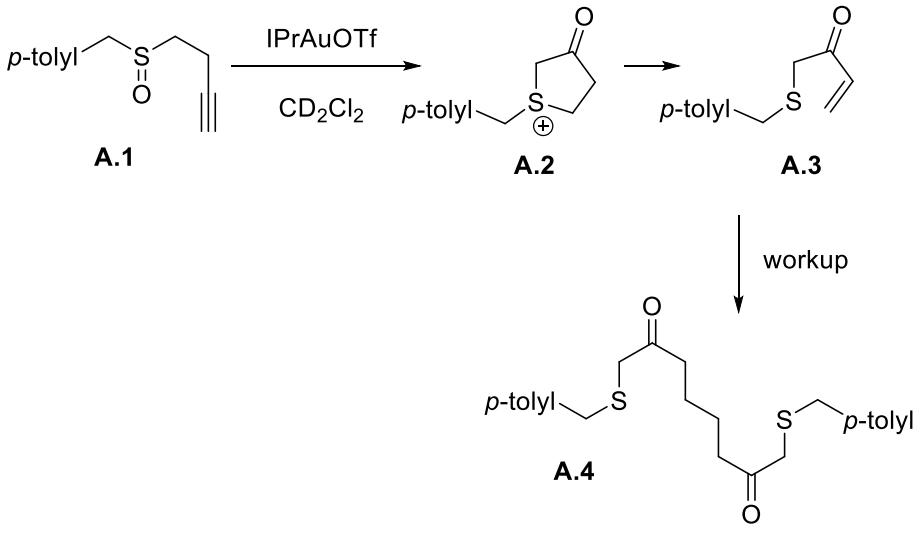

Scheme 40. Reaction pathway of formation of thiophenium compound (A.2) and degradation into α,β-unsaturated ketone (A.3) and resulting dimerization product (A.4).

A.3 Attempted Synthesis of Cyclic β-Oxosulfonium Salts

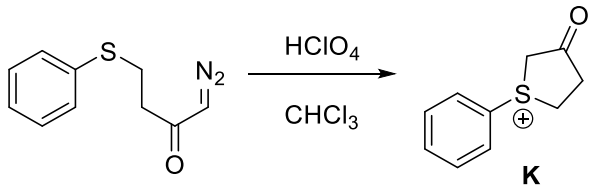

Scheme 41. Reported synthesis of cyclic β-oxosulfonium complex B.

If the rearrangement of alkynyl sulfoxides discussed in chapter 4 were forming an α-oxo carbene, it is hypothesized the more stable isomer (Scheme 38, **B**) would be observed.[60] To independently synthesize **B**, the analogous β-oxosulfonium salt could be synthesized, then treated with base and (IPr)AuOTf. The synthesis of cyclic β-oxosulfonium salt **K** was reported in 1981 by Purkiss from diazo sulfoxide complex, 1-diazo-4-(phenylthiol)butan-2-one) (Scheme 41).[132] Unfortunately, the diazo sulfoxide complex was reported to be synthesized using diazomethane. Due to the hazardous conditions and safety concerns surrounding diazomethane, we attempted to derive alternate routes to synthesize **A.5** (Scheme 42). Furthermore, it should be noted that in the presence of a nucleophile, Purkiss reported the ring of **B** to open and form an α,β-unsaturated ketone, a result that was observed during our studies.

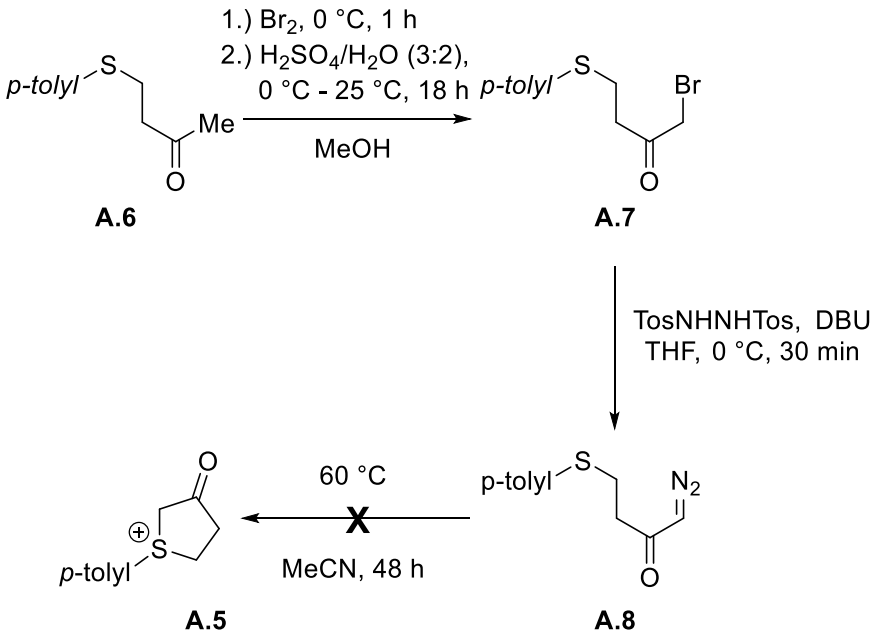

Scheme 42. Synthesis of α-carbonyl diazo to for β-oxosulfonium complex.

In an attempt to synthesize **A** without diazomethane (Scheme 42), 4-(*p*-tolylthio)butan-2-one (**A.6**) was treated with bromine in methanol at 0 °C followed by acidification with H_2SO_2/H_2O to afford 1-bromo-4-(*p*-tolyl)butan-2-one (**A.7**) in 77 % yield, which was used in the next step without purification. Crude **A.7** (360 mg, 1.3 mmol) was treated with N,N-ditosylhydrazine and DBU (0.3 mL, 1.98 mmol) in THF at 0 °C for 30 min. Work up and chromatography led to isolation of 1-diazo-4-(*p*-tolylthio)butan-2-one (**A.8**) in 15 % yield. 1-Diazo-4-(*p*-tolylthio)butan-2-one **A.8** was then dissolved in MeCN and heated at 60 °C for 48 h in an attempt to cyclize **A.8** to yield

the desired thiophenium complex (**A.5**) (Scheme 42). However, no reaction was observed and starting material **A.8** was recovered.

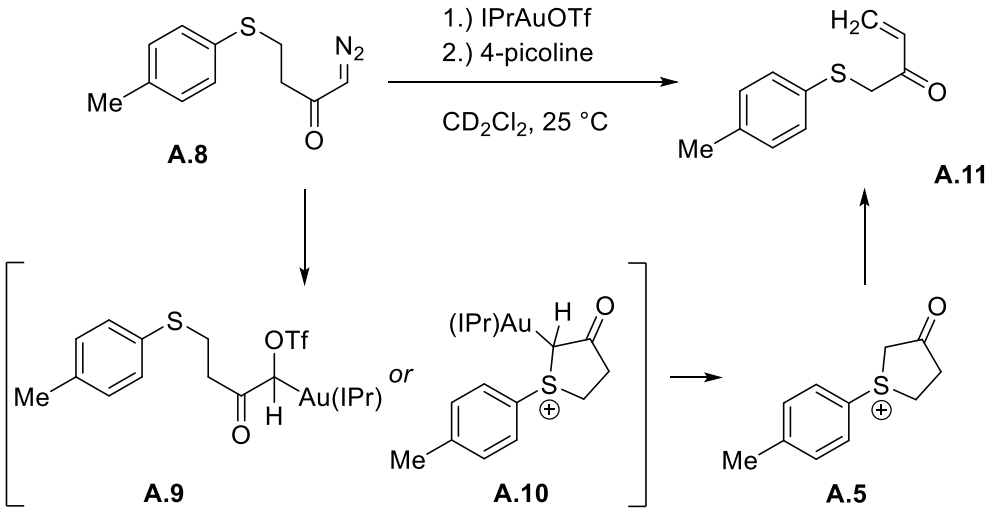

Scheme 43. Reaction pathway to observe desired product (A.5), but instead obtaining α,β-unsaturated ketone (A.11).

Treatment of **A.8** with (IPr)AuOTf in CD_2Cl_2 (<1 min, 25 °C) led to immediate effervescence and the solution turned from colorless to yellow (Scheme 43). ^{1}H NMR analysis of the resulting mixture displayed a resonance at δ 5.24 which was attributed to the α-H resonance indicative of the formation of **A.9** or **A.10** Additionally, methylidene resonances at δ 2.99 and δ 2.83 were observed, which indicate carbenoid **A.9** is intermediate formed, as the methylidene resonances of **A.8** are δ 3.12 and δ 2.94 whereas the methylidene resonance of β-oxosulfonium salt (**B**) are reported at δ 4.13 and δ 3.07. However, similar triflate carbenoid complexes reported in previous work[79] had an α-C resonance at δ 96.2 or δ 104, and no similar resonance was observed in the spectrum for

this intermediate, indicating it may not be **A.9**. As there is no reported carbon NMR spectrum for a compound similar to **A.10**, we do not if our spectrum has characteristics indicative of this compound. After workup filtration through Celite followed by concentration under vacuum and recrystallization, the resonance at δ 5.24 attributed to the α-H of **A.9** or **A.10** was no longer observed in the crude mixture. Instead, 1-(p-tolylthio)but-3-en-2-one (**A.11**) was obtained in 87% yield. As we know vinyl ketones are often decomposition products of β-oxosulfonium salts,[132] we can assume **A.5** formed but was not observed.

Additionally, addition of 1 equivalent of 4-picoline to the intermediate (either **A.9** or **A.10**) formed after **A.8** was mixed with (IPr)AuOTf resulted in the immediate formation of **A.11** *in situ* in similar yields to when **A.11** was obtained from working up the reaction mixture containing the unknown intermediate. This heightened reactivity could possibly be attributed to displacement of triflate group in carbenoid **A.9**, which could potentially afford a more reactive species, as was seen with the carbenoids reported in chapter three. However, once the 4-picolinium carbenoids formed, they showed no further reactivity, so this explanation could be unlikely. Alternatively, the heightened activity could be attributed to 4-picoline reacting with the gold, wherein **A.10** forms and the 4-picoline reacts quickly to form (IPr)Au-(4-picoline) and **A.5**, but this explanation is also problematic, as a similar effect should also have been observed

when 4-picoline was added to the rearrangement of alkynyl sulfoxides investigated in chapter four, and the effect was actually slowing down the reaction. Therefore, we still do not know which proposed intermediate is the compound observed, nor why 4-picoline leads to direct formation of **A.11**.

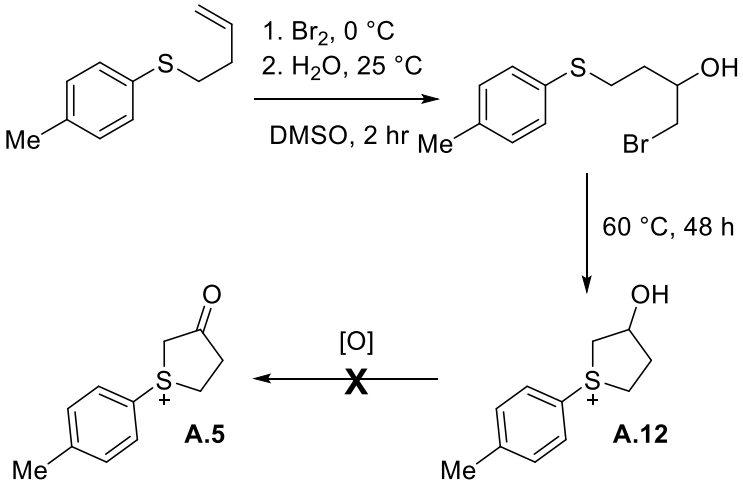

Scheme 44. Synthesis of A.12 was made to then oxidize into desired product A.5.

Complex **A.5** was also attempted to be synthesized from an alternate route. First, compound **A.12** was made via hydrobromination of 1-(3-buten-1-ylthio)-4-methylbenzene to form 1-bromo-4-(p-tolylthio)butan-2-ol, which was then heated in the same pot to at 60 °C for 48 hours to yield 3-Hydroxy-1-(*p*-tolyl)tetrahydro-1*H*-thiophen-1-ium (**A.12**) in 21 % yield. Compound A.11 was then subjected of a wide range of oxidants, however, no oxidizing agent (e.g. Dess-Martin periodinane, pyridinium chlorochromate, or Swern's reagent) was able to form the ketone (**A.5**) (Scheme 44).

A.4 Summary

The above thiophenium complexes syntheses were carried out in an attempt to characterize intermediates in previous reactions and gain mechanistic insight. However, none of the outcomes achieved were applicable to the above research. While, in some cases, a thiophenium complex was able to be observed *in situ*, there was no chance to isolate nor characterize the species. Alternatively, there were cases where the product obtained from a reaction indicated the formation of a thiophenium complex, but none were observed. While we may not know if the gold bound thiophenium complex (**B**) is stable enough to exist, the thiophenium complex along (**A.2** and **A.5**) appear to be too unstable to isolate.

A.5 Experimental Data

A.1.1 General Methods

Reactions were run under a nitrogen atmosphere in flame-dried glassware using standard glovebox and Schlenk techniques. NMR spectra were obtained on a 400 MHz Varian Inova spectrometer and a 500 MHz Bruker spectrometer. ^{13}C NMR spectra were referenced to residual $CDCl_3$ (δ 77.2) or CH_2Cl_2 (δ 53.8). The ^{1}H NMR spectra were referenced to residual $CDCl_3$ (δ 7.26) or CH_2Cl_2 (δ 5.32). Diethyl ether, CH_2Cl_2, and tetrahydrofuran were purified by passage through columns of activated alumina under nitrogen. Silver-free (IPr)AuOTf was synthesized employing published procedures.[119,120]

A.1.2 Synthesis of Benzyl Thiophenium Complex and Precursors

***S*-(4-methylbenzyl) pent-4-ynethionate (A.1).** Hydrogen peroxide (30 % w/w, 3.7 mL, 32.4 mmol) was added dropwise to a solution of but-3-yn-1-yl(4-methylbenzyl)sulfane (1.43 mg, 8.11 mmol) in MeOH (10 mL) based on similar reported procedures.[129] The solution was stirred for 18 h and then quenched with water (20 mL). The product was then extracted with diethyl ether (3x10 mL), washed with brine (20 mL), and dried over $MgSO_4$. After filtering and concentrating the solution under vacuum, the resulting oil was purified by column chromatography (SiO_2, hexanes/EtOAc = 1:1) and yielded **A.1** as a pale yellow oil (72% yield). ^{1}H NMR (500 MHz, $CDCl_3$): δ 7.19 (s, 4H), 4.10 – 3.98 (m, 2H), 2.82 – 2.70 (m, 2H), 2.70 – 2.61 (m, 2H), 2.35 (s, 3H), 2.05 (t, *J* = 2.6 Hz, 1H). ^{13}C{^{1}H} NMR (126 MHz, $CDCl_3$): δ 138.6, 130.1, 129.9, 126.3, 81.0, 70.6, 58.1, 49.0, 21.3, 12.5. HRMS (ESI) calcd. (found) for $C_{12}H_{14}OS$ (M^+): 206.3030 (207.0842).

1,8-Bis[(4-methylbenzyl)thio]octane-2,7-dione (A.4). (IPr)AuOTf (61.2 mg, 8.3 x 10-2 mmol) was dissolved in dichloromethane (4 mL) at room temperature. *S*-(4-methylbenzyl) pent-4-ynethionate (**A.1**) (17.2 mg, 8.3 x 10^{-2} mmol) was dissolved in dichloromethane (1 mL) and added dropwise to the (IPr)AuOTf solution. The resulting mixture was stirred for two hours. Before workup, an aliquot of the rection mixture was analyzed by ^{1}H NMR spectroscopy in CD_2Cl_2. In the crude reaction mixture, there was

an ABq at δ 4.38 with J_{AB} = 11.2 Hz, corresponding to **A.2**, and vinylic protons at δ 6.29 (dd, *J* = 17.7, 10.5 Hz), 6.17 (d, *J* = 17.7 Hz), and 5.90 (d, *J* = 10.5 Hz), corresponding to **A.3**. These compounds were present in a 2:1 mixture ratio (**A.2:A.3**). The micture was then filtered through Celite, then concentrated under vacuum. The resulting residue was then recrystallized with by layering dichloromethane and hexanes and cooling to -20 °C overnight. The mother liquor was then decanted from the solids and concentrated under vacuum to afford a mixture of compounds including **A.4**. The yellow oil mixture was purified by column chromatography (SiO_2: hexanes-EtOAc = 9:1) to cleanly isolate **A.4** as a pale yellow oil (31 % yield). The peaks attributed to **A.2** and **A.3** in the crude mixture were not observed in the crude product mixture after recrystallization.

For **A.2:** ^{1}H NMR (500 MHz, CD_2Cl_2): δ 4.38 (ABq, J_{AB} = 11.2 Hz, 2H)

For **A.3:** ^{1}H NMR (500 MHz, CD_2Cl_2): δ 6.29 (dd, *J* = 17.7, 10.5 Hz), 6.17 (d, *J* = 17.7 Hz), 5.90 (d, *J* = 10.5 Hz)

For **A.4:** ^{1}H NMR (500 MHz, $CDCl_3$): δ 7.32 (d, *J* = 7.8 Hz, 2H), 7.22 (d, *J* = 7.8 Hz, 2H), 4.22 (s), 3.13 (t, *J* = 7.4 Hz, 2H), 2.92 (t, *J* = 7.4 Hz, 2H), 2.37 (s, 3H), 2.20 (s, 3H).

A.1.2 Synthesis of *p*-Tolyl Thiophenium Complex and Precursors

1-Bromo-4-(*p*-tolylthio)butan-2-one (A.7). 4-(*p*-Tolylthio)butan-2-one (**A.6**) (1.6 g, 8.3 mmol) was dissolved in MeOH (10 mL) and was cooled to 0 °C. Bromine (0.43 mL, 8.3 mmol) was added dropwise to the reaction solution and stirred for 1 h at 0 °C. A

mixture of H_2SO_2/H_2O (3:2, 7mL) was added dropwise at 0 °C. The solution was then allowed to come to room temperature and stirred for 18 h. The solution was then diluted with H_2O (20 mL) and organic products extracted with diethyl ether (20 mL). The organic layer was then washed with $NaHCO_3$ (20 mL) followed by H_2O (20 mL) and dried over $MgSO_4$. The mixture was then filtered and the solution as concentrated under vacuum to afford 1-bromo-4-(*p*-tolylthio)butan-2-one (**A.7**) as a dark yellow oil (1.6 g, 77 %). The product was used in the next step without purification. ^1H NMR (500 MHz, $CDCl_3$): δ 7.27 (d, *J* = 6.2 Hz, 2H), 7.12 (d, *J* = 8.0 Hz, 2H), 3.85 (s, 2H), 3.12 (t, *J* = 7.1 Hz, 2H), 2.94 (t, *J* = 7.1 Hz, 2H), 2.33 (s, 3H). $^{13}C\{^1H\}$ NMR (126 MHz, $CDCl_3$): δ 200.5, 137.1, 131.9, 130.9, 130.0, 39.8, 34.3, 28.8, 21.2.

1-Diazo-4-(*p*-tolylthio)butan-2-one (A.8). 1-Bromo-4-(*p*-tolylthio)butan-2-one (**A.7**) (360 mg, 1.3 mmol) and N,N-ditosylhydrazine(496 mg, 1.5 mmol) were combined and dissolved with THF (5 mL), then cooled to 0 °C and stirred for 30 min. 1,8-Diazabicyclo[5.4.0]undec-7-ene (DBU) (0.3 mL, 1.98 mmol) was then added dropwise and stirred for 30 min at 0 °C. The solution was then washed with $NaHCO_3$ (10 mL) and extracted with diethyl ether (3 x 10 mL). The organic layers were combined and washed with brine (30 mL), then dried over $MgSO_4$, filtered, and concentrated under vacuum. The resulting oil was then purified by column chromatography (SiO_2, hexanes/EtOAc = 3/1) and yielded a yellow oil (**A.8**, 44.3 mg, 15 %). When **A.8** was dissolved in MeCN and

heated at 60 °C for 48 h, the ring did not close to yield a five membered ring (**A.5**). ^{1}H NMR (500 MHz, $CDCl_3$): δ 7.27 (d, *J* = 6.2 Hz, 2H), 7.12 (d, *J* = 8.0 Hz, 2H), 3.85 (s, 2H), 3.12 (t, *J* = 7.1 Hz, 2H), 2.94 (t, *J* = 7.1 Hz, 2H), 2.33 (s, 3H). ^{13}C{^{1}H} NMR (126 MHz, $CDCl_3$): δ 192.7, 136.9, 131.6, 130.7, 129.9, 55.0, 40.4, 29.6, 21.1.

1-(*p*-Tolylthio)but-3-en-2-one (A.11). (IPr)AuOTf (14.6 mg, 2.0 x 10^{-2} mmol) was added to an NMR tube and dissolved in CD_2Cl_2 (0.5 mL). 1-Diazo-4-(*p*-tolylthio)butan-2-one (**A.8**) (4.4 mg, 2.0 x 10^{-2} mmol) from a stock solution was added to the gold solution in the NMR tube. The mixture immediately bubbled and turned from colorless to yellow. When the reaction mixture was analyzed by ^{1}H NMR spectroscopy, an α-H resonance at δ 5.24 was observed and attributed to the formation of **A.9** or **A.10**. The reaction mixture was transferred to a vial and layered with pentane, then cooled to -20 °C for 12 hours to yield a clear oil in the bottom of the vial. The mother liquor was decanted and concentrated to a yellow oil, which was analyzed by ^{1}HNMR and found to be 1-(*p*-tolylthio)but-3-en-2-one (**A.11**) (3.3 mg, 87%). ^{1}H NMR (500 MHz, $CDCl_3$): δ 7.27 (d, *J* = 8.0 Hz, 2H), 7.12 (d, *J* = 8.0 Hz, 2H), 6.56 (dd, *J* = 17.5, 10.5 Hz, 1H), 6.24 (d, *J* = 17.4 Hz, 1H), 5.83 (d, *J* = 10.5 Hz, 1H), 3.77 (s, 2H), 2.31 (s, 3H).

A.5.6.1 Synthesis of Tetrahydro-thiophenium Compound

3-Hydroxy-1-(*p*-tolyl)tetrahydro-1*H*-thiophen-1-ium (A.12) 1-(3-Buten-1-ylthio)-4-methylbenzene[129] (1.7 g, 9.6 mmol) was dissolved in DMSO (8 mL) and cooled to 0 °C

in an ice bath. Bromine (500 μL, 9.6 mmol) was added dropwise, and stirred for one minute before the addition of water (3.5 mL). After ten minutes, the reaction mixture was removed from the ice bath and stirred for three hours at 25 °C. After three hours, the mixture was heated to 60 °C and stirred for 48 hours. The reaction mixture was then poured over $NaHCO_3$ and extracted with diethyl ether (3 x 10 mL). The organic layers were combined, washed with brine, dried ($MgSO_4$), filtered, and concentrated under vacuum. The resulting orange oil was chromatographed (SiO_2: hexanes-EtOAc = 9:1) to afford a yellow oil (**A.12**, 390 mg, 21 %). ^1H NMR (500 MHz, $CDCl_3$): δ 7.30(d, *J* = 8.2 Hz, 2H), 7.12 (d, *J* = 7.9, 2H), 4.06 (dd, *J* = 9.0, 6.4 Hz, 1H), 3.94 (td, *J* = 8.1, 6.7 Hz, 1H), 3.85 (td, *J* = 8.0, 5.7 Hz, 1H), 3.73 (dq, *J* = 7.8, 5.7 Hz, 1H) 3.67 (dd, *J* = 9.0, 5.5 Hz, 1H), 2.33 (s, 3H), 2.28 (ddt, *J* = 13.1, 7.8, 6.6, 1H), 1.91 (ddt, *J* = 13.1, 7.6, 6.5 Hz, 1H). $^{13}C\{^1H\}$ NMR (126 MHz, $CDCl_3$): δ 137.2, 131.8, 131.7, 129.9, 73.7, 67.8, 45.6, 33.2, 21.2. HRMS (ESI) calcd. (found) for $C_{11}H_{15}OS^+$ (M^+): 195.0838 (195.0844).

References

(1) Teles, J. H.; Brode, S.; Chabanas, M. "Cationic Gold(I) Complexes: Highly Efficient Catalysts for the Addition of Alcohols to Alkynes," *Angew. Chem., Int. Ed.* 1998, *37* (10), 1415-1418.

(2) Miró J.; del Pozo, C. "Fluorine and Gold: A Fruitful Partnership," *Chem. Rev.* 2016, *116*, 11924–11966.

(3) Dorel, R.; Echavarren, A. M. "Gold(I)-Catalyzed Activation of Alkynes for the Construction of Molecular Complexity," *Chem. Rev*. 2015, *115,* 9028–9072.

(4) Gorin, D. J.; Sherry, B. D.; Toste, F. D. "Ligand Effects in Homogeneous Au Catalysis," *Chem. Rev*. 2008, *108* (8), 3351-3378.

(5) Bandini, M. "Gold-catalyzed decorations of arenes and heteroarenes with C–C multiple bonds," *Chem. Soc. Rev.* 2011, *40*, 1358-1367.

(6) Corma, A.; Leyva-Pérez, A.; Sabater, M. J. "Gold-Catalyzed Carbon-Heteroatom Bond-Forming Reactions," *Chem. Rev*. 2011, *111* (3), 1657-1712.

(7) Gorin, D. J.; Toste, F. D. "Relativistic effects in homogeneous gold catalysis," *Nature* 2007, *446* (7134), 395-403.

(8) Schwerdtfeger, P. *Relativistic effects in properties of gold. Heteroatom Chemistry: An International Journal of Main Group Elements*. 2002, *13* (6), 578-584.

(9) Pyykkö, P. "Theoretical chemistry of gold. III." *Chemical Society Reviews* 2008, *37* (9), 1967-1997.

(10) Pyykkö, P. "Theoretical chemistry of gold. II." *Inorganica Chimica Acta* 2005, *358* (14), 4113-4130.

(11) Nakanishi, W.; Yamanaka, M.; Nakamura, E. "Reactivity and stability of organocopper (I), silver (I), and gold (I) ate compounds and their trivalent derivatives," *J. Am. Chem. Soc.*, 2005, *127* (5), 1446-1453.

(12) Komiya, S.; Kochi, J. "Electrophilic cleavage of organogold complexes with acids. The mechanism of the reductive elimination of dialkyl (aniono) gold (III) species," ," *J. Am. Chem. Soc.*, 1976, *98* (24), 7599-7607.

(13) Komiya, S.; Albright, T. A.; Hoffmann, R.; Kochi, J. K. "Reductive elimination and isomerization of organogold complexes. Theoretical studies of

trialkylgold species as reactive intermediates," *J. Am. Chem. Soc.*, 1976, *98* (23), 7255-7265.

(14) Joost, M.; Amgoune, A.; Bourissou, D. "Reactivity of gold complexes towards elementary organometallic reactions," *Angew. Chem. Int. Ed.*, 2015, *54* (50), 15022-15045.

(15) Shen, H. C. "Recent advances in synthesis of heterocycles and carbocycles via homogeneous gold catalysis. Part 1: Heteroatom addition and hydroarylation reactions of alkynes, allenes, and alkenes," *Tetrahedron*, 2008, *64* (18), 3885-3903.

(16) Li, Z.; Brouwer, C.; He, C. "Gold-Catalyzed Organic Transformations," *Chem. Rev.*, 2008, *108* (8), 3239-3265.

(17) Jiménez-Núñez, E.; Echavarren, A. M. "Gold-Catalyzed Cycloisomerization of Enynes: A Mechanistic Perspective," *Chem. Rev*., 2008, *108*, 3326-3350.

(18) Echavarren, A. M.; Jiménez-Núñez, E. "Complexity via Gold-Catalyzed Molecular Gymnastics," *Top. Catal*., 2010, *53*, 924-930.

(19) Zhang, L.; Sun, J.; Kozmin, S. A. "Gold and Platinum Catalysis of Enyne Cycloisomerization," *Adv. Synth. Catal*., 2006, *348*, 2271-2296.

(20) Fürstner, A. "Gold and Platinum Catalysis−A Convenient Tool for Generating Molecular Complexity," *Chem. Soc. Rev*., 2009, *38*, 3208-3221.

(21) López, F.; Mascareñas, J. L. "Recent Developments in Gold-Catalyzed Cycloaddition Reactions," *Beilstein J. Org. Chem.*, 2011, *7*, 1075-1094.

(22) Michelet, V.; Toullec, P. Y.; Genêt, J.-P. "Cycloisomerization of 1,*n*-Enynes: Challenging Metal-Catalyzed Rearrangements and Mechanistic Insights," *Angew. Chem. Int., Ed*. 2008, *47*, 4268-4315.

(23) Hussong, M. W.; Rominger, F.; Krämer, P.; Straub, B. F. "Isolation of a Non-Heteroatom-Stabilized Gold–Carbene Complex" *Angew. Chem. Int. Ed.*, 2014, *53*, 9372 –9375.

(24) Harris, R. J.; Widenhoefer, R. A. "Synthesis, Structure, and Reactivity of a Gold Carbenoid Complex that Lacks Heteroatom Stabilization" *Angew. Chem. Int. Ed.*, 2014, *53*, 9369–9371.

(25) Harris, R. J.; Widenhoefer, R. A. "Generation and Characterization of a Gold Vinylidene Complex Lacking π-Conjugated Heteroatoms," *Angew. Chem. Int. Ed*., 2015, *54*, 6867-6869.

(26) Werlt, C.; Goddard, R.; Fürstner, A. "The First Crystal Structure of a Reactive Dirhodium Carbene Complex and a Versatile Method for the Preparation of Gold Carbenes by Rhodium-to-Gold Transmetalation," *Angew. Chem. Int. Ed*. 2015, *54*, 15452 –15456.

(27) Seidel, G.; Fürstner, A. "Structure of a Reactive Gold Carbenoid," *Angew. Chem. Int. Ed*. 2014, *53*, 4807 –4811.

(28) Carden, R. G.; Lam, N.; Widenhoefer, R. A. "Experimental Evaluation of (L)Au Electron Donor Ability in Cationic Gold Carbene Complexes," *Chem. Eur. J.* 2017, *23*, 17992-18001.

(29) Qian, D.; Zhang, J. "Gold-catalyzed cyclopropanation reactions using a carbenoid precursor toolbox" *Chem. Soc. Rev.* 2015, *44*, 677–698.

(30) Brooner, R. E. M.; Widenhoefer, R. A. "Cationic, Two-Coordinate Gold π-Complexes," *Angew. Chem*. 2013, *125*, 11930-11941; *Angew. Chem. Int. Ed*. 2013, *52*, 11714-11724.

(31) Nieto-Oberhuber, C.; Lopez, S.; Munoz, M. P.; Jiménez-Núñez, E.; Buñuel, E.; Cárdenas, D. J.; Echavarren, A. M. "Gold(i)-Catalyzed Intramolecular Cyclopropanation of Dienynes" *Chem. Eur. J.* 2006, *12*, 1694–1702.

(32) Pérez-Galán, P.; Herrero-Gómez, E.; Hog, D. T.; Martin, N. J. A.; Maseras, F.; Echavarren, A. M. "Mechanism of the gold-catalyzed cyclopropanation of alkenes with 1,6-enynes" *Chem. Sci.* 2011, *2*, 141–149.

(33) Batiste, L.; Fedorov, A.; Chen, P. "Gold carbenes via 1,2-dialkoxycyclopropane ring-opening: a mass spectrometric and DFT study of the reaction pathways" *Chem. Commun*. 2010, *46*, 3899–3901.

(34) Fedorov, A.; Batiste, L.; Bach, A.; Birney, D. M.; Chen, P. "Potential Energy Surface for (Retro)Cyclopropanation: Metathesis with a Cationic Gold Complex" *J. Am. Chem. Soc*. 2011, *133*, 12162–12171.

(35) Wang, Y.; Muratore, M. E.; Echavarren, A. M. "Gold Carbene or Carbenoid: Is There a Difference? " *Chem. Eur. J.* 2015**,** *21*, 7332–7339.

(36) Brookhart, M.; Studabaker, W. B. "Cyclopropanes from Reactions of Transition-Metal-Carbene Complexes with Olefins " *Chem. Rev.* 1987, *87*, 411–432.

(37) Ringger, D. H.; Chen, P. "Rational Design of a Gold Carbene Precursor Complex for a Catalytic Cyclopropanation Reaction" *Angew. Chem. Int. Ed*. 2013, *52*, 4686 –4689.

(38) Sarria Toro, J. M.; García-Morales, C.; Raducan, M.; Smirnova, E. S.; Echavarren, A. M. "Gold(I) Carbenoids: On-Demand Access to Gold(I) Carbenes in Solution" *Angew. Chem. Int. Ed.* 2017, *56*, 1859 –1863.

(39) Fedorov, A.; Moret, M.; Chen, P. "Gas-Phase Synthesis and Reactivity of a Gold Carbene Complex" *J. Am. Chem. Soc.* 2008, *130*, 8880–8881.

(40) Fedorov, A.; Chen, P. "Electronic Effects in the Reactions of Olefin-Coordinated Gold Carbene Complexes" *Organometallics* 2009, *28*, 1278–1281.

(41) Ringger, D. H.; Kobylianskii, I. J.; Serra, D.; Chen, P. "Quantitative Description of Structural Effects on the Stability of Gold(I) Carbenes" *Chem. Eur. J*. 2014, *20*, 14270 –14281.

(42) Kneuper, H.; Harms, K.; Boche, G. "Fuuktionalisierte ijbergangsmetallalkyle: Synthese und Kristallstruktur von Ph,PAu-CHPh-SO,-t-Bu" *J. Organomet. Chem.* 1989, *364*, 275–279.

(43) Vicente, J.; Chicote, M. T.; Saura-Llamas, I.; Turpin, J.; Femandez-Baeza, J. "Keto-stabilized phosphorus ylide gold(I) and gold(III) complexes" *J. Organomet. Chem.* 1987, *333*, 129–137.

(44) Steinborn, D.; Becke, S.; Herzog, R.; Ggnther, M.; Kircheisen, R.; Stoeckli-Evans, H.; Bruhn, C. " Heteroatomfunktionalisierte Methylgold-Komplexe: Synthese und Struktur von Chlormethyl(triphenylphosphin)- und Phenylthiomethyl(trimethylphosphin)gold" *Z. Anorg. Allg. Chem.* 1998, *624*, 1303–1307.

(45) Swift, C.A.; Gronert, S. "Formation and Reactivity of Gold Carbene Complexes in the Gas Phase" *Organometallics* 2014, *33,* 7135–7140.

(46) Yamamoto, Y.; Kanda, Z. "Ylide-Metal Complexes. III. Preparation and Properties of Gold(I) Complexes of Alylidenetriphenylphsphorates and arsoranes" *Bull. Chem. Soc. Jpn*. 1979, *52*, 2560–2562.

(47) Fructos, M. R.; Diáz-Requejo, M. M.; Pérez, P. J. "Gold and diazo reagents: a fruitful tool for developing molecular complexity" *Chem. Commun.* 2016, *52*, 7326–7335.

(48) Liu, L.; Zhang, J. "Gold-catalyzed transformations of α-diazocarbonyl compounds: selectivity and diversity" *Chem. Soc. Rev.* 2016, *45*, 506–516.

(49) Wei, F.; Song, C.; Ma. Y.; Zhou, L.; Tung, C.; Xu, Z. "Gold carbene chemistry from diazo compounds" *Sci. Bull.* 2015, *60*,1479–1492.

(50) Fructos, M. R.; Belderrain, T. R.; de Frémont, P.; Scott, N. M.; Nolan, S. P.; Díaz-Requejo, M. M.; Pérez, P. J. "A Gold Catalyst for Carbene-Transfer Reactions from Ethyl Diazoacetate" *Angew. Chem. Int. Ed.* 2005, *44*, 5284–5288.

(51) de Frémont, P.; Stevens, E. D.; Fructos, M. R.; Díaz-Requejo, M. M.; Pérez, P. J.; Nolan, S. P. "Synthesis, isolation and characterization of cationic gold(I) *N*-heterocyclic carbene (NHC) complexes" *Chem. Commun.* 2006, 2045–2047.

(52) Flores, J. A.; Dias, H. V. R. "Gold(I) Ethylene and Copper(I) Ethylene Complexes Supported by a Polyhalogenated Triazapentadienyl Ligand" *Inorg. Chem.* 2008, *47*, 4448-4450.

(53) Yeom, H.; Shin, S. "Catalytic Access to a-Oxo Gold Carbenes by N-O Bond Oxidants" *Acc. Chem. Res.* 2014, *47*, 966–977.

(54) Xiao, J.; Li, X. "Gold α-Oxo Carbenoids in Catalysis: Catalytic Oxygen- Atom Transfer to Alkynes" *Angew. Chem. Int. Ed*. 2011, *50*, 7226–7236.

(55) Zhang, L. "A Non-Diazo Approach to r-Oxo Gold Carbenes via Gold-Catalyzed Alkyne Oxidation" *Acc. Chem. Res.* 2014, *47*, 877–888.

(56) Zheng, Z.; Wang, Z.; Wang, Y.; Zhang, L. "Au-Catalysed oxidative cyclisation" *Chem. Soc. Rev.* 2016, *45*, 4448–4458.

(57) Shin S. (2014) Gold-Catalyzed Carbene Transfer Reactions. In: Slaughter L. (eds) Homogeneous Gold Catalysis. Topics in Current Chemistry, vol 357. Springer, Cham.

(58) Fructos, M. R.; Urbano, J.; Díaz-Requejo, M. M.; Pérez, P. J. "Evidencing an inner-sphere mechanism for NHC-Au(I)-catalyzed carbene-transfer reactions from ethyl diazoacetate" *Beilstein J. Org. Chem.* 2015, *11*, 2254–2260.

(59) Noey, E.; Luo, Y.; Zhang, L.; Houk, K. N. "Mechanism of Gold(I)-Catalyzed Rearrangements of Acetylenic Amine-N-Oxides: Computational Investigations Lead to a New Mechanism Confirmed by Experiment" *J. Am. Chem. Soc.* 2012, *134*, 1078−1084.

(60) Lu, B.; Li, Y.; Wang, Y.; Aue, D. H.; Luo, Y.; Zhang, L. "[3,3]-Sigmatropic Rearrangement versus Carbene Formation in Gold-Catalyzed Transformations of Alkynyl Aryl Sulfoxides: Mechanistic Studies and Expanded Reaction Scope" *J. Am. Chem. Soc.* 2013, *135*, 8512−8524.

(61) Henrion, G.; Chavas, T. E. J.; Le Goff, X.; Gagosz, F. "Biarylphosphonite Gold(I) Complexes as Superior Catalysts for Oxidative Cyclization of Propynyl Arenes into Indan-2-ones" *Angew. Chem. Int. Ed.* 2013, *52*, 6277−6282.

(62) Schulz, J.; Jašíková, L.; Škríba, A.; Roithová, J. "Role of Gold(I) α-Oxo Carbenes in the Oxidation Reactions of Alkynes Catalyzed by Gold(I) Complexes" *J. Am. Chem. Soc.* 2014, *136*, 11513−11523.

(63) Salomon, R. G.; Kochi, J. K. "Copper(I) catalysis in cyclopropanations with diazo compounds. Role of olefin coordination" *J. Am. Chem. Soc.* 1973, *95*, 3300–3310.

(64) Maxwell, J. L.; Brown, K. C.; Bartley, D. W.; Kodadek, T. "Mechanism of the rhodium porphyrin-catalyzed cyclopropanation of alkenes" *Science* 1992, 256, 1544–1547.

(65) Klimczyk, S.; Huang, X.; Kahlig, H.; Veiros, L. F.; Maulide, N. "Stereoselective Gold(I) Domino Catalysis of Allylic Isomerization and Olefin Cyclopropanation: Mechanistic Studies" *J. Org. Chem.* 2015, *80*, 5719−5729.

(66) Huang, X.; Klimczyk, S.; Veiros, L. F.; Maulide, N. "Stereoselective intramolecular cyclopropanation through catalytic olefin activation" *Chem. Sci.* 2013, *4*, 1105–1110.

(67) Sabbatani, J.; Huang, X.; Veiros, L. F.; Maulide, N. "Gold-Catalyzed Intermolecular Synthesis of Alkylidenecyclopropanes through Catalytic Allene Activation" *Chem. Eur. J.* 2014, *20*, 10636–10639.

(68) Davies, H. M. L.; Beckwith, R. E. J. "Catalytic enantioselective C-H activation by means of metal carbenoid-induced C-H insertion." *Chem. Rev*. 2003, *103*, 2861-2903.

(69) Doyle, M. P.; Duffy, R.; Ratnikov, M.; Zhou, L. "Catalytic carbene insertion into C-H bonds." *Chem. Rev*. 2010, *110*, 704-724.

(70) Gillingham, D.; Fei, N. "Catalytic X-H insertion reactions based on carbenoids." *Chem. Soc. Rev.* 2013, *42*, 4918-4931.

(71) Sun, X. L.; Tang, Y. "Ylide-initiated Michael additions-cyclization reactions beyond cyclopropanes." *Acc. Chem. Res.* 2008, *41*, 937-948.

(72) Zhou, J.; Tang, Y. "The development and application of chiral trioxazolines in asymmetric catalysis and molecular recognition." *Chem. Soc. Rev*. 2005, *34*, 64-676.

(73) Lebel, H.; Marcoux, J. F.; Molinaro, C.; Charette, A. B. "Stereoselective cyclopropanation reactions." *Chem. Rev*., 2003, *103*, 977-1050.

(74) Xia, Y.; Feng, S.; Liu, Z. "Rhodium(I)-catalyzed sequential C(sp)-C(sp^3) and C(sp^3)-C(sp^3) bond formation through migratory carbene insertion. *Angew. Chem. Int. Ed*. 2015, *54*, 7891-7894.

(75) Shapiro, N. D.; Toste, F. D. "Rearrangement of Alkynyl Sulfoxides Catalyzed by Gold(I) Complexes." *J. Am. Chem. Soc.* 2007. *129*, 4160-4161.

(76) Li, G.; Zhang, L. "Gold-Catalyzed Intramolecular Redox Reaction of Sulfinyl Alkynes: Efficient Generation of α-Oxo Gold Carbenoids and Application in Insertion into R-CO Bonds." *Angew. Chem. Int. Ed.* 2007. *46*, 5156-5159.

(77) Cui, L.; Peng, Y.; Zhang, L. "A Two-Step, Formal [4+2] Approach toward Piperidin-4-ones via Au Catalysis." *J. Am. Chem. Soc.* 2009, *131*, 8394-8395.

(78) Cui, L.; Yu, Y.; Zhang, L. "Gold-catalyzed efficient synthesis of azepan-4-ones *via* a two step [5+2] annulation." *Chem. Commun.* 2010, *46*, 3351-3353.

(79) Stow, C. P.; Widenhoefer, R. A. "Synthesis, Structure, and Reactivity of Gold(I) α-Oxo Carbenoid Complexes." *Organometallics*, 2020, *39*, 1249-1257.

(80) Zi, W.; Toste, F. D. "Recent advances in enantioselective gold catalysis." *Chem. Soc. Rev.* 2016, *45*, 4567−4589.

(81) Asiri, A. M.; Hashmi, A. S. K. "Goldcatalysed reactions of diynes." *Chem. Soc. Rev*. 2016, *45*, 4471−4503.

(82) Goodwin, J. A.; Aponick, A. "Regioselectivity in the Au-catalyzed hydration and hydroalkoxylation of alkynes." *Chem. Commun*. 2015, *51*, 8730−8741.

(83) Jia, M.; Bandini, M. "Counterion Effects in Homogeneous Gold Catalysis." *ACS Catal*. 2015, *5*, 1638−1652.

(84) Fürstner, A. "Gold Catalysis for Heterocyclic Chemistry: A Representative Case Study on Pyrone Natural Products." *Angew. Chem., Int. Ed.* 2018, *57*, 4215−4233.

(85) Akram, M. O.; Banerjee, S.; Saswade, S. S.; Bedi, V.; Patil, N. T. "Oxidant-free oxidative gold catalysis: the new paradigm in cross-coupling reactions." *Chem. Commun.* 2018, *54*, 11069−11083.

(86) Harris, R. J.; Widenhoefer, R. A. "Gold Carbenes, Gold Stabilized Carbocations, and Cationic Intermediates Relevant to Gold-Catalyzed Cycloaddition." *Chem. Soc. Rev.* 2016, *45*, 4533−4551.

(87) Zeineddine, A.; Rekhroukh, F.; Sosa Carrizo, E. D.; Mallet-Ladeira, S.; Miqueu, K.; Amgoune, A.; Bourissou, D. "Isolation of a Reactive Tricoordinate α-Oxo Gold Carbene Complex." *Angew. Chem., Int. Ed.* 2018, *57*, 1306−1310.

(88) Straub, B. F.; Hofmann, P. "Copper(I) Carbenes: The Synthesis of Active Intermediates in Copper-Catalyzed Cyclopropanation." *Angew. Chem., Int. Ed.* 2001, *40*, 1288−1290.

(89) Ikeno, T.; Iwakura, I.; Yamada, T. "Cobalt−Carbene Complex with Single-Bond Character: Intermediate for the Cobalt Complex-Catalyzed Cyclopropanation." *J. Am. Chem. Soc*. 2002, *124*, 15152−15153.

(90) Chen, M.; Chen, Y.; Sun, N.; Zhao, J.; Liu, Y.; Li, Y. "Gold-Catalyzed Oxidative Ring Expansion of 2-Alkynyl-1,2- Dihydropyridines or -quinolines: Highly Efficient Synthesis of Functionalized Azepine or Benzazepine Scaffolds." *Angew. Chem., Int. Ed.* 2015, *54*, 1200−1204.

(91) Qian, D.; Hu, H.; Liu, F.; Tang, B.; Ye, W.; Wang, Y.; Zhang, J. "Gold(I)-Catalyzed Highly Diastereo- and Enantioselective Alkyne Oxidation/Cyclopropanation of 1,6-Enynes." *Angew. Chem., Int. Ed*. 2014, *53*, 13751−13755.

(92) Schulz, J.; Jasík, J.; Gray, A.; Roithová, J. "Formation of Oxazoles from Elusive Gold(I) α-Oxocarbenes: A Mechanistic Study." *Chem. - Eur. J.* 2016, *22*, 9827−9834.

(93) Neuhaus, J. D.; Oost, R.; Merad, J.; Maulide, N. "Sulfur Based Ylides in Transition-Metal-Catalysed Processes." *Top. Curr. Chem.* (Z) 2018, 376, 15.

(94) Lu, L.-Q.; Li, T.-R.; Wang, Q.; Xiao, W.-J. "Beyond sulfide-centric catalysis: recent advances in the catalytic cyclization reactions of sulfur ylides." Chem. Soc. Rev. 2017, *46*, 4135− 4149.

(95) Burtoloso, A. C. B.; Dias, R. M. P.; Leonarczyk, I. A. "Sulfoxonium and Sulfonium Ylides as Diazocarbonyl Equivalents in Metal-Catalyzed Insertion Reactions." *Eur. J. Org. Chem.* 2013, *2013*, 5005−5016.

(96) Kramer, S.; Skrydstrup, T. "Gold-Catalyzed Carbene Transfer to Alkynes: Access to 2,4-Disubstituted Furans." *Angew. Chem., Int. Ed*. 2012, *51*, 4681−4684.

(97) Huang, X.; Peng, B.; Luparia, M.; Gomes, L. F. R.; Veiros, L. F.; Maulide, N. "Gold-Catalyzed Synthesis of Furans and Furanones from Sulfur Ylides." *Angew. Chem., Int. Ed*. 2012, *51*, 8886−8890.

(98) Klimczyk, S.; Misale, A.; Huang, X.; Maulide, N. "Dimeric TADDOL Phosphoramidites in Asymmetric Catalysis: Domino Deracemization and Cyclopropanation of Sulfonium Ylides." *Angew. Chem., Int. Ed*. 2015, *54*, 10365−10369.

(99) Oost, R.; Neuhaus, J. D.; Misale, A.; Meyrelles, R.; Veiros, L. F.; Maulide, N. "Catalyst-dependent selectivity in sulfonium ylide cycloisomerization reactions." *Chem. Sci.* 2018, *9*, 7091−7095.

(100) Mangion, I. K.; Weisel, M. "Gold (I) catalysis of X−H bond insertions." *Tetrahedron Lett.* 2010, *51*, 5490−5492.

(101) Urriolabeitia, E. P. "Ylide Ligands." *Top. Organomet. Chem*. 2010, *30*, 15−48.

(102) Fedorov, A.; Chen, P. "Electronic Effects in the Reactions of Olefin-Coordinated Gold Carbene Complexes." *Organometallics* 2009, *28*, 1278−1281.

(103) Carden, R. G.; Widenhoefer, R. A. "Gold Sulfonium Benzylide Complexes Undergo Efficient Benzylidene Transfer to Alkenes." *Chem. - Eur. J.* 2019, *25*, 11026−11030.

(104) Tskhovrebov, A. G.; Lingnau, J. B.; Fürstner, A. "Gold Difluorocarbenoid Complexes: Spectroscopic and Chemical Profiling." *Angew. Chem., Int. Ed*. 2019, *58*, 8834−8838.

(105) Nesmeyanov, A. N.; Perevalova, E. G.; Smyslova, E. I.; Dyadchenko, V. P.; Grandberg, K. I. "Reaction of Gold Compounds and Diazomethane." *Bull. Acad. Sci. USSR, Div. Chem. Sci*. 1977, *26*, 2417−2419.

(106) Perevalova, E. G.; Smyslova, E. I.; Grandberg, K. I. "Auration of chloroform." *Bull. Acad. Sci. USSR, Div. Chem. Sci.* 1982, *31*, 2506−2506.

(107) Perevalova, E. G.; Struchkov, Y. T.; Dyadchenko, V. P.; Smyslova, E. I.; Slovokhotov, Y. L.; Grandberg, K. I. "Cyanomethyl Derivatives of Gold." *Bull. Acad. Sci. USSR, Div. Chem. Sci*. 1983, *32*, 2529−2536.

(108) Vicente, J.; Chicote, M.-T.; Lagunas, M.-C. "Gold(I) and Palladium(II) Complexes Containing the Functionalized Ylides Triarylphosphonium Cyanomethylide or 2-Cyanoethylide, (R3P.CHR', R'.CN, CH2CN)." *Helv. Chim. Acta* 1999, *82*, 1202− 1210.

(109) Arnup, P. A.; Baird, M. C. "Transition Metal Ylid Complexes." *Inorg. Nucl. Chem. Lett*. 1969, *5*, 65−68.

(110) Vicente, J.; Chicote, M.- T.; Saura-Llamas, I.; Jones, P. G.; Meyer-Base, K.; Erdbrügger, C. F. "Synthesis of Gold(I), Gold(III), and Silver(I) Complexes with Ylide Ligands Derived from Carbonylbis(methylenetriphenylphosphonium) Diperchlorate. Crystal and Molecular Structures of $[Au_2\{\mu\text{-}\{\{CH\text{-}(PPh_3)\}_2CO\}\}_2](ClO_4)_2$, $[(Ph_3PCCl_2)_2CO][AuCl_4](ClO_4)$, $[(AuL)_2\{\mu\text{-}\{C(PPh_3)C(O)CH(PPh_3)(AuL)\}\}](ClO_4)_2$ (L = PPh_3), and $[\{Au(PMe_2Ph)\}_4\{\mu\text{-}\{\{C(PPh_3)\}_2CO\}\}](ClO_4)_2$." *Organometallics* 1988, *7*, 997−1006.

(111) Vicente, J.; Chicote, M.-T.; Lagunas, M.- C.; Jones, P. G. "Synthesis and Structural Characterization of Gold-(I), -(III) and Silver(I) Complexes of the Ylide Ligand $Ph_3P = CHC(O)NMe_2$. Crystal Structure of $[(AuPPh_3)_2\{\mu\text{-}C(PPh_3)C(O)\text{-}NMe_2\}]ClO_4$." *J. Chem. Soc., Dalton Trans*. 1991, 2579−2583.

(112) Vicente, J.; Chicote, M.-T.; Cayuelas, J. A.; Fernandez-Baeza, J.; Jones, P. G.; Sheldrick, G. M.; Espinet, P. "Synthesis of Gold-(I) and -(III) Complexes with Carbonyl-stabilized Phosphorus Ylides. Crystal Structure of $[\{Au(PPh_3)\}_2\{\mu\text{-}C(PPh_3)CO_2Et\}]ClO_4$." *J. Chem. Soc., Dalton Trans.* 1985, 1163−1168.

(113) Bayat, M.; Sedghi, A.; Ebrahimkhani, L.; Sabounchei, S. J. N "Heterocyclic carbene or phosphorus ylide: which one forms a stronger bond with group 11 metals? A theoretical study." *Dalton Trans*. 2017, *46*, 207−220.

(114) Zhdanko, A.; Ströbele, M.; Maier, M. E. "Coordination Chemistry of Gold Catalysts in Solution: A Detailed NMR Study." *Chem. - Eur. J.* 2012, *18*, 14732−14744.

(115) Rastogi, G. K.; Deka, B.; Deb, M. L.; Baruah, P. K. "Disastereoselective sp^3-C-H Functionalization of Arylmethyl Ketones and Transformation of E- to Z-Product through Photocatalysis." *Eur. J. Org. Chem*. 2020, *2020*, 424−428.

(116) Dai, X.; Warren, T. H. "Discrete Bridging and Terminal Copper Carbenes in Copper-Catalyzed Cyclopropanation." *J. Am. Chem. Soc.* 2004, *126*, 10085−10094.

(117) Joost, M.; Estevez,´ L.; Mallet-Ladeira, S.; Miqueu, K.; Amgoune, A.; Bourissou, D. "Enhanced π-Backdonation from Gold(I): Isolation of Original Carbonyl and Carbene Complexes." *Angew. Chem., Int. Ed*. 2014, *53*, 14512−14516.

(118) Brown, T. J.; Widenhoefer, R. A. "Synthesis and Equilibrium Binding Studies of Cationic, Two-coordinate Gold(I) π-Alkyne Complexes." *J. Organomet. Chem.* 2011, *696*, 1216−1220.

(119) Kim, N.; Brooner, R. E. M.; Widenhoefer, R. A. "Unexpected Skeletal Rearrangement in the Gold(I)/Silver(I)-Catalyzed Conversion of 7-Aryl-1,6-enynes to Bicyclo[3.2.0]hept-6-enes via Hidden Brønsted Acid Catalysis." *Organometallics* 2017, *36*, 673−678.

(120) Tsui, E. Y.; Müller, P.; Sadighi, J. P. "Reactions of Stable Monomeric Gold(I) Hydride Complex." *Angew. Chem., Int. Ed*. 2008, *47*, 8937−8940.

(121) Toma, T.; Shimokawa, J.; Fukuyama, T. "N,N′-Ditosylhydrazine: A Convenient Reagent for Facile Synthesis of Diazoacetates." *Org. Lett*. 2007, *9*, 3195−3197.

(122) Müller, P.; Fernandez, D.; Nury, P.; Rossier, J.-C. "Transition-Metal-Catalyzed Carbenoid Reactions of Sulfonium Ylides." *Helv. Chim. Acta* 1999, *82*, 935−945.

(123) Payne, G. B. "Cyclopropanes from Reactions of Ethyl (Dimethylsulfuranylidene)acetate with α,β Unsaturated Compounds." *J. Org. Chem*. 1967, *32* (11), 3351−3355.

(124) Shevchenko, V. V.; Zhegalova, N. G.; Borzenko, A. O.; Nikolaev, V. A. "On the Most Powerful Chemical Traps for Bis(methoxycarbonyl)carbene(=2-Methoxy-1-(methoxycarbonyl)-2- oxoethylidene)." *Helv. Chim. Acta* 2008, *91*, 501−509.

(125) Takebayashi, M.; Ibata, T.; Kohara, H.; Ueda, K. "Reactions of Diazoketones in the Presence of Metal Chelates. II. Reactions with Olefinic Compounds." *Bull. Chem. Soc. Jpn.* 1969, *42*, 2938−2944.

(126) Wessig, P.; Mühling, O. "Photochemical Synthesis of Highly Functionalized Cyclopropyl Ketones." *Helv. Chim. Acta* 2003, *86*, 865−893.

(127) Wang, Y.; Zhang, L. "Recent Developments in the Chemistry of Heteroaromatic *N*-Oxides." *Synthesis*, 2015, *47*, 289-305.

(128) Witham, C.A.; Mauleón, P.; Shapiro, N.D.; Sherry, B.D.; Toste, F.D. "Gold(I)-Catalyzed Oxidative Rearrangements." *J. Am. Chem. Soc.* 2007, *129*, 5838-5839.

(129) Emerson, C. R.; Zakharov, L. N.; Blakemore, P. R. "Investigation of Functionalized α-Chloroalkyllithiums for a Stereospecific Reagent-Controlled Homologation Approach to the Analgesic Alkaloid (-)-Epibatidine." *Chem Eur. J.* 2013, *19,* 16342-16356.

(130) Brummond, K. M.; McCabe, J. M. "Trimethylaluminium (TMA)-Catalyzed Reaction of Alkynyllithiums with Ethylene Oxide: Increased Yields and Purity of Homopropargylic Alcohols." *Synlett*. 2005, *16*, 2457-2460.

(131) Pileio, G.; Hill-Cousins, J. T.; Mitchell, S.; Kuprov, I.; Brown, L. J.; Brown, R. C. D.; Levitt, M. H. "Long-Lived Nuclear Singlet Order in Near-Equivalent ^{13}C Spin Pairs." *J. Am. Chem. Soc.* 2012, *134*, 17494-17497.

(132) Flowers, W. T.; Freitas, A. M.; Holt, G.; Purkiss, S. C. "Preparation and Reactions of Novel Cyclic β-Oxosulphonim Salts obtained by the Acid-induced cyclisation of 1-Diazo-ω-phenylthio-2-alkanones." *J. Chem. Soc., Perkin Trans. 1* 1981, 1119-1124.

(133) Brooner, R. E. M.; Brown, T. J.; Widenhoefer, R. A. "Synthesis and Study of Cationic, Two-Coordinate Triphenylphosphine-Gold-π-Complexes." *Chem. Eur. J.* 2013, *19*, 8276-8284.

(134) Brown, T. J.; Widenhoefer, R. A. "Cationic Gold(I) π-Complexes of Terminal Alkynes and Their Conversion to Dinuclear σ,π-Acetylide Complexes." *Organometallics,* 2011**,** *30*, 6003-6009.

(135) Oare, D. A.; Henderson, M. A.; Sanner, M. A., Heathcock, C. H. "Stereochemistry of the Michael Addition of N,N-Disubstituted Amide and Thioamide Enolate to Thioamide Enolates to α,β-Unsatureated Ketones." *J. Org. Chem.* 1990, *55,* 132-157.

(136) Akana, J. A.; Bhattacharyya, K. X.; Muller, P.; Sadighi, J. P. "Reversible C-F Bond Formation and the Au-Catalyzed Hydrofluorination of Alkynes." *J. Am. Chem. Soc.*, 2007, *129* (25), 7736-7737.

(137) Jonsson H. F.; Fiksdahl, A. "Studies on gold-nitrone systems." *Dalton Trans.* 2019, *48*, 142-149.

(138) Davies, P. W.; Albrecht, S. J.-C. "Gold- or Platinum-Catalyzed Synthesis of Sulfur Heterocycles Access to Sulfur Ylides without Using Sacrificial Functionality." *Angew, Chem. Int. Ed.* **2009**, *48*, 8372-8375.

(139) Davies, P. W. "Alkynes as "masked" ylides under noble-metal catalysis." *Pure Appl. Chem.* 2010, *82*, 1537-1544.

(140) Mei, H; Pan, G; Zhang, X; Lin, L.; Liu, X.; Feng, X. "Catalytic Asymmetric Ring-Opening/Cyclopropanation of Cyclic Sulfur Ylides: Construction of Sulfur-Containing Spirocyclopropyloxindoles with Three Vicinal Stereocenters." *Org. Lett.* 2018, *20*, 7794-7797.

(141) Obradors, C.; Echavarren, A. M. "Gold-Catalyzed Rearrangements and Beyond." *Acc. Chem. Res.* 2014, *47* (3), 902-912.

(142) Fürstner, A. "From Understanding to Prediction: Gold- and Platinum- Based π-Acid Catalysis for Target Oriented Synthesis." *Acc. Chem. Res.* 2014, *47* (3), 925-938.

(143) Obradors, C.; Echavarren, A. M. "Intriguing mechanistic labyrinths in gold(I) catalysis." *Chem. Commun.* 2014, *50*, 16-28.

(144) Doyle, M. P.; Griffin, J. H.; Bagheri, V.; DorowR. L., "Correlations between catalytic reactions of diazo compounds and stoichiometric reactions of transition metal-carbenes with alkenes. Mechanism of the cyclopropanation reactions." *Organometallics,* 1984, *3* (1), 53-61.

(145) Doyle, M. P. "Catalytic methods for metal carbene transformations." *Chem. Rev.* 1986, *86* (5), 919-939.

(146) Rodríguez-García, C.; Olivia, A.; Ortuño, R. M.; Branchadell, V. "Mechanism of olefin cyclopropanation by diazomethane catalyzed by palladium dicarboxylates, a density functional study." *J. Am. Chem. Soc.* 2001, *123* (25), 6157-6163.

(147) Fraile, J. M.; Garcia, J. L.; Martínez-Merino, V.; Mayoral, J. A.; Salvatella, L. "Theoretical (DFT) insights into the mechanism of copper-catalyzed

cyclopropanation reactions. Implications for enantioselective catalysis." *J. Am. Chem. Soc.* 2001, *123* (31), 7616-7625.

(148) Bernardi, F.; Bottoni, A.; Miscione, G. P., "DFT Study of the palladium-catalyzed cyclopropanation reaction." *Organometallics* 2001, *20* (13), 2751-2758.

(149) Straub, B. F. "Pd (0) mechanism of palladium-catalyzed cyclopropanation of alkenes by CH_2N_2: a DFT study." *J. Am. Chem. Soc.* 2002, *124* (47), 14195-14201.

(150) Iwakura, I.; Ikeno, T.; Yamada, T.; "Proposal for the metallacycle pathway during the cyclopropanation catalyzed by cobalt-Schiff base complexes." *Org. Lett.* 2004, *6* (6), 949-952.

(151) Hasmi, A. S. K.; Haufe, P.; Rivas Nass, A. "On the Enantioselective Rhodium-Catalyzed Enyne Cyclization." *Adv. Synth. Catal.* 2003, *345* (11), 1237-1241.

(152) Nakamura, A.; Konishi, A.; Tsujitani, R.; Kudo, M.; Otsuka, S. "Enantioselective carbenoid cyclopropanation catalyzed by chiral vic-dioximatocobalt(II) complexes prepared from natural camphor and beta-pinene. Mechanism and stereochemistry." *J. Am. Chem. Soc.* 1978, *100* (11), 3449-3461.

(153) Nakamura, A.; Koyama, T.; Otsuka, S. "Some Aspects on the Mechanism of Palladium-complex-catalyzed Decomposition of an Cyclopropanation with Ethyl Diazoacetate." *Bulletin of the Chemical Society of Japan.* 1978, *51* (11), 593-595.

(154) Seo, S.; Yu, X.; Marks, T. J. "Intramolecular Hydroalkoxylation/Cyclization of Alkynyl Alcohols Mediated by Lanthanide Catalysts. Scope and Reaction Mechanism." *J. Am. Chem. Soc.* 2009, *131* (1), 263-276.

(155) Fananas-Mastral, M; Aznar, F. "Carbene transfer reactions from chromium (0) to gold (I): Synthesis and reactivity of new Fischer-type gold (I) alkenyl carbene complexes." *Organometallics*. 2009, *28* (3), 666-668.

(156) Brooner, R. E.; Widenhoefer, R. A. "Experimental evaluation of electron donor ability of a gold phosphine fragment in a gold carbene complex." *Chemical Communications.* 2014, *50* (19), 2420-2423.

(157) Fernandex, E. J.; Laguna, A.; Olmos, M. E. "Recent developments in arylgold (I) chemistry" *Advancements in Organometallic Chemistry*. 2005, *52,* 77-142.

Biography

Caroline Stow graduated *summa cum laude* from St. Joseph's University in 2017 with a Bachelor of Science in Chemistry. During her undergraduate research career, she conducted research with Professor Mark A. Forman focusing on the synthesis of pentacyclo-[4.3.0.$0^{2,4}$.$0^{3,8}$.$0^{5,7}$]-non-4-ene. During her time at St. Joseph's, she was inducted as a member of Sigma Xi, Sigma Zeta, and Phi Beta Kappa. Upon graduation, she was awarded with the ACS Scholastic Achievement Award, and ACS Undergraduate Awards in the fields of inorganic, organic, and physical chemistry.

In August of 2017, Caroline then began her graduate career at Duke University, and joined the lab of Professor Ross Widenhoefer to begin her research on mechanistic analysis of gold(I) catalysis of reactive intermediates, with a specific interested in α-oxo gold(I) carbenoids and *N*-alkenoxypyridinium/sulfonium complexes. She published her research in 2020 in *Organometallics* and presented her research both locally and nationally throughout her graduate career.

From 2018-2020, she served on the Graduate Chemistry council as President, Vice President, and Recruitment Chair. In 2021 she was awarded the C.R. Hauser Memorial Fellowship. As she concludes graduate research, she plans to publish her remaining research and obtain her Doctor of Philosophy in chemistry in November of 2022.